arXiv:cond-mat/0502465v1 [cond-mat.mtrl-sci] 18 Feb 2005

Accuracy of ab initio methods in predicting the crystal structures of metals: review of 80 binary alloys.

Stefano Curtarolo[1,3], Dane Morgan[2], Gerbrand Ceder[2]
[1] *Department of Mechanical Engineering and Materials Science, Duke University, Durham, NC 27708*
[2] *Department of Materials Science and Engineering, MIT, Cambridge, MA 02139*
[3] *corresponding author, e-mail: stefano@duke.edu*

(February 2, 2008)

Predicting and characterizing the crystal structure of materials is a key problem in materials research and development. We report the results of *ab initio* LDA/GGA computations for the following systems: AgAu, AgCd, AgMg, AgMo*, AgNa, AgNb*, AgPd, AgRh*, AgRu*, AgTc*, AgTi, AgY, AgZr, AlSc, AuCd, AuMo*, AuNb, AuPd, AuPt*, AuRh*, AuRu*, AuSc, AuTc*, AuTi, AuY, AuZr, CdMo*, CdNb*, CdPd, CdPt, CdRh, CdRu*, CdTc*, CdTi, CdY, CdZr, CrMg*, MoNb, MoPd, MoPt, MoRh, MoRu, MoTc*, MoTi, MoY*, MoZr, NbPd, NbPt, NbRh, NbRu, NbTc, NbY*, NbZr*, PdPt, PdRh*, PdRu*, PdTc, PdTi, PdY, PdZr, PtRh, PtRu, PtY, PtTc, PtTi, PtZr, RhRu, RhTc, RhTi, RhY, RhZr, RuTi, RuTc, RuY, RuZr, TcTi, TcY, TcZr, TiZr*, YZr* (* = systems in which the *ab initio* method predicts that no compounds are stable). A detailed comparison to experimental data confirms the high accuracy with which *ab initio* methods can predict ground states.

Keywords: Binary Alloys, Ab initio, Intermetallics, Transition Metals, Structure Prediction, Phase Stability, Aluminum, Cadmium, Gold, Magnesium, Molybdenum, Niobium, Palladium, Platinum, Rhodium, Ruthenium, Scandium, Silver, Sodium, Titanium, Technetium, Yttrium, Zirconium.

CONTENTS

I. Introduction 1
II. The library: alloys and structures 2
III. High-throughput First Principles calculations 3
IV. Discussion and summary of results 4
  A. Discussion of disagreement between experimental and ab initio results 5
V. Conclusions 6
VI. Alloys without ab initio compounds 8
VII. Alloys with ab initio compounds 9
VIII. Trend for Technetium alloys 45
IX. Acknowledgments 46
X. Tables of Results 47
  A. Experimental compounds in agreement with ab initio solutions 47
  B. Experimentally unknown, non-identified or speculated compounds and ab initio predictions 48
  C. Experimental solid solutions, two-phases and "not studied" regions and possible ab initio predictions 49
  D. Experimental compounds that could not be checked by our calculations 51
  E. Experimental compounds in disagreement with other ab initio compounds or two-phase regions 52
XI. Appendix: new structure prototypes which are superstructures of FCC, BCC, HCP 53
XII. Appendix: relaxed structure prototypes 53
References 54

I. INTRODUCTION

First principles computation, whereby the properties of materials are predicted starting from the principles of quantum mechanics, is becoming well integrated with more traditional materials research. A list of *ab initio* studies on binary and ternary alloy phase stability up to 1994 can be found in reference [1]. Since the earliest, completely *ab initio* computation of a binary phase diagram [2], the approaches to compute the total energy of a solid have significantly improved, and computing resources have continued to become faster and less expensive. We believe that a point has been reached where, with a reasonable amount of resources, high throughput first principles studies of a large number of alloys can be performed [3–8]. In this paper we present the results of a first principles study of 14080 computed total energies on 176 crystal structures in 80 binary alloys. To our knowledge this is the largest first principles study of its kind on alloys. As we have compared the results in every system to experimental compilations, this study also offers a statistical test on the accuracy of some current *ab initio* approaches in correctly predicting the structure of materials.

For 89 compounds we find unambiguous agreement between experiment and the *ab initio* computation (Table 5), giving some indication of the predictive power of modern *ab initio* electronic structure methods. For many systems, verification of the *ab initio* results is difficult, as the systems have been poorly or incompletely characterized, or only high-temperature information is available experimentally. For most of these system, we make predictions that are consistent with the limited available information. Even though our library of 176 crystal structures is, to our knowledge, the largest library of *ab initio* energies ever produced, there are still 27 compounds for which we cannot verify the experimental structures as they are not in our library. We have not included such prototypes because they are extremely rare and complicated (many atoms per unit cell) (Table 8).

Overall, we find remarkably few significant discrepancies between the *ab initio* predictions and the experimental observations (Table 9). Based on the experimental data in references [9,10], we find only nine compounds for which LDA/GGA seems to predict the ground state incorrectly. For four of these nine systems, the experimental ground state is within less than 10meV/atom of the *ab initio* ground state. For the remaining five systems, there are at least two in which further investigation indicates that the experimental structure assignment is poorly justified, leaving three compounds in which a significant disagreement between experiment and *ab initio* LDA/GGA is likely. Such disagreements are addressed in Section (IV).

We believe that the low ratio of unambiguous errors (3) to the number of unambiguous correct predictions (89) is encouraging, and establishes clearly the potential of predicting crystal structure correctly with *ab initio* methods.

We also predict the stability of five new crystal structures which, to the best of our knowledge, have not yet been observed in any system. An AB_3 superstructure of the fcc lattice, stable for $CdPt_3$, $PdPt_3$ and Pd_3Pt, an AB bcc superstructure for MoTi, an AB_3 bcc superstructure for $MoTi_3$, Mo_3Ti, Nb_3Tc, $RuTi_3$ and $TcTi_3$, an A_2B_2 hcp superstructure for RhRu, and an A_2B_4 hcp superstructure for $RhRu_2$ (Appendix (XI)). In addition, we find two new crystal structures which are not superstructures of fcc, bcc or hcp: $MoZr_3$ and Mo_5Ti (for Mo_5Ti, $MoZr_5$, and Nb_5Ru) (Appendix (XII)).

II. THE LIBRARY: ALLOYS AND STRUCTURES

Binary alloys. Our calculated library contains 80 binary intermetallic alloys. The alloys include the binaries that can be made from row 5 transition metals, as well as some systems with Aluminum, Gold, Magnesium, Platinum, Scandium, Sodium, Titanium, and Technetium. The alloys are: AgAu, AgCd, AgMg, AgMo*, AgNa, AgNb*, AgPd, AgRh*, AgRu*, AgTc*, AgTi, AgY, AgZr, AuCd, AuMo*, AuNb, AuPd, AuPt*, AuRh*, AuRu*, AuSc, AuTc*, AuTi, AuY, AuZr, AlSc, CdMo*, CdNb*, CdPd, CdPt, CdRh, CdRu*, CdTc*, CdTi, CdY, CdZr, CrMg*, MoNb, MoPd, MoPt, MoRh, MoRu, MoTc*, MoTi, MoY*, MoZr, NbPd, NbPt, NbRh, NbRu, NbTc, NbY*, NbZr*, PdPt, PdRh*, PdRu*, PdTc, PdTi, PdY, PtRh, PtRu, PtY, PtTc, PdZr, PtTi, PtZr, RhRu, RhTc, RhTi, RhY, RhZr, RuTi, RuTc, RuY, RuZr, TcTi, TcY, TcZr, TiZr*, YZr*, where the superscript * indicates the systems in which the *high throughput ab initio* method predicts that no compounds are stable: 57 alloys form compounds and 23 are non compound forming.

Structures and their prototypes. The library contains 176 crystal structures. Many of these have the same structure type but with different compositions of occupancies, for example, AB_3 and A_3B (also AB and BA if the point groups of atomic positions of A and B are different), so the number of distinct prototypes is 101. The various concentrations are listed in the table below.

Compounds composition	Conc. of B	number of prototypes
A & B	0%	4
A_5B & AB_5	16.66%	3
A_4B & AB_4	20%	2
A_3B & AB_3	25%	27
A_2B & AB_2	33.33%	32
A_5B_3 & A_3B_5	37.5%	2
A_3B_2 & A_2B_3	40%	1
A_4B_3 & A_3B_4	42.85%	1
AB (& BA*)	50%	29 (+3)

TABLE 1. Compositions, concentrations and number of prototypes inside the library. The library has 176 structures, and 101 distinct prototypes (* at composition AB, 3 prototypes have different point groups in atomic positions A and B, therefore they represent distinct structure types).

Of such prototypes, 65 are chosen from the most common intermetallic binary structures in the CRYSTMET database [11] and in the Pauling File [10]. Such prototypes can be described by their Strukturbericht designation and/or natural prototypes [9,10]: A1, A2, A3, A4, A15, B_h, B1, B2, B3, B4, $B8_1$, $B8_2$, B10, B11, B19, B27, B32, B33 (B_f), C_c, C2, C6, $C11_b$, C14, C15, $C15_b$, C16, C18, C22, C32, C33, C37, C38, C49, $D0_a$, $D0_3$, $D0_9$, $D0_{11}$, $D0_{19}$, $D0_{22}$, $D0_{23}$, $D0_{24}$, $D1_3$, $D1_a$, $D2_d$, $D7_3$, $D8_8$, $L1_0$, $L1_1$, $L1_2$, $L6_0$, $CaIn_2$, CuTe, $CuZr_2$, $GdSi_2$ (1.4), $MoPt_2$, NbAs (NbP), $NbPd_3$, Ni_2Si, Ω (with z=1/4), Pu_3Al (Co_3V), Ti_3Cu_4, W_5Si_3, YCd_3, $ZrSi_2$, γ-Ir. The rest of the structures (36) are fcc, bcc or hcp superstructures. Twelve of these superstructures consist of stacking of pure A and B planes along some direction. Of such prototypes, 12 contain a stacking direction, therefore we can name them following the parent lattice and the stacking direction:

$$LATTICE^{[direction]}_{stacking}. \tag{1}$$

For example the designation $FCC^{[001]}_{A2B2}$ indicates a structure prototype with FCC parent lattice and A2B2 stacking along direction [001]. The 12 prototypes of the library that can be labeled in this manner are: $\mathrm{BCC}^{[011]}_{AB2}$, $\mathrm{BCC}^{[211]}_{AB2}$, $\mathrm{FCC}^{[001]}_{A2B2}$, $\mathrm{FCC}^{[011]}_{A2B2}$, $\mathrm{FCC}^{[111]}_{A2B2}$, $\mathrm{FCC}^{[311]}_{A2B2}$, $\mathrm{FCC}^{[100]}_{AB2}$, $\mathrm{FCC}^{[111]}_{AB2}$, $\mathrm{FCC}^{[001]}_{AB3}$, $\mathrm{FCC}^{[011]}_{AB3}$, $\mathrm{FCC}^{[011]}_{AB3}$, $\mathrm{FCC}^{[111]}_{AB3}$. For the FCC superstructures, a conversion table between the lattice-stacking-direction, the Sanchez - de Fontaine notation [12], and the Lu *et al.* designations [13,14] is included below.

	Space Group	Sanchez - de Fontaine [12]	Lu *et al.* [13,14]	Here and [15]
AB_2	I4/mmm #139	AB_2(c)	$\beta1/\beta2$	$FCC^{[100]}_{AB2}$
AB_2	P$\bar{3}$m1 #164		$\alpha1/\alpha2$	$FCC^{[111]}_{AB2}$
AB_3	P4/mmm #123		Z1/Z3	$FCC^{[001]}_{AB3}$
A_2B_2	P4/nmm #129	AB(a)	Z2	$FCC^{[001]}_{A2B2}$
A_2B_2	C2/m #12		W2	$FCC^{[311]}_{A2B2}$
AB_3	Pmmm #47		Y1/Y3	$FCC^{[011]}_{AB3}$
A_2B_2	Pmmn #59	AB(e)	Y2	$FCC^{[011]}_{A2B2}$
A_2B_2	I4_1/amd #141		CH or "40"	$FCC^{[201]}_{A2B2}$
AB_3	R$\bar{3}$m #166		V1/V3	$FCC^{[111]}_{AB3}$
A_2B_2	R$\bar{3}$m #166		V2	$FCC^{[111]}_{A2B2}$

TABLE 2. Conversion table between the lattice-stacking-direction, the Sanchez - de Fontaine notation [12], and the Lu *et al.* designations [13,14].

The prototypes of stable structures, that cannot be described by Strukturbericht designation, natural prototypes or lattice-stacking-direction convention, are described in Appendix XI. The complete geometrical description of all the fcc, bcc, and hcp superstructures of the library can be found in reference [15].

III. HIGH-THROUGHPUT FIRST PRINCIPLES CALCULATIONS

Ultra Soft Pseudopotentials LDA calculations (US-LDA). Most of the energy calculations of the library were performed using Density Functional Theory in the Local Density Approximation (LDA), with the Ceperley-Alder form for the correlation energy as parameterized by Perdew-Zunger [18] with ultra soft Vanderbilt type pseudopotentials [19], as implemented in VASP [20]. Calculations are at zero temperature and pressure, and without zero-point motion. The energy cutoff in an alloy was set to 1.5 times the larger of the suggested energy cutoffs of the pseudopotentials of the elements of the alloy (suggested energy cutoffs are derived by the method described in [20]). Brillouin zone integrations were done using 2000/(number of atoms in unit cell) **k**-points distributed as uniformly as possible on a Monkhorst-Pack mesh [21,22]. For a sample set of calculations, we verified that with these energy cutoffs and **k**-points meshes the absolute energy is converged to better than 10 meV/atom. Energy differences between structures are expected to be converged to much smaller tolerances. Spin polarization was used only for magnetic alloys. For the non-magnetic ones, spin polarization was used only to verify the energies of the ground state structures. All structures were fully relaxed. With such methodology, we consider degenerate structures the ones that have energies closer than about 5meV/atom.

We have decided to calculate the entire library within the LDA formalism instead of the PAW-GGA method (discussed below) because of the faster execution speed of LDA.

PAW-GGA calculations. When several structures are in close competition for the ground state, we also performed calculations in the Generalized Gradient Approximation (GGA), with Projector Augmented-Wave (PAW) pseudopotentials, as implemented in VASP [20,23,24]. One would expect the PAW-GGA approach to be somewhat more accurate than the US-LDA. For the GGA correlation energy, we used the Perdew-Wang parameterization (GGA-PW91) [25]. Similar to the US-LDA case, all PAW-GGA calculations are performed at zero temperature and pressure, and without zero-point motion. The energy cutoff in each calculation was set to 1.75 times the larger of the suggested energy cutoffs of the pseudopotentials of the elements of the alloy. Brillouin zone integrations were done using at least ~3500/(number of atoms in unit cell) **k**-points distributed as uniformly as possible on a Monkhorst-Pack mesh [21,22]. Spin polarization was used in all calculations. We expect such calculations to be able to distinguish energies of structures previously degenerate. This is because the increased density of the **k**-points mesh, the reduced radial cutoff of the PAW potentials versus the ultrasoft pseudopotentials, and the GGA correlation energy implementation. With such methodology, we consider degenerate structures the ones that have energies closer than $\lesssim$1meV/atom.

For some structures both the US-LDA and PAW-GGA calculations are presented. To avoid confusion, we specify the type of calculation in brackets: "(us-lda)" or "(paw-gga)". *In addition, all the results of the PAW-GGA calculations are described in italics.*

Symmetries of the pure elements. Both the US-LDA and PAW-GGA calculations reproduce the correct experimental crystal structures of the pure elements at room temperature. The only exception is Sodium. In the two formalisms, Na-hcp is very slightly favored over Na-bcc and Na-fcc, in agreement with other first principle calculations [26–30]. At room temperature Sodium has the bcc structure, and undergoes a martensitic transformation below 35K, to a closed packed structure [31–38]. Therefore our results, Na-hcp stable and the very small energy differences with Na-bcc and Na-fcc, are consistent with the behavior at low temperature only.

High-throughput computing. To perform the high number of calculations, we have implemented a set of automatic tools to prepare initial data, perform calculations and analyze results.

Preparation of input files. All input files are prepared by starting from the templates based on the prototype chemistry. The volume of the unit cells is determined as a linear combination of atomic volumes of pure elements with Vegard's law [39]. The internal position of the atoms have been taken from geometrical configurations (for fcc, bcc, hcp superstructures) or have been extracted from the CRYSTMET and the Pauling File databases [11,10].

Ab initio Calculations. The calculations are performed by a high-throughput tool, called AFLOW (automatic flow), which searches inside the library for potential input files and performs the proper *ab initio* calculations. AFLOW is able to balance the CPU loads in a multiprocessor and cluster environment, maximizing the total throughput of the process [15]. AFLOW extracts the energy and initiates further relaxations with the atomic positions and unit cell geometries obtained from VASP. Therefore, all the structures are relaxed at least twice, and many ($\sim 10\%$ of the total) are relaxed three or more times, until proper geometrical and energetic convergence is obtained. To conclude, for a library of 176 crystal structures in 80 binary alloys, with a total of 14080 structures, AFLOW performed 32,402 VASP calculations. The total computing time used for this project was $\sim 9.05{\cdot}10^8$ CPU seconds ($\sim$ 28.7 CPU years), which was spread over a large set of computers [40]. Given the different types of CPUs used, we can only *estimate* the total amount of computation for the project at roughly $\sim 1.2 \cdot 10^6$ TERAFLOP.

Collection and error check of the results. Once each structure has been calculated, space group symmetry, bond distances, coordination numbers and unit volumes are compared for all the structures of that alloy with the same concentration in the library. Frequently, several structures, starting from different prototypes, relax to the same final structure with the same energy. Therefore, to identify the correct stable phase, it is mandatory to be able to determine the final relaxed structure with the highest possible reliability. Details of the high-throughput error checking tool can be found in reference [15]. A few stable structures remain unidentified. For those we report the unit cell and atomic positions in Appendix XI. Such prototypes might be new phases to be checked experimentally.

Calculation of the formation energies and the convex hull. The formation energy for each structure is determined with respect to the most stable structure of the pure elements. To determine the ground states of a system one needs to find, as a function of composition, the ordered compounds that have an energy lower than any other structure or any linear combination of structures that gives the proper composition. This set of ground state structures forms a *convex hull*, as all other structures have an energy that falls above the set of tie lines that connects the energy of the ground states. In thermodynamical terms, the *convex hull* represents the Gibbs free energy of the alloy at zero temperature.

Comparison with experiments. To compare the *ab initio* results to experimental information, we relied on the information and references in the Binary Alloy Phase Diagrams (Massalski [9]) and in the Pauling File [10]. Though in some cases references not included in these were also used, no systematic approach to go beyond information in the Pauling File or Binary Alloy Phase Diagrams was used.

IV. DISCUSSION AND SUMMARY OF RESULTS

In comparing the stable structures predicted by the *ab initio* computations with available experimental information, we have attempted to classify the results in a few distinct categories. Table 5 gives the compounds where the *ab initio* result and experiments are in unambiguous agreement. The fact that there are a large number of compounds (89) in Table 5 is a positive statement about the accuracy of LDA/GGA in capturing the close energetic competition between the 176 structures in our library. For one of the systems in Table 5 ($PdTi_3$) we took the liberty of modifying the experimental result [9] which shows the A15 structure (stoichiometry AB_3) as a line compound at composition $PdTi_4$. While off-stoichiometric compounds are obviously possible, this usually goes together with significant width of the single-phase field. Hence, we concluded (maybe erroneously) that the placement of A15 at composition $PdTi_4$ in reference [9] is likely a typographical error.

Table 6 shows compositions which are experimentally known to form compounds, but lack a complete identification of the structure type. Hence, the *ab initio* prediction should be seen as a likely crystal structure for the compound. In most cases, the *ab initio* structure is consistent with the conditions imposed by the limited experimental data (e.g. bcc-ordering is seen for Ag-Cd, and we predict B19; or C37 is speculated for Au-Sc, in agreement with what we predict). Hence, it is likely that with further experimental characterization, many of these systems would move to Table 5.

Table 7a-b contains compositions which are experimentally characterized as solid solutions, high-temperature two-phase regions, or have not been studied at all in a particular composition range. Because of the lack of low-temperature information in these systems, an unambiguous statement about the accuracy of the LDA/GGA prediction cannot be made. For some systems, the *ab initio* result is very consistent with the experimentally observed behavior. For example, in Ag-Au we find many fcc ordered superstructures with low formation energies, indicating a weak ordering interaction. So it is likely that the *ab initio* predicted structures are stable at low temperature, but disorder into a solid solution at elevated temperature, a rather common occurrence for noble-metal alloys. For other systems in this table the comparison between experiments and *ab initio* is more troubling. For example, while Mo-Ti is experimentally described as a two-phase system with no known compounds down to 400°C, we find very strong compound formation. While it is possible that these compounds disappear through peritectoid reactions below 400°C, the large negative formation energies make this unlikely. It is more likely that either the experimental characterization of this system, or the *ab initio* result is significantly in error. A system such as Mo-Nb, on the other hand, is not at all studied experimentally, and no statement about the accuracy of our prediction in this system can be made.

Table 8 contains the compounds whose crystal structure is not present in the library, and hence, it is not possible to make a comparison with the *ab initio* data. In some cases (e.g. $Au_{10}Zr_7$), this is because the crystal structure is uncommon and has a large unit cell, making it less worthwhile to include it in the library. In other cases (e.g. Rh_5Ti) the structure is simply unknown. Table 8 also includes structures that are only stable at off-stoichiometric compositions (e.g. B19 in Au-Ti), as we did not include disorder in the library prototypes.

Finally, Table 9 contains the compositions for which there seems to be a clear disagreement between the experimental data in references [9,10] and the *ab initio* results. Because these systems can point at either experimental errors, or shortcomings of the *ab initio* method, we discuss them here in more detail. Note that *ab initio* errors are most likely due to the LDA or GGA approximations or the pseudopotentials being used. In general, one should consider that our calculations only produce the zero-K energy, whereas all the experimental results are at non-zero temperature. Given that entropic differences between structures can be of the order $0.1 \sim 1.0 k_B$ per atom [381], very small energy differences between the experimentally observed structure and our *ab initio* results, could be reversed at elevated temperature. In particular, $AuNb_3$-A15, $NbRh_3$-$L1_2$, $NbRu_3$-$L1_2$ and NbRu'-$L1_0$ may be in this category. This phenomenon is quite common. As an example, Wolverton and Ozilins have shown that, in the case of the aluminum-copper system, the vibrational entropy difference is responsible for stabilizing the θ phase Al_2Cu (tetragonal C16) over the competing Al_2Cu-θ' phase (distortion of θ_c-C1, the cubic fluorite phase with CaF_2 prototype), which has the lowest energy, and, therefore, is the stable structure at zero Kelvin [382]. At temperatures higher than T$\sim 150 - 200$°C, Al_2Cu-θ is more favorable.

A. Discussion of disagreement between experimental and ab initio results

$AuNb_3$. The structure $AuNb_3$-A15 has been reported a number of times [9,10,127–141]. In particular, Röschel *et al.* [132] observed the A15 structure to grow in quenched samples. Ball-milling samples of the material to form disordered bcc, revert upon heat treatment in an exothermic reaction to A15, suggesting that A15 could be the ground state for this composition at low temperature. The relatively small energy difference between A15 and the $AuNb_2 \leftrightarrow Nb$ tie-line in our calculation could lead to finite temperature stability of A15. Alternatively, the ∼7meV/atom energy difference (US-LDA and PAW-GGA) could simply be an error of the *ab initio* approach.

AuY. While we predict the B33 structure to be stable by 26meV/atom below the B2 structure, this system is experimentally listed as having a B2 structure. This experimental classification is based on a paper by Chao *et al.* [170,10]. Chao's work mentioned that they only see B2 when performing a rapid quench. Further work by Kusma [172] and Dwight [158] did not observe the B2 structure. The experimental results in this system are therefore somewhat suspect. It is possible that B2 is a high temperature structure while B33 is the low temperature form. However, it should also be pointed out that the mixing energies in this system are very large (∼1eV), and that the potential error of ∼25meV/atom (US-LDA and PAW-GGA) is a small fraction of this.

Cd_3Nb. The structure of this compound is one of the more interesting discrepancies between *ab initio* and experiments to emerge from our study. Based on experimental work of Von Holleck [178], a single $L1_2$ compound is claimed to be stable in this system. Computationally, no compounds are stable at all, and we find this system to be immiscible. The compound with lowest energy is a bcc superstructure at composition CdNb, and energy ∼55meV/atom above the $Cd \leftrightarrow Nb$ tie-line *(∼62meV/atom with PAW-GGA)*. The Cd_3Nb-$L1_2$ is 70meV/atom above that same tie-line *(>100meV/atom with PAW-GGA)*. It is not common for LDA/GGA to make such large and qualitative errors in metals, and further investigation of this system is suggested, as it will likely lead to a reconsideration of the experimental classification, or to some novel understanding of the errors that *ab initio* methods can produce in metals.

$CdPt_3$. Experimentally this compound is claimed to form in the $L1_2$ structure, while we predict it to form in a new structure for which no prototype yet exists

($CdPt_3^{proto}$ in Appendix VIII). We believe the experimental assignment to be uncertain. It is based on a single paper by Nowotny [181] which actually does not observe the $L1_2$ structure in this system, but assigns it by chemical similarity with the Pt_3Zn system.

$NbRh_3$. This compound is characterized as an $L1_2$ structure, whereas our *ab initio* results find the Al_3Pu prototype to be 8meV/atom lower in energy *(5.3meV/atom with PAW-GGA)*. This small energy difference could very well be an LDA/GGA error, or could be reversed at elevated temperature by entropic effects.

$NbRu_3$. $NbRu_3$ is similar to the discrepancy of compound $NbRh_3$. Experimentally it is found to be an $L1_2$ structure, whereas we find a $D0_{24}$ structure that is 8meV/atom below the $L1_2$. With PAW pseudopotentials and the GGA exchange correlation corrections the $D0_{24}$-$L1_2$ energy difference reduces to 2.5meV/atom. Because this number is so small, extremely large **k**-points sets and high energy cutoff were used to converge it. The results indicate that $L1_2$ and $D0_{24}$ are all but degenerate in this system. Since $D0_{24}$ and $L1_2$ are very similar ($D0_{24}$ is a periodically anti-phased version of $L1_2$) subtle entropic effects can easily reverse the stability between these two.

NbRu. Experimentally this system is classified to have the $L1_0$ structure, whereas the *ab initio* results indicate an unusual two-phase region between Nb_3Ru ($D0_3$) and $NbRu_2$ (C37) covering this composition [9,10,233,237]. The most recent experimental result is based on the assignment by Chen [237] who observes a disordered bcc solution at high temperature and a transformation to a tetragonal structure near 1000°C. Between 720∼920°C they see a further symmetry reduction to an orthorhombic phase. Hence, even if the tetragonal structure below 1000°C would be $L1_0$ (which is only speculated by Chen) its further transformation to an orthorhombic structure indicates that $L1_0$ is not the ground state structure. Based on a diffusion couple study, Hurley [235] believes that a two-phase region exists near 50% Ru, though the results seem to be irreproducible. Besides the difficulty with interpreting the experimental data, significant problems also exists on the *ab initio* side with this compound. The PAW-GGA result is substantially different from the US-LDA result. GGA gives $L1_0$ only 4meV/atom above the tie-line (versus 20meV/atom in LDA), whereas B19 seems to be >100meV/atom above the tie-line (versus 13meV/atom with LDA).

PtY. Experimental assignment of the structure of this compound as B27 is based on two papers [277,316]. The *ab initio* work finds B33 to be lowest in energy with B27 higher by 50meV/atom *(60meV/atom with PAW-GGA)*. Given that the experimental results seem sound, this is probably a true *ab initio* error.

Pt_3Zr_5. The work of Schubert *et al.* [323] establishes Pt_3Zr_5 as a $D8_8$ structure, whereas our *ab initio* (LDA) results put the $D8_8$ structure 36meV/atom above the tie-line formed by $PtZr_2$-C16 and PtZr-B33. The GGA result is 26meV/atom above the tie-line. In each case the W_5Si_3 structure is lower in energy than the $D8_8$. Given the large mixing energies in this system (of the order of 1 eV/atom), these *ab initio* errors seem plausible.

V. CONCLUSIONS

Overall, the comparison between experimental data and *ab initio* results is encouraging. A large number of the ground states are predicted correctly, even though significant competition exists between various structures, indicating that relative energy differences are well reproduced by LDA/GGA. In many cases, the direct comparison between *ab initio* and experiments is difficult, as systems have often not been studied completely, or have not been studied to low enough temperature to make a reliable statement about the ground state structures. For only a small number of cases, there is a clear discrepancy between *ab initio* and experiments (Table 9). On further investigations, we find that some of the experimental assignments are poorly justified (e.g. $CdPt_3$). In a few of the "error systems", the energy difference between the observed structure and the *ab initio* structure is small, which makes it fall within the uncertainty one would expect from LDA/GGA or from a lack of entropic considerations.

A few systems display, in our opinion, such a significant discrepancy between available experimental data and *ab initio* results as to make them worthwhile for further study. These include Cd_3Nb ($L1_2$ observed, but no compounds from *ab initio*), Nb-Ru and Pt_3Zr_5 (respectively $L1_0$ and $D8_8$ observed, but no stable compounds at that composition in *ab initio*), PtY (significant error between B33 and B27) and the complete Mo-Ti system (which from experiments appears to be a miscibility gap, but in the *ab initio* results display a number of novel and strongly stabilized compounds). These systems should be investigated further, either to find experimental errors, or to shed new light on *ab initio* problems.

Our findings are summarized in Table 3. By comparing all the available *ab initio* calculations with the experimental results [9,10], we obtain 284 potential structure comparisons. A subset of these, (48), are not available due by the lack of the proper prototype or the unknown experimental compound. The rest of the structure comparisons, (236), can be divided in 89 *agreements* in ordered systems (N_{ac}), 21 *agreements* in immiscible systems (N_{ai}), 9 *disagreements* (N_d), 21 *good predictions* (N_{gp}), and 96 *possible predictions* (N_{pp}). This division is summarized in the following table.

<table>
<tr><th colspan="6">Total Experiments comparisons: 284</th></tr>
<tr><th colspan="6">Available comparisons: 236</th></tr>
<tr><td></td><td>Experimental</td><td><i>Ab initio</i></td><td></td><td>#</td><td>Table</td></tr>
<tr><td>Agreements</td><td>Compound</td><td>Compound</td><td>N_{ac}</td><td>89</td><td>5</td></tr>
<tr><td>Agreements</td><td>Immiscibility</td><td>Immiscibility</td><td>N_{ai}</td><td>21</td><td>3</td></tr>
<tr><td>Disagreements</td><td>Comp./ Immisc.</td><td>Incorrect</td><td>N_d</td><td>9</td><td>9</td></tr>
<tr><td>Good predictions</td><td>Comp. unknown, uncertain, guessed</td><td>Compound prediction</td><td>N_{gp}</td><td>21</td><td>6</td></tr>
<tr><td>Possible predictions</td><td>not-studied, solid-solution, two-phase region</td><td>Possible compound</td><td>N_{pp}</td><td>96</td><td>7a-b</td></tr>
<tr><th colspan="6">Unavailable comparisons: 48</th></tr>
<tr><td colspan="4">Reason</td><td>#</td><td>Table</td></tr>
<tr><td colspan="4">unavailable <i>ab initio</i> prototype</td><td>21</td><td>8</td></tr>
<tr><td colspan="4">unknown experimental compound</td><td>27</td><td>8</td></tr>
</table>

TABLE 3. Summary of the 284 structure comparisons between experimental and *ab initio* calculations. When available, we use the PAW-GGA calculations, otherwise we use the US-LDA ones. If only US-LDA calculations were used, we would obtain N_{ac}^{LDA}=84 agreements and N_d^{LDA}=14 disagreements.

The reliability of our *ab initio* method can be defined as the fraction of correct compounds (agreements) over the number of accessible compounds (agreements and disagreements):

$$\eta_c \equiv \frac{N_{ac}}{N_{ac}+N_d} \approx 90.8\%. \tag{2}$$

Such quantity, η_c, contains the reliability of the experimental results, which can be removed by considering only the *true unambiguous disagreements* of Table 9 ($N_d^\star = 3$). Hence the reliability of the method becomes:

$$\eta_c^\star \equiv \frac{N_{ac}}{N_{ac}+N_d^\star} \approx 96.7\%. \tag{3}$$

Such quantities, η_c and $\eta_c^\star$, can be considered as the probabilities that the most stable *ab initio* compounds reproduce the correct experimental compound. The quantity $\eta_c^\star$ should be used if the experimental compound is certain.

If we extend the argument to the agreements with experimental compounds and immiscible systems, then the reliabilities become:

$$\eta \equiv \frac{N_{ac}+N_{ai}}{N_{ac}+N_{ai}+N_d} \approx 92.4\%, \tag{4}$$

$$\eta^\star \equiv \frac{N_{ac}+N_{ai}}{N_{ac}+N_{ai}+N_d^\star} \approx 97.3\% \tag{5}$$

where the quantity $\eta_c^\star$ should be used if the experimental compound or immiscibility is certain. Such quantities, η and $\eta^\star$, can be considered as the probabilities that *ab initio* results reproduce the correct experimental compounds or immiscibilities.

Given the large number of calculations of this project, we believe η, $\eta^\star$, η_c, and $\eta_c^\star$ to be good estimations of state of the art pseudopotential *ab initio* accuracies in phase stability prediction.

VI. ALLOYS WITHOUT AB INITIO COMPOUNDS

Table 4 gives the alloys for which we find no compounds with negative formation energy, and the structure with lowest formation energy in the system. All of these agree with experiments except for the ones described below.

System	Structure with lowest E_f	E_f (us-lda) meV/atom	References [9–11] and
Ag-Mo	$AgMo_3$-BCC proto. #72 in [16]	208	[81,82]
Ag-Nb	$AgNb_3$-BCC proto. #72 in [16]	62	[86,87]
Ag-Rh	$AgRh_3$-$FCC^{[111]}_{AB3}$	116	[50,94–96]
Ag-Ru	$AgRu_3$-HEX proto. #127 in [16]	199	[41,43,96–98]
Ag-Tc	AgTc-HEX proto. #126 in [16]	147	[99]
Au-Mo	$AuMo_3$-$D0_{19}$	75	[41,46,118–122]
Au-Pt	Au_2Pt-$FCC^{[111]}_{AB2}$	9	[41,117,119,146–148]
Au-Rh	$AuRh_3$-$FCC^{[001]}_{AB3}$	91	[116,119,149,150]
Au-Ru	$AuRu_3$-HEX proto. #125 in [16]	165	[116,119,151,152]
Au-Tc	AuTc-HEX proto. #126 in [16]	74	[116,159]
Cd-Mo	Cd_5Mo-HEX proto. #128 in [16]	173	[9]
Cd-Nb	CdNb-BCC proto. #71 in [16]	55 (us-lda) *58 (paw-gga)*	[178] see note "Cd-Nb"
Cd-Ru	CdRu-$FCC^{[001]}_{A2B2}$	88	see note "Cd-Ru"
Cd-Tc	CdTc-B11	92	[182]
Cr-Mg	CrMg-B11	251	[45,191]
Mo-Tc	Mo_5Tc-A15	53	[44,217] see note "Mo-Tc"
Mo-Y	Mo_2Y-C15	40	[222,223]
Nb-Y	Nb_2Y-C49	132	[244–248]
Nb-Zr	$NbZr_2$-HEX proto. #129 in [16]	22	[249–253,90] [238–240,254–258]
Pd-Rh	$PdRh_3$-$FCC^{[111]}_{AB3}$	35	[13,263–270]
Pd-Ru	PdRu-HEX proto. #126 in [16]	44	[271–274]
Ti-Zr	Ti_2Zr-$B8_2$	18	[48,49,371–374]
Y-Zr	YZr_5-HEX proto. #141 in [16]	35	[49,375–380]

TABLE 4. Systems without intermetallic compounds. The second and third columns give, for each system, the structure with the lowest formation energy E_f (US-LDA calculations). The table contains 23 entries. 21 of these are in agreement with experiments. References include both experimental and *ab initio* studies.

Cd-Nb. One compound, Cd_3Nb-$L1_2$, has been reported for the system Cd-Nb [9,178]. However, we did not find any stable phase (Cd_3Nb-$L1_2$ has formation energy of ∼70meV/atom). The disagreement of compound Cd_3Nb-$L1_2$ is further discussed in the Section (IV).

Cd-Ru. The authors are not aware of any experimental result for the Cd-Ru system.

Mo-Tc. Two compounds have been suggested based on thermodynamic models: βMo_2Tc_3-A15 and σMo_3Tc_7-$D8_b$ [9,44]. However, we did not find any stable phase for the system, nor can we check the suggested compounds, since our library does not have the σ phase or the off-stoichiometry A15.

VII. ALLOYS WITH AB INITIO COMPOUNDS

Ag-Au (Silver - Gold). The system Ag-Au has not been studied in great detail at low temperatures, and no intermetallic compounds have been reported [9,10,52–55,119]. The solid is reported to be short-range ordered fcc, though it is suggested that long-order might exist at low temperature. At low temperature we find several stable compounds: Ag_4Au, Ag_3Au, Ag_2Au, AgAu-$L1_0$, $AgAu_2$ and $AgAu_3$. In our electronic structure approach, the ground states are degenerate for Ag_3Au, Ag_2Au, $AgAu_2$ and $AgAu_3$. Our best candidates are $L1_2$, $D0_{23}$, Al_3Pu, $NbPd_3$, $D0_{22}$ and $D0_{24}$ for Ag_3Au, C37 and $MoPt_2$ for Ag_2Au and $AgAu_2$, and $L1_2$, $D0_{22}$ and $D0_{23}$ for $AgAu_3$, as shown in figure (1). The considerable degeneracy of the ground states indicates that only very small effective interactions exist between Ag and Ag, consistent with the experimentally observed complete solid solubility. For composition Ag_4Au, the structure $D1_a$ is degenerate with the tie-line of the two-phase region Ag↔Ag_3Au. We conclude that further experimental and theoretical investigations are necessary to determine the behavior of AgAu. *To address the degenerate structures, we further investigate Ag_3Au, Ag_2Au, $AgAu_2$ and $AgAu_3$ with PAW-GGA potentials, as described in Section (III). With PAW, for composition Ag_3Au, $L1_2$ is the most stable compound and $D0_{22}$, $D0_{23}$, Al_3Pu, $NbPd_3$, $D0_{24}$ are higher by 0.9, 1.6, 2.2, 2.4, and 3.0meV/atom, respectively. For both composition Ag_2Au and $AgAu_2$, C37 is the most stable compound and $MoPt_2$ is higher by 1.9meV/atom and 4.3meV/atom, respectively. For composition $AgAu_3$, $L1_2$ is the most stable compound and $D0_{23}$ and $D0_{22}$ are higher by 3.4meV/atom and 3.9meV/atom, respectively.*

Other *ab initio* studies, relevant for this system, can be found in references [56–66].

Ag-Au system		
Low Temperature Phases comparison chart		
Composition % Au	Experimental (Massalski [9])	*Ab initio* result
20	short-range order $\gtrsim$ 950°C	Ag_4Au-$D1_a$/tie-line
25	short-range order $\gtrsim$ 950°C	Ag_3Au $L1_2$/$D0_{23}$/Al_3Pu/ (us-lda) /$NbPd_3$/$D0_{22}$/$D0_{24}$ (us-lda) *$L1_2$ stable (paw-gga)* *$D0_{22}$~0.9meV/at.* *$D0_{23}$~1.6meV/at.* *Al_3Pu~2.2meV/at.* *$NbPd_3$~2.4meV/at.* *$D0_{24}$~3.0meV/at.* *above $L1_2$ (paw-gga).*
33.3	short-range order $\gtrsim$ 950°C	Ag_2Au-C37/$MoPt_2$ (us-lda) *C37 stable (paw-gga)* *$MoPt_2$~1.9meV/at.* *above C37 (paw-gga).*
50	short-range order $\gtrsim$ 950°C	AgAu-$L1_0$
66.6	short-range order $\gtrsim$ 950°C	$AgAu_2$-C37/$MoPt_2$ (us-lda) *C37 stable (paw-gga)* *$MoPt_2$~4.3meV/at.* *above C37 (paw-gga).*
75.0	short-range order $\gtrsim$ 950°C	$AgAu_3$ $L1_2$/$D0_{22}$/$D0_{23}$ (us-lda) *$L1_2$ stable (paw-gga)* *$D0_{23}$~3.4meV/at.* *$D0_{22}$~3.9meV/at.* *above $L1_2$ (paw-gga).*

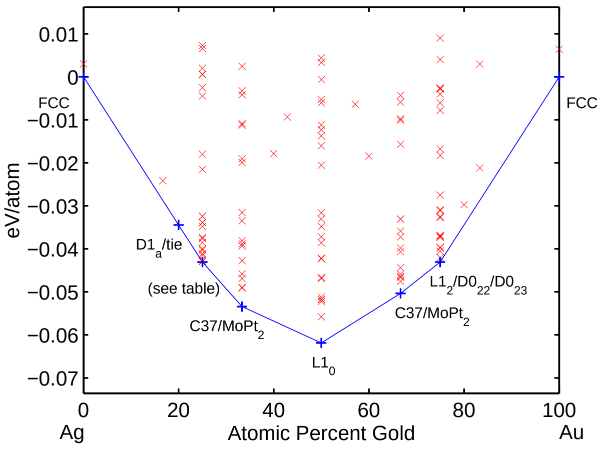

FIG. 1. AgAu (Silver - Gold) ground state convex hull.

Ag-Cd (Silver - Cadmium). At composition $AgCd_3$ we find $D0_{19}$ stable, while only disordered hcp solid solution has been reported at this composition. Hence, $D0_{19}$, an ordered hcp superstructure, probably is stable at low temperature in this system. At composition $AgCd_2$ we find a previously unknown compound $AgCd_2$-$ZrSi_2$. The low temperature β', near AgCd stoichiometry, is reported to be ordered bcc in Massalski [9]. In particular, the Pauling File reports AgCd-B2 [10,67–70]. We find B2, B19 and B27 to have degenerate energies (B19 is quite common for Cd alloys). The experimental phase diagram only displays solid solution on the Ag-rich side [9,10]. We find C37 at Ag_2Cd and a stable phase with stoichiometry Ag_3Cd. The ground state of Ag_3Cd is degenerate: three distinct structure ($D0_{19}$, $D0_{22}$, $D0_{24}$) have similar energy. *To address the degenerate structures, we further investigate AgCd and* Ag_3Cd *with PAW-GGA potentials, as described in Section (III). With PAW, for compound AgCd, B19 is the most stable structure, and B27 and B2 are higher by 2.8meV/atom and 3.4meV/atom, respectively. For compound* Ag_3Cd*,* $D0_{22}$ *and* $D0_{24}$ *are still degenerate ground states and* $D0_{19}$ *is higher by only 2.2meV/atom. It is possible that these compounds have not yet been observed, or that they have low ordering temperatures.*

Ag-Cd system		
Low Temperature Phases comparison chart		
Composition % Cd	Experimental (Massalski [9])	*Ab initio* result
25.0	fcc solid solution	Ag_3Cd $D0_{19}/D0_{22}/D0_{24}$ (us-lda) $D0_{22}/D0_{24}$ *(paw-gga)* $D0_{19}\sim$*2.2meV/at.* *above* $D0_{22}/D0_{24}$ *(paw-gga)*
33.3	fcc solid solution	Ag_2Cd-C37
48.5 to 50	β'-bcc B2 [10]	AgCd-B2/B19/B27 (us-lda). *B19 stable (paw-gga)* *B27$\sim$2.8meV/at.* *B2 $\sim$3.4meV/at.* *above B19 (paw-gga).*
66.6	none	$AgCd_2$-$ZrSi_2$.
64.5 to 81	hcp solid solution	$AgCd_3$-$D0_{19}$

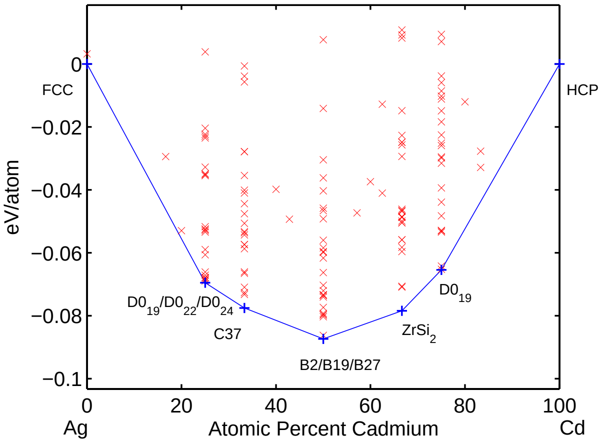

FIG. 2. AgCd (Silver - Cadmium) ground state convex hull.

Ag-Mg (Silver - Magnesium). The phase diagram of the system Ag-Mg is known with reasonable accuracy [9,10,71,72,75,77]. Our *ab initio* method confirms the stability of AgMg-B2. In the Ag-rich side of the phase diagram, at stoichiometry Ag_3Mg, we find $D0_{23}$ and $D0_{24}$ to be degenerate. While Massalski [9] indicates Ag_3Mg to be $L1_2$, it is known from detailed High Resolution Electronic Microscopy (HREM) that Ag_3Mg forms Long Period Superstructure (LPS) modulations of $L1_2$ [73,74] (LPS $D0_{23}$ is present in our library). For a detailed discussion of this system see Kulik *et-al.* [76]. $L1_2$ is 15.2meV/atom above $D0_{23}/D0_{24}$. On the Mg-rich side, our library does not have prototypes at 80% Mg concentration, so we are not able to find any hexagonal $AgMg_4$ (with unknown prototype [75,77]). However we find a stable compound $AgMg_3$. Two phases, $AgMg_3$-$D0_a$ and $AgMg_3$-$D0_{19}$, have degenerate energies. This is important, since experiments suggest that $AgMg_4$ was probably identified as hexagonal $AgMg_3$ in early studies. Unfortunately, we cannot determine the correct *ab initio* solution since we lack the hexagonal $AgMg_4$ prototypes in our library. *To address the degenerate structures, we further investigate* Ag_3Mg *and* $AgMg_3$ *with PAW-GGA potentials, as described in Section (III). For compound* Ag_3Mg*, with PAW,* $D0_{23}$ *is the most stable compound (in agreement with [73,74,76]),* $D0_{24}$ *and* $L1_2$ *are 1.1meV/atom and 11.3meV/atom higher than* $D0_{23}$*, respectively. In addition, for compound* $AgMg_3$*,* $D0_{19}$ *is the most stable structure and* $D0_a$ *is* $\sim$*6.8meV/atom higher than* $D0_{19}$*.*

Other *ab initio* studies, relevant for this system, can be found in references [78–80].

Ag-Mg system		
Low Temperature Phases comparison chart		
Composition % Mg	Experimental (Massalski [9])	*Ab initio* result
25.0	$L1_2$ $D0_{23}$ [73,74,76]	Ag_3Mg-$D0_{23}/D0_{24}$ (us-lda) $L1_2\sim$15meV/atom above. $D0_{23}$ *stable (paw-gga)* $D0_{24}$ $\sim$*1.1meV/at.* $L1_2$ $\sim$*11.3meV/at.* *above* $D0_{23}$ *(paw-gga)*
35.5 to 65.4	B2	AgMg-B2
75.8 to 78.2	cF* (unknown)	$AgMg_3$ $D0_{19}$ (hP8)/$D0_a$ (oP8) (us) $D0_{19}$ *stable (paw-gga)* $D0_a$ $\sim$*6.8meV/at.* *above* $D0_{19}$ *(paw-gga)*
80.0	hP* (unknown)	unavailable (see text)

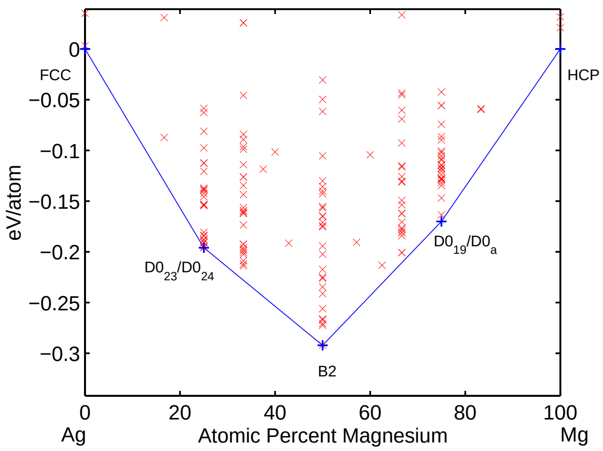

FIG. 3. AgMg (Silver - Magnesium) ground state convex hull.

Ag-Na (Silver - Sodium). The phase diagram of the system Ag-Na is known with reasonable accuracy and has only one intermetallic compound [9,10,83–85]. We confirm the stability of Ag_2Na-C15 and find almost all the other compounds to have positive formation energies energies. Both with US-LDA and PAW-GGA, Na-hcp is very slighly favored over Na-bcc and Na-fcc, in agreement with other first principle calculations [26–30]. At room temperature Sodium has the bcc structure, and undergoes a martensitic transformation below 35K, to a closed packed structure [31–38]. Therefore our results, Na-hcp stable and the very small energy differences with Na-bcc and Na-fcc, are consistent with the behaviour at low temperature.

Ag-Na system		
Low Temperature Phases comparison chart		
Composition % Na	Experimental (Massalski [9])	*Ab initio* result
33.0	C15	Ag_2Na-C15

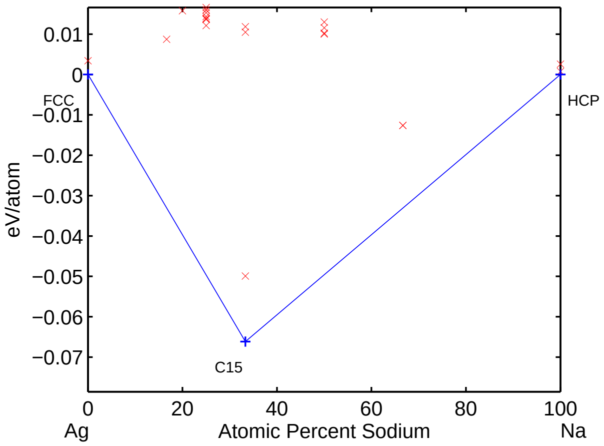

FIG. 4. AgNa (Silver - Sodium) ground state convex hull.

Ag-Pd (Silver - Palladium). The system Ag-Pd has not been studied in great detail and no intermetallic compounds have been reported [9,10,41,88]. The solid is reported to be disordered fcc. At low temperature we find three stable compounds: AgPd-$L1_1$, Ag_2Pd and Ag_3Pd. In our computations, for Ag_2Pd and Ag_3Pd, the ground states are degenerate: our best candidates are C49 or C37 for Ag_2Pd, and $L1_2$ or $D0_{22}$ for Ag_3Pd, as shown in figure (5). *To address the degenerate structures, we further investigate Ag_2Pd and Ag_3Pd with PAW-GGA potentials, as described in Section (III). With PAW, for composition Ag_2Pd, C37 is the most stable compound and C49 is higher by 4meV/atom. For composition Ag_3Pd, $L1_2$ and $D0_{22}$ remain degenerate. In fact, $D0_{22}$ has an energy 0.4meV/atom greater than $L1_2$, too small compared to the numerical accuracy of the ab initio calculation.*

Other *ab initio* studies, relevant for this system, can be found in references [89–93].

Ag-Pd system

Low Temperature Phases comparison chart

Composition % Ag	Experimental (Massalski [9])	*Ab initio* result
50	solid solution > 900°C	AgPd-$L1_1$
66.6	solid solution > 900°C	Ag_2Pd C37/C49 (us-lda) *C37 stable (paw-gga)* *C49∼4meV/at. above C37 (paw-gga)*
75.0	solid solution > 900°C	Ag_3Pd $L1_2/D0_{22}$ (us & paw-gga)

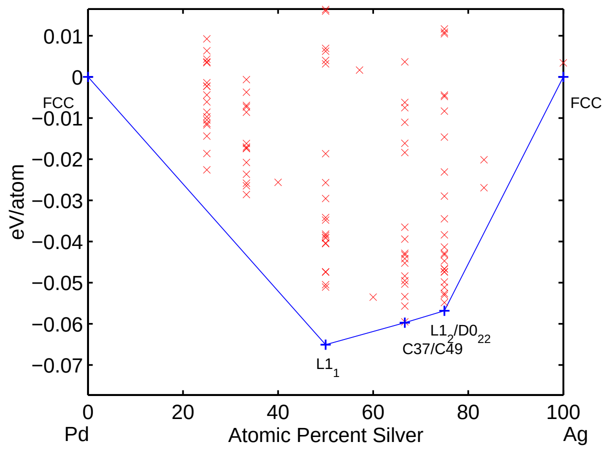

FIG. 5. AgPd (Silver - Palladium) ground state convex hull.

Ag-Ti (Silver - Titanium). The stability of $AgTi_2$-$C11_b$ and AgTi-B11 is confirmed [9,10,100,101], and no other stable phases are found computationally. Hence, we conclude that the low temperature part of the phase diagram of AgTi is probably accurate.

Ag-Ti system

Low Temperature Phases comparison chart

Composition % Ag	Experimental (Massalski [9])	*Ab initio* result
33.3	$C11_b$	$AgTi_2$-$C11_b$
50	B11	AgTi-B11 (γCuTi)

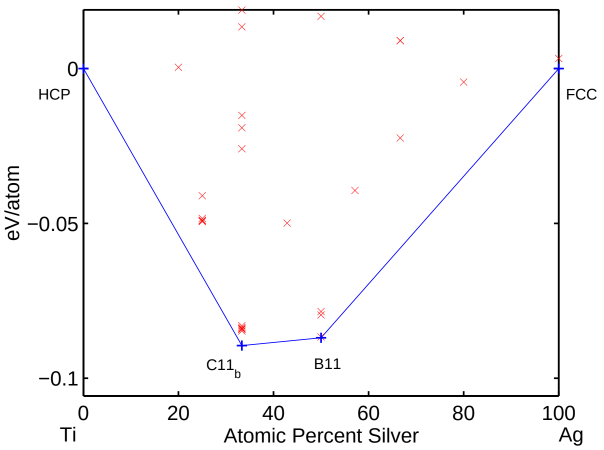

FIG. 6. AgTi (Silver - Titanium) ground state convex hull.

Ag-Y (Silver - Yttrium). The stability of AgY-B2 and Ag_2Y-$C11_b$ is confirmed [9,10,102]. In the Ag-rich region, we do not determine the stability of $Ag_{51}Y_{14}$, since we do not have the prototype in our library [103,104]. Instead, we find Ag_3Y with $D0_a$ structure stable with an energy ∼22meV/atom below the energy of a two-phase region Ag↔Ag_2Y. In the real system, the presence of $Ag_{51}Y_{14}$ probably makes structure $D0_a$ metastable. In the Y-rich region we find AgY_2-C37 degenerate with the two-phase region Y↔AgY (within ∼1.7meV/atom) as shown in figure (7).

Ag-Y system		
Low Temperature Phases comparison chart		
Composition % Ag	Experimental (Massalski [9])	*Ab initio* result
33.3	two-phase region above 200°C	AgY_2-C37/tie-line
50	B2	AgY-B2
66.6	$C11_b$	Ag_2Y-$C11_b$
75	two-phase region above 200°C	Ag_3Y-$D0_a$ (uncertain)
78.5	$Ag_{51}Gd_{14}$	unavailable

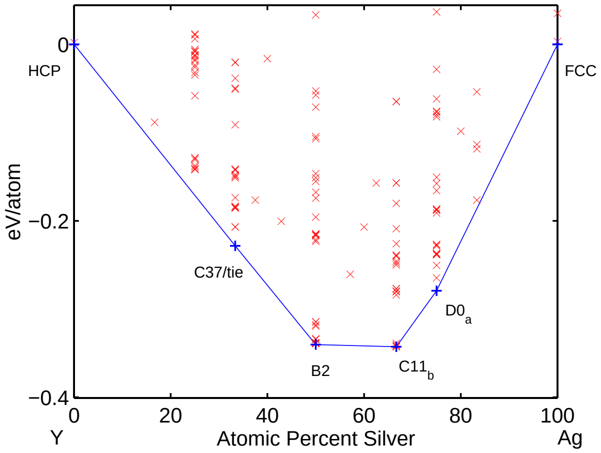

FIG. 7. AgY (Silver - Yttrium) ground state convex hull.

Ag-Zr (Silver - Zirconium). The phase diagram of Ag-Zr is known partially, and it has been estimated from thermodynamic properties [9,10,105,106]. The stability of the two known phases AgZr-B11 (γ-CuTi prototype) and $AgZr_2$-$C11_b$ is confirmed by our calculation. In addition to the known intermetallic compounds, we find a stable phase Ag_2Zr, which is not present in Massalski [9]: the C6 and C32 structures are degenerate. To conclude, we find $AgZr_3$-$FCC^{[001]}_{AB3}$ degenerate with the two-phase region Zr↔$AgZr_2$ (within ∼1.3meV/atom). *To address the degenerate structures, we further investigate Ag_2Zr with PAW-GGA potentials, as described in Section (III). With PAW, C32 is the most stable compound and C6 is 2meV/atom above C32.*

Ag-Zr system		
Low Temperature Phases comparison chart		
Composition % Ag	Experimental (Massalski [9])	*Ab initio* result
25.0	two-phase region estimated above 700°C	$AgZr_3$ $FCC^{[001]}_{AB3}$/tie-line
33.3	$C11_b$	$AgZr_2$-$C11_b$
50	B11	AgZr-B11 (γCuTi)
66.6	two-phase region estimated above 700°C	Ag_2Zr C6/C32 (us-lda) *C32 stable (paw-gga)* *C6∼2meV/at. above C32 (paw-gga)*

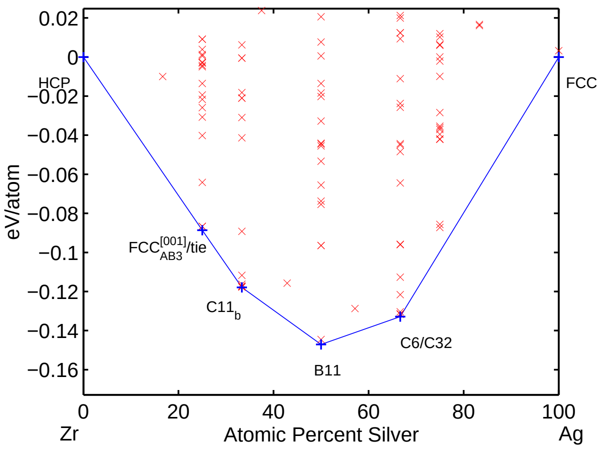

FIG. 8. AgZr (Silver - Zirconium) ground state convex hull.

Al-Sc (Aluminum - Scandium). The experimental phase diagram has compounds at compositions: Al_3Sc, Al_2Sc, AlSc, and $AlSc_2$ [9,10,107–109]. The *ab initio* technique confirms the stability of Al_3Sc-$L1_2$, Al_2Sc-C15, AlSc-B2, and $AlSc_2$-$B8_2$. In the Sc-rich region of the phase diagram, we find a new hexagonal stable phase $AlSc_3$-$D0_{19}$, which is not present in Massalski [9]. Only very limited experimental data is available for this side of the phase diagram.

Other *ab initio* studies, relevant for this system, can be found in references [110–115].

Al-Sc system		
Low Temperature Phases comparison chart		
Composition % Al	Experimental (Massalski [9])	*Ab initio* result
25.0	two-phase region above 0°C	$AlSc_3$-$D0_{19}$
33.3	$B8_2$	$AlSc_2$-$B8_2$
50	B2	AlSc-B2
66.6	C15	Al_2Sc-C15
75	$L1_2$	Al_3Sc-$L1_2$

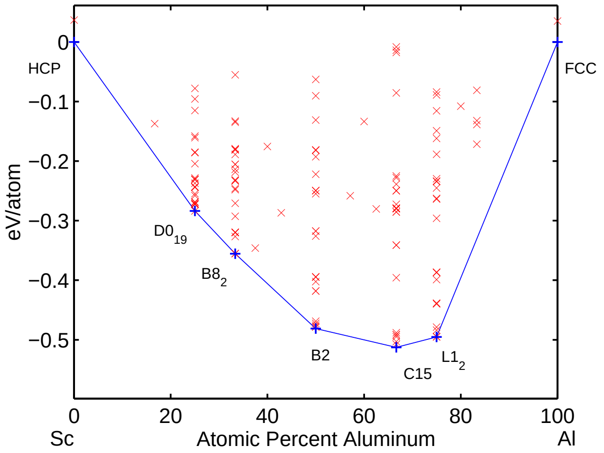

FIG. 9. AlSc (Aluminum - Scandium) ground state convex hull.

Au-Cd (Gold - Cadmium). Several compounds have been reported for the system Au-Cd, and the phase diagram is known with reasonable accuracy [9,10,41,117,119,123–126]. We confirm β'-AuCd-B19 and the high-temperature phase β-AuCd-B2 (with energy ∼6meV/atom higher than B19). At 25% Cd composition, we do not find the compound $\alpha_1 Au_3Cd$-Ag_3Mg because we do not have the proper prototype in our library. Instead, we find structures $D0_{24}$, $D0_{19}$, and Al_3Pu (Co_3V) with degenerate energies. Such structures have hexagonal lattices and they are candidates for the phase field α_2 which has been reported to be a long-period superstructure with hP lattice [9]. At 33% Cd composition, we find three phases Au_2Cd-C37, Au_2Cd-$MoPt_2$, and Au_2Cd-C49 with energies 4meV/atom, 14meV/atom and 16meV/atom above the tie-line $Au_3Cd \leftrightarrow AuCd$, respectively. At 50% Cd composition, the prototype of the phase β''-AuCd is not known, but it is reported to have a hexagonal structure. For β'', we suggest two candidates: AuCd-$L1_0$ and AuCd-$FCC^{[201]}_{A2B2}$ (CH "40" in reference [262]), which have energies higher by 5.4meV/atom and 5.5meV/atom with respect to B19. None of these structures has hexagonal lattice type, and all our hexagonal prototypes have much higher energies.

Au-Cd system		
Low Temperature Phases comparison chart		
Composition % Cd	Experimental (Massalski [9])	*Ab initio* result
∼25	α_1-Ag_3Mg	unavailable
∼25.5 to 35.5	α_2-hP? (unknown)	Au_3Cd $D0_{24}/D0_{19}/Al_3Pu$ hP candidates for α_2
33.3	two-phase region	$Au_3Cd \leftrightarrow AuCd$ Au_2Cd-C37, $MoPt_2$, C49 above tie-line
∼47.5 ∼50 43 to 57	β'-B19 β'' unknown β-B2 (high T)	AuCd-B19 $L1_0/FCC^{[201]}_{A2B2}$ ∼5meV/at. B2 ∼6meV/at. above B19
61.6 to 62.1	Au_3Cd_5-$D8_m$	unavailable
72 to 76	ϵ'-unknown tentative phase field	$AuCd_3$-$L6_0$
∼82	η'-unknown tentative phase field	nothing stable at 83.3%

At concentration ∼75% Cd, a stable phase ϵ', with unknown structure, is believed to exists [9]. We confirm the existence of a stable compound and our best prediction is $AuCd_3$-$L6_0$. At concentration ∼82% Cd another stable phase η' is believed to exist. We are not able to confirm η'. In fact at 83.3% Cd, the phase with lowest energy is ∼60meV/atom higher than the two tie-line $AuCd_3 \leftrightarrow Cd$. *To address the degenerate structures, we further investigate Au_3Cd with PAW-GGA potentials, as described in Section (III). Also with PAW, $D0_{24}$, Al_3Pu and $D0_{19}$ remain degenerate.*

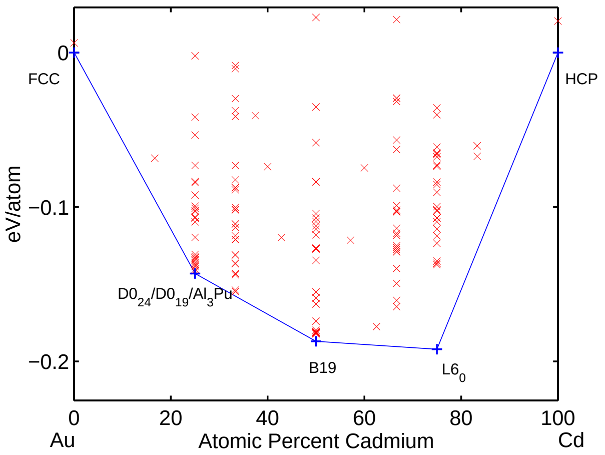

FIG. 10. AuCd (Gold - Cadmium) ground state convex hull.

Au-Nb (Gold - Niobium). The phase diagram of the system Au-Nb is based on three known compounds (Au_2Nb, Au_2Nb_3, $AuNb_3$) [9,10,47,117,119,127–141]. We do not confirm the stability of phase Au_2Nb-C32 [9,10,47]. Instead of C32, we find a stable compound Au_2Nb-C6 and C32 with energy higher by ∼12meV/atom with respect to C6. We can not conclude anything about stability of Au_2Nb_3 since our library does not contain any A_2B_3 prototype. The Nb-rich side of the experimental phase diagram is drawn with the assumption that $AuNb_3$-A15 is stable at low temperature (∼500°C) [9]. Our calculations suggest that $AuNb_3$-A15 might not be stable at low-temperature as it is ∼7meV/atom above the two phase field $AuNb_2 \leftrightarrow Nb$. In addition, we find a stable phase $AuNb_2$ at 66.6% Nb composition, with bcc parent lattice, and space group Fmmm #69. The compound, labeled as $BCC_{AB2}^{[011]}$, has AB2 stacking along [011] direction. If the prototype $BCC_{AB2}^{[011]}$ were not included in the calculation, the phase $AuNb_3$-A15 would be stable, as shown in figure (11). To conclude, we think it might be worthwhile to reconsider the thermodynamic modeling of the Nb-rich side of the phase diagram with the inclusion of $AuNb_2$-$BCC_{AB2}^{[011]}$, to obtain the proper temperature and concentration ranges of phase A15. *To address the disagreements with the experimental results, we further investigate Au_2Nb and $AuNb_3$ with PAW-GGA potentials, as described in Section (III). For the compound Au_2Nb C32 is the most stable compound and C6 is higher by 3.2meV/atom. For composition $AuNb_3$, A15 is still unstable, being ∼6.5meV/atom above the tie-line $AuNb_2 \leftrightarrow Nb$.* The disagreement at composition $AuNb_3$ is further discussed in Section (IV).

Au-Nb system		
Low Temperature Phases comparison chart		
Composition % Nb	Experimental (Massalski [9])	*Ab initio* result
33.3	C32	Au_2Nb-C6 (us-lda). C32 ∼12meV/at. above C6 (us-lda). *C32 stable (paw-gga) C6∼3.2meV/at. above C32 (paw-gga).*
60	Au_2Nb_3 (unknown) tI10 I4/mmm	unavailable
66.6	two-phase region (calculated)	$AuNb_2$-$BCC_{AB2}^{[011]}$
73 to 83	A15	two-phase region $AuNb_2 \leftrightarrow Nb$. $AuNb_3$-A15 is ∼7meV/at. above tie-line (us-lda). *A15 is ∼6.5meV/at. above tie-line (paw-gga).* See Section (IV).

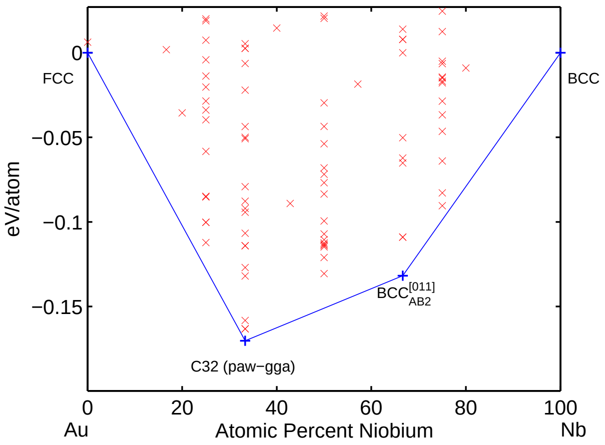

FIG. 11. AuPd (Gold - Niobium) ground state convex hull.

Au-Pd (Gold - Palladium). Two ordered compounds have been suggested for the system Au-Pd in the fcc solid solution (Au,Pd): Au_3Pd and $AuPd_3$ [142–145]. The low-temperature part of the phase diagram has been constructed with the addition of a phase field AuPd that is believed to exist below ∼100°C [9,10,117,119]. In the Au-rich part of the phase diagram, we confirm the stability of a compound Au_3Pd, but we find three structures, $D0_{23}$, $D0_{22}$ and $L1_2$, with degenerate energy. At composition Au_4Pd, we find the structure $D1_a$ to be degenerate with the tie-line Au↔Au_3Pd. At composition 33.3% Pd, we find a stable compound Au_2Pd, but again, two structures C49 and C37 are degenerate. At composition 50%, we confirm the existence of a stable phase AuPd. The prototype is not known. Our best guess is AuPd-$FCC^{[201]}_{A2B2}$ (CH "40" in reference [262]), and $L1_0$ with an energy higher by 8meV/atom with respect to $FCC^{[201]}_{A2B2}$. Finally, in the Pd-rich part of the phase diagram, we find a compound $AuPd_3$ to be degenerate with the tie-line of the two-phase region AuPd↔Pd. For this compound, three structures, $D0_{23}$, $D0_{22}$ and $L1_2$, have degenerate energies. The considerable degeneracy of the ground states is indicative of week effective interactions and consistent with the significant miscibility of the two elements inside each other. The near degeneracy of structures such as $D0_{23}$, $D0_{22}$ and $L1_2$, which are related to each other by periodic antiphase boundaries, indicates that more complicated Long Period Superstructures (LPS) might be present. *To address the small energy differences between structures, we further investigate* Au_3Pd*,* Au_2Pd*, AuPd, and* $AuPd_3$ *with PAW-GGA potentials, as described in Section (III). For the compound* Au_3Pd*,* $D0_{23}$ *is the most stable compound and* $D0_{22}$ *and* $L1_2$ *are higher by 9.4meV/atom and 12.7meV/atom, respectively. For the compound* $AuPd_3$*,* $D0_{23}$ *is the most stable compound and* $L1_2$ *and* $D0_{22}$ *are higher by 1.8meV/atom and 4.8meV/atom, respectively. Also with PAW, for the compound* Au_2Pd*, C37 and C49 remain degenerate. For the compound AuPd,* $FCC^{[201]}_{A2B2}$ *is the most stable compound and* $L1_0$ *is higher by 10.8meV/atom.*

Another *ab initio* study, relevant for this system, can be found in reference [60].

Au-Pd system		
Low Temperature Phases comparison chart		
Composition % Pd	Experimental (Massalski [9])	*Ab initio* result
12 to 32	Au_3Pd-$L1_2$ (guessed)	Au_3Pd $D0_{23}/D0_{22}/L1_2$ (us-lda) *$D0_{23}$ stable (paw-gga)* *$D0_{22}\sim 9.4$meV/at.* *$L1_2\sim 12.7$meV/at.* *above $D0_{23}$ (paw-gga)*
20		Au_4Pd-$D1_a$/tie-line (us-lda)
33.3	solid solution	Au_2Pd C49/C37 (us-lda/*paw-gga*)
50	AuPd (guessed) unknown prototype	AuPd-$FCC^{[201]}_{A2B2}$ (us-lda) $L1_0$ ∼8meV/at. above $FCC^{[201]}_{A2B2}$ (us-lda) *$FCC^{[201]}_{A2B2}$ stable (paw-gga)* *$L1_0$ ∼10.8meV/at.* *above $FCC^{[201]}_{A2B2}$ (paw-gga).*
68 to 90	$L1_2$ (guessed)	$AuPd_3$-$D0_{23}/D0_{22}/$ $/L1_2$/tie-line (us-lda) *$D0_{23}$ stable (paw-gga)* *$L1_2\sim 1.8$meV/at.* *$D0_{22}\sim 4.8$meV/at.* *above $D0_{23}$ (paw-gga)*

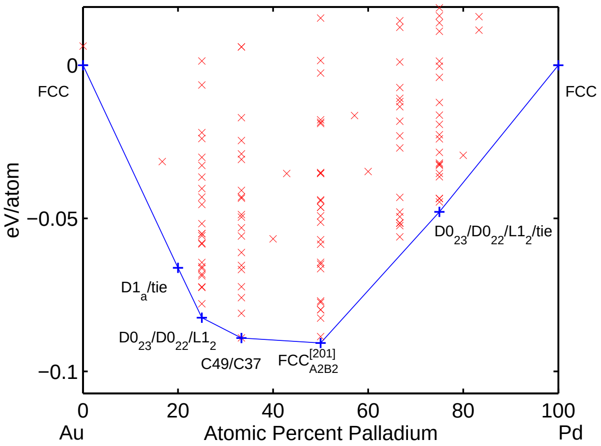

FIG. 12. AuPd (Gold - Palladium) ground state convex hull.

Au-Sc (Gold - Scandium). The phase diagram of the system Au-Sc is known only in the Au-rich region, and a total of three intermetallic compounds have been reported: Au_4Sc, Au_3Sc, and AuSc [9,10,119,153–158]. At 20% Sc, we confirm Au_4Sc-$D1_a$. At 25% Sc, we find a two-phase region, in agreement with experiments. In fact, Au_3Sc-$D0_a$, the structure with lowest energy, is higher by ∼7meV/atom with respect to the tie-line Au_4Sc-$D1_a$↔Au_2Sc-$C11_b$. At 33% and at 50% concentrations of Sc, we find two stable phases Au_2Sc and AuSc, but in both cases two structures are degenerate $C11_b$ and $MoPt_2$ for Au_2Sc, and B2 and B19 for AuSc. The experimental results indicate Au_2Sc-$C11_b$ and AuSc-B2. The $AuSc_2$-C37 (Co_2Si prototype) compound has been speculated to exist by similarity with other Au-(Rare Earth)$_2$ systems [153]. Our *ab initio* method confirms $AuSc_2$-C37. *To address the degenerate structures, we further investigate Au_2Sc and AuSc with PAW-GGA potentials, as described in Section (III). For compound Au_2Sc, with PAW, Au_2Sc-$C11_b$ is the most stable compound and Au_2Sc-$MoPt_2$ is higher by 1.0meV/atom. In addition, for compound AuSc, Au_2Sc-B2 is the most stable compound and Au_2Sc-B19 is higher by 2.2meV/atom. While these energy differences are very small, both calculations are in agreement with experiments.*

Au-Sc system		
Low Temperature Phases comparison chart		
Composition % Sc	Experimental (Massalski [9])	*Ab initio* result
20	$D1_a$	Au_4Sc-$D1_a$
25	two-phase region	two-phase region Au_3Sc-$D0_a$ ∼7meV/at. above Au_4Sc↔Au_2Sc.
33.3	$C11_b$	Au_2Sc-$C11_b/MoPt_2$ (us-lda) *$C11_b$ stable (paw-gga)* *$MoPt_2$ ∼1.0meV/at.* *above $C11_b$ (paw-gga).*
50	B2	AuSc-B2/B19 (us-lda) *B2 stable (paw-gga)* *B19 ∼2.2meV/at.* *above B2 (paw-gga).*
66.6	C37 (Co_2Si) (guessed)	$AuSc_2$-C37

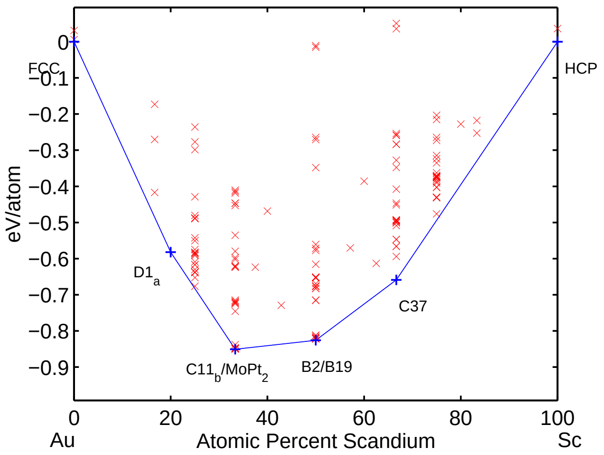

FIG. 13. AuSc (Gold - Scandium) ground state convex hull.

Au-Ti (Gold - Titanium). Five ordered compounds have been reported for the system Au-Ti at low temperature: Au$_4$Ti, Au$_2$Ti, αAuTi, βAuTi, and AuT$_3$ [9,10,48,101,160–169,311,283,321,298]. We confirm the stability of αAuTi-B11, Au$_4$Ti-D1$_a$ and AuTi$_3$-A15. At 25% Ti, we find a two-phase region, in agreement with experiments. In fact, Au$_3$Ti-D0$_a$, the structure with lowest energy, is higher by ∼11meV/atom with respect to the tie-line Au$_4$Ti↔Au$_2$Ti. For compound Au$_2$Ti, the experimental phase is C11$_b$. At such composition we find two structures with degenerate energies: Au$_2$Ti-C11$_b$ and Au$_2$Ti-MoPt$_2$. We do not confirm an off-stoichiometry stable phase βAuTi-B19, because we do not have such prototype in our library. The stoichiometric B19 has an energy ∼50meV/atom above αAuTi-B11. At 42.8% concentration of Ti, we find a previously unknown compound Au$_4$Ti$_3$-Cu$_4$Ti$_3$. This compound is degenerate with the tie-line of the two-phase field Au$_2$Ti↔AuTi, therefore its existence is uncertain. *To address the degenerate structures Au$_2$Ti-C11$_b$/MoPt$_2$ and the energy difference between αAuTi-B11 and βAuTi-B19 phases, we further investigate Au$_2$Ti and AuTi with PAW-GGA potentials, as described in Section (III). With PAW, Au$_2$Ti-C11$_b$ is the most stable compound and Au$_2$Ti-MoPt$_2$ is higher by 3.7meV/atom. For phase AuTi, AuTi-B11 is the most stable compound (as in the ultrasoft pseudopotential case), and AuTi-B19 is higher by 53.6meV/atom.*

Au-Ti system		
Low Temperature Phases comparison chart		
Composition % Ti	Experimental (Massalski [9])	*Ab initio* result
18-21	D1$_a$	Au$_4$Ti-D1$_a$
25	two-phase region above 500°C	two-phase region Au$_3$Ti-D0$_a$ ∼11meV/at. above Au$_4$Ti↔Au$_2$Ti.
33.3	C11$_b$	Au$_2$Ti C11$_b$/MoPt$_2$ (us-lda) *C11$_b$ stable (paw-gga)* *MoPt$_2$∼3.7meV/at.* *above C11$_b$ (paw-gga).*
42.8	two-phase region above 500°C	Au$_4$Ti$_3$ Cu$_4$Ti$_3$/tie
50 50-51	αAuTi-B11 βAuTi-B19	AuTi-B11 B19∼50meV/at. *B19∼53.6meV/at. (us-lda)* *above B11 (paw-gga).*
38-52	γAuTi-B2 high-temperature	B2∼135meV/at. above B11 (us-lda).
75	A15	AuTi$_3$-A15

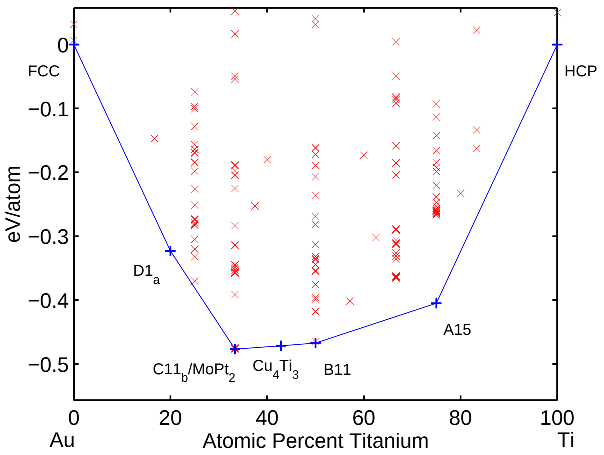

FIG. 14. AuTi (Gold - Titanium) ground state convex hull.

Au-Y (Gold - Yttrium). Four intermetallic compounds have been reported for the system Au-Y: Au_3Y, Au_2Y, AuY, and AuY_3 [9,10,119,155–158,170–173]. With our *ab initio* method, we confirm stability of Au_3Y-$D0_a$ and Au_2Y-$C11_b$. At equal composition, AuY, we do not confirm B2: we find a stable B33 and phase B2 higher by ∼26meV/atom. No experimental compound is reported for composition AuY_2, though we obtain AuY_2-C37. At 75% composition of Y, we do not find a stable AuY_3 compound reported experimentally [10,156]: the structure with lowest energy is AuY_3-$D0_{11}$ with an energy higher by ∼30meV/atom with respect to the tie-line. *We further investigate AuY with PAW-GGA potentials, as described in Section (III). With PAW, B33 is the most stable compound and B2 is ∼25meV/atom higher than B33.* The disagreement at composition AuY is further discussed in Section (IV).

<table>
<tr><th colspan="3">Au-Y system</th></tr>
<tr><th colspan="3">Low Temperature Phases comparison chart</th></tr>
<tr><th>Composition
% Y</th><th>Experimental
(Massalski [9])</th><th><i>Ab initio</i>
result</th></tr>
<tr><td>25</td><td>$D0_a$</td><td>Au_3Y-$D0_a$</td></tr>
<tr><td>33.3</td><td>$C11_b$</td><td>Au_2Y-$C11_b$</td></tr>
<tr><td>50</td><td>B2</td><td>AuY-B33 (us-lda)
B2∼26meV/at.
above B33 (us-lda).
<i>B33 stable (paw-gga)</i>
<i>B2∼25meV/at.</i>
<i>above B33 (paw-gga).</i>
See Section (IV).</td></tr>
<tr><td>66.6</td><td>not studied</td><td>AuY_2-C37</td></tr>
<tr><td>75</td><td>hyp
(uncertain prototype)</td><td>nothing stable
$D0_{11}$∼30meV/at.
above tie-line</td></tr>
</table>

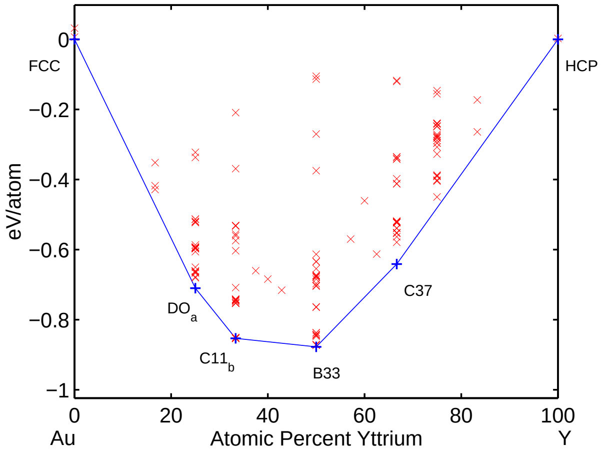

FIG. 15. AuY (Gold - Yttrium) ground state convex hull.

Au-Zr (Gold - Zirconium). Several ordered compounds have been reported for the system Au-Zr: Au_4Zr, Au_3Zr, Au_2Zr, $Au_{10}Zr_7$, Au_4Zr_5, $AuZr_2$, and $AuZr_3$ [9,10,163,174–177]. Our *ab initio* method confirms the stability of Au_3Zr-$D0_a$, Au_2Zr-$C11_b$ and $AuZr_3$-A15. At composition $AuZr_2$, Massalski and the Pauling file report $C11_b$ and $CuZr_2$ type compounds, respectively [9,10]. $C11_b$ ($MoSi_2$ prototype) and $CuZr_2$ are very similar structures, both tetragonal (tI6) and with the same space group #139. $C11_b$ belongs to the bcc superstructure family while $CuZr_2$, a slightly distorted version of $C11_b$, is a closed packed structure [10], therefore, within the formalism of the atomic environments, they represents two different prototypes [10]. Our library contains both prototypes. However, in our calculations, $AuZr_2$-$C11_b$ and $AuZr_2$-$CuZr_2$ are both unstable with degenerate energies higher by ~20meV/atom with respect to the tie-line AuZr↔$AuZr_3$. We can not say anything about Au_4Zr, $Au_{10}Zr_7$ and Au_4Zr_5, because our library lacks prototypes at the proper concentrations. At AuZr composition we find two structures with degenerate energies: B11 and $FCC_{A2B2}^{[001]}$. This prediction is unreliable because such compounds appear in the two-phase region $Au_{10}Zr_7$↔Au_4Zr_5, that we are not able to describe properly. At 42.8% concentration of Zr, we find Au_4Zr_3-Cu_4Ti_3. As before, this prediction is unreliable because it appears in the two-phase region Au_2Zr↔$Au_{10}Zr_7$, that we are not able to describe. To conclude, the inclusion of prototypes of $Au_{10}Zr_7$ and Au_4Zr_5 in our calculations, might change the stability of the predicted AuZr and Au_4Zr_3 phases. *To address the degenerate structures, we further investigate $AuZr_2$ with PAW-GGA potentials, as described in Section (III). With PAW, $AuZr_2$-$CuZr_2$ and $AuZr_2$-$C11_b$ are still degenerate, but become stable with an energy 6.6meV/atom lower than the tie-line AuZr↔$AuZr_3$.*

Au-Zr system		
Low Temperature Phases comparison chart		
Composition % Zr	Experimental (Massalski [9])	*Ab initio* result
20	Au_4Zr oP20 - Pnma	unavailable
25	$D0_a$	Au_3Zr-$D0_a$
33.3	$C11_b$	Au_2Zr-$C11_b$
42.8	two-phase region Au_2Zr↔$Au_{10}Zr_7$	Au_4Zr_3-Cu_4Ti_3 unreliable, see text.
45	$Au_{10}Zr_7$ tI34	unavailable
50	two-phase region $Au_{10}Zr_7$↔Au_4Zr_5	AuZr-B11/$FCC_{A2B2}^{[001]}$ unreliable, see text.
55.5	Au_4Zr_5 unknown prototype	unavailable
66.6	$C11_b$ [9] $CuZr_2$ [10]	two-phase region (us-lda) $AuZr_2$-$CuZr_2$/$C11_b$ ~20meV/at. above tie-line AuZr↔$AuZr_3$ (us-lda). *$CuZr_2$/$C11_b$ stable ~ 6.6meV/at. below AuZr↔$AuZr_3$ (paw-gga).*
75	A15	$AuZr_3$-A15

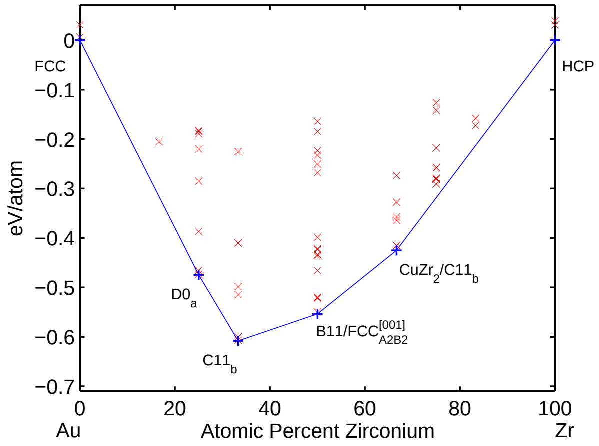

FIG. 16. AuZr (Gold - Zirconium) ground state convex hull.

Cd-Nb (Cadmium - Niobium). The phase diagram for the system Cd-Nb is not known [9]. It has been reported that Cd_3Nb has $L1_2$ prototype [178]. However, we are not able to find any stable compound, so we propose that the system is not compound-forming, but will display low-temperature immiscibility. In our calculations, Cd_3Nb-$L1_2$ is ~70meV/atom higher in energy than the phase separation of Cd↔Nb. In addition, the structure with the lowest formation energy is a bcc superstructure at composition CdNb and energy ~55meV/atom higher then Cd↔Nb. *To address the disagreement with the experimental result, we further investigate the relevant compounds with PAW-GGA potentials, as described in Section (III). With PAW, Cd_3Nb-$L1_2$ is >100meV/atom higher in energy than the tie-line Cd↔Nb. The structure with the lowest formation energy is a bcc superstructure at composition $CdNb_3$, and energy ~58meV/atom above Cd↔Nb.* It is unlikely that the *ab initio* calculations have such a large errors. The disagreement at composition Cd_3Nb is further discussed in Section (IV).

Cd-Nb system

Low Temperature Phases comparison chart

Composition % Nb	Experimental (Massalski [9])	*Ab initio* result
25	Cd_3Nb-$L1_2$	immiscible See Section (IV).

Cd-Pd (Cadmium - Palladium). Four Cd-Pd compounds have been identified experimentally at low-temperature (γ, γ_1, γ' and β_1 [179,180,9]). However, the phase boundaries are unknown. We confirm β_1-CdPd-$L1_0$. In the Cd-rich part of the phase diagram, we find Cd_3Pd (near γ' at 74%Cd). We are not able to determine the exact structure of Cd_3Pd but our best candidates are $D0_{19}$, $D0_{24}$, $NbPd_3$-type, and Al_3Pu-type (Co_3V). In the Pd-rich part of the phase diagram, we find a stable phase $CdPd_3$. As before, we cannot determine its structure, precisely. Our guesses are $D0_{22}$ and $NbPd_3$-type, which have degenerate energies. At concentration 33.3% Cd, we find a new compound $CdPd_2$-C37 which is not present in Massalski [9]. *To address the degenerate structures, we further investigate $CdPd_3$ and Cd_3Pd with PAW-GGA potentials, as described in Section (III). Compounds $CdPd_3$-$D0_{22}$ and $CdPd_3$-$NbPd_3$ remain degenerate with PAW (the energy difference is 1.1meV/atom). In addition, for Cd_3Pd composition, $NbPd_3/Al_3Pu$ remain degenerate compounds, and $D0_{22}$, $D0_{19}$, $D0_{24}$ are higher by 4.7meV/atom, 5.6meV/atom, 6.7meV/atom, respectively.*

Cd-Pd system

Low Temperature Phases comparison chart

Composition % Cd	Experimental (Massalski [9])	*Ab initio* result
25	Pd phase above 100°C	$CdPd_3$ $D0_{22}/NbPd_3$ (us-lda) $D0_{22}/NbPd_3$ (paw-gga)
33.3	two-phase region above 100°C, between β_1-Pd	$CdPd_2$-C37
37-55	β_1-$L1_0$	CdPd-$L1_0$
74	γ'-(unknown)	Cd_3Pd-$D0_{19}$ or $D0_{24}/NbPd_3/Al_3Pu$ (us-lda) *$NbPd_3/Al_3Pu$ stable (paw-gga)* *$D0_{22}$ ~ 4.7meV/at.,* *$D0_{19}$ ~ 5.6meV/at.,* *$D0_{24}$ ~ 6.7meV/at.* *above $NbPd_3/Al_3Pu$ (paw-gga)*
77-80	γ_1-(unknown)	unavailable
81-83	γ-$D8_3$	unavailable

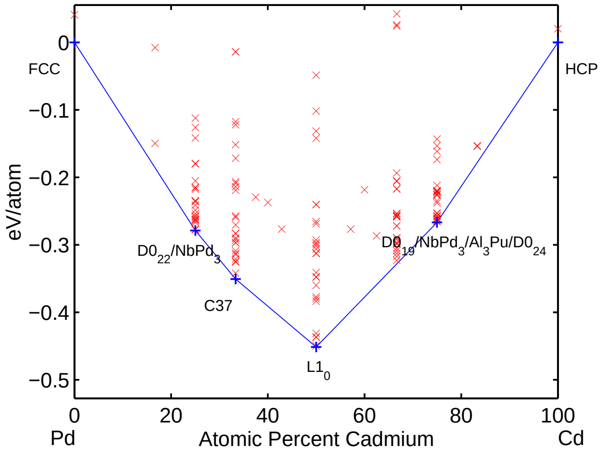

FIG. 17. CdPd (Cadmium - Palladium) ground state convex hull.

Cd-Pt (Cadmium - Platinum). The phase diagram of the system Cd-Pt is partially known [181,9], with several compounds of unknown structure. We confirm the stability of phase α_1'-CdPt-$L1_0$. In the Cd-rich part of the phase diagram, the prototypes of Cd_2Pt and γ_1 are unknown. For Cd_2Pt, our best guess are two degenerate structures, Cd_2Pt-C37 and Cd_2Pt-C16, which are also degenerate with the hull. For γ_1, at stoichiometry Cd_3Pt, we find two degenerate structures $D0_{11}$, $D0_a$ and $D0_{22}$. In the Pt-rich part of the phase diagram, we do not find a stable compound α'-$CdPt_3$-$L1_2$. Instead, we find a stable orthorhombic $CdPt_3$ with fcc superstructure and Cmmm #65 space group. The prototype, labeled as $CdPt_3^{proto}$, is described in Appendix (XI). In addition, $CdPt_3$-$L1_2$ is found with an energy ∼25meV/atom above $CdPt_3^{proto}$. *To address the degenerate structures and the disagreement with experimental results for compound $CdPt_3$, we further investigate $CdPt_3$, Cd_2Pt and Cd_3Pt with PAW-GGA potentials, as described in Section (III). With PAW, $CdPt_3$-$CdPt_3^{proto}$ is the most stable structure and $CdPt_3$-$L1_2$ higher by ∼10.4meV/atom. For compound Cd_2Pt, C16 is the most stable compound and C37 is ∼33meV/atom higher than C16. For compound Cd_3Pt, $D0_{11}$ is the most stable compound and $D0_a$ and $D0_{22}$ are higher by ∼52meV/atom and ∼60meV/atom, respectively.* The disagreement at composition $CdPt_3$ is further discussed in Section (IV).

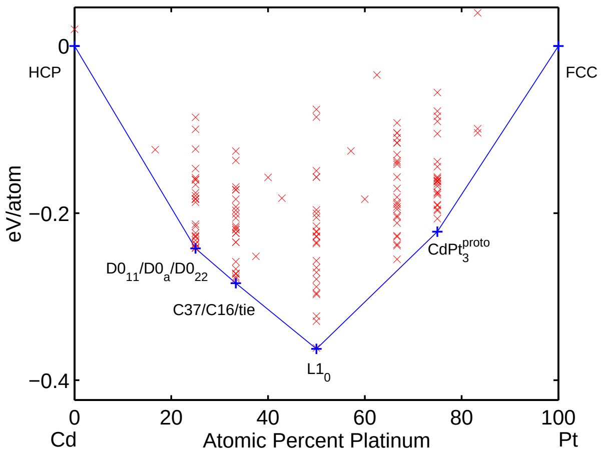

FIG. 18. CdPt (Cadmium - Platinum) ground state convex hull.

Cd-Pt system		
Low Temperature Phases comparison chart		
Composition % Pt	Experimental (Massalski [9])	*Ab initio* result
∼13 to 17	γ-(unknown)	two-phase region
24 to 26	γ_1-(unknown)	Cd_3Pt $D0_{11}/D0_a/D0_{22}$ (us-lda) *$D0_{11}$ stable (paw-gga)* *$D0_a$∼52meV/at.* *$D0_{22}$∼60meV/at.* *above $D0_{11}$ (paw-gga)*
∼26 to 28	γ_2-(unknown)	unavailable
∼31 to 38	Cd_2Pt-(unknown)	Cd_2Pt C37/C16/tie-line (us-lda) *C16 stable (paw-gga)* *C37∼33meV/at.* *above C16 (paw-gga)*
∼49 to 51	α_1'-$L1_0$	CdPt-$L1_0$
∼75	α'-$L1_2$	$CdPt_3^{proto}$ Appendix (XI) $L1_2$∼25meV/at. above $CdPt_3^{proto}$. *$CdPt_3^{proto}$ stable (paw-gga)* *$L1_2$∼10.4meV/at. above* *$CdPt_3^{proto}$ (paw-gga).* See Section (IV).

Cd-Rh (Cadmium - Rhodium). No experimental phase diagram is available [9]. With our *ab initio* technique we find two stable compounds, Cd_2Rh-C37, and Cd_3Rh. Our best guesses for Cd_3Rh are Cd_3Rh-$D0_{24}$ and Cd_3Rh-Al_3Pu-type (Co_3V), which have degenerate energies (2meV/atom difference). Interesting metastable phases are Cd_3Rh-$D0_{19}$, (11 meV/atom above Cd_3Rh), and Cd_2Rh-C49 (8meV/atom above Cd_2Rh-C37). *To address the degenerate structures, we further investigate Cd_3Rh with PAW-GGA potentials, as described in Section (III). With PAW, Cd_3Rh-Al_3Pu is the ground state, and Cd_3Rh-$D0_{24}$ has an energy 5meV/atom higher.*

Cd-Rh system		
Low Temperature Phases comparison chart		
Composition % Cd	Experimental (Massalski [9])	*Ab initio* result
66.6	not studied	Cd_2Rh-C37 C49 metastable
75	not studied	Cd_3Rh $D0_{24}/Al_3Pu$ (us-lda) $D0_{19}$ ~ 11meV/at. above $D0_{24}/Al_3Pu$ (us-lda) *Al_3Pu stable (paw-gga)* *$D0_{24}$ ~ 5meV/at. above Al_3Pu (paw-gga)*

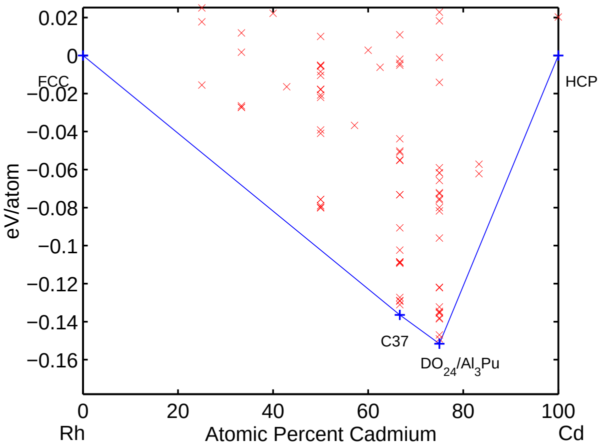

FIG. 19. CdRh (Cadmium - Rhodium) ground state convex hull.

Cd-Ti (Cadmium - Titanium). Little is known for the system Cd-Ti at high-temperature [9,10,183,184]. At low temperature only two stable intermetallic compounds have been reported [184]. We confirm the stability of Ti_2Cd-$C11_b$. At composition CdTi, Massalski and the Pauling file, report B11 and CdTi compounds, respectively [9,10]. B11 (γCuTi prototype) and CdTi are very similar structures, both tetragonal (tP4) and with the same space group #129. B11 belongs to the bcc superstructure family while CdTi, a slightly distorted version of B11, is a closed packed structure [10]. Therefore, within the formalism of the atomic environments, they represents two different prototypes [10]. The *ab initio* calculation is able to relax one structure into the other, easily. For CdTi we confirm the experimental results. In addition, at concentration 42.8%Cd, we find a compound Cd_3Ti_4-Cu_4Ti_3, degenerate with the tie-line of the two-phase region $CdTi_2 \leftrightarrow CdTi$. We have not found any other stable or metastable compound: we conclude that the low temperature part of the phase diagram is complete. Note that this system is very similar to Ag-Ti.

Cd-Ti system		
Low Temperature Phases comparison chart		
Composition % Cd	Experimental (Massalski [9])	*Ab initio* result
33.3	$C11_b$	$CdTi_2$-$C11_b$
42.8	two-phase region above 200°C	Cd_3Ti_4 Cu_4Ti_3/tie-line
50	B11 CdTi [10]	CdTi-B11 (CdTi)

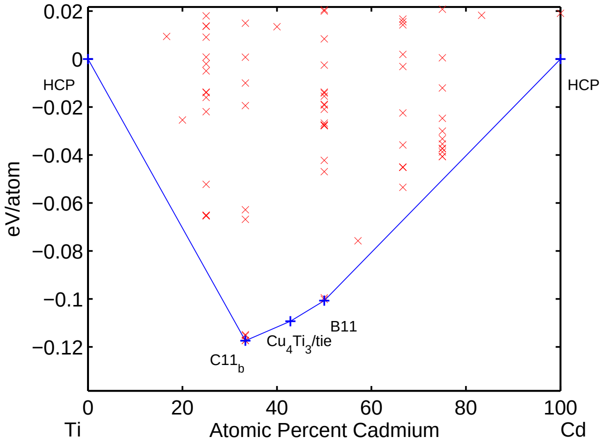

FIG. 20. CdTi (Cadmium - Titanium) ground state convex hull.

Cd-Y (Cadmium - Yttrium). The stability of compounds YCd-B2, YCd_2-C6 and YCd_3 (Cd_3Er prototype) [9,10,185–187] is confirmed. The Yttrium-rich side of the phase diagram is poorly known. In that region we find two degenerate phases Y_2Cd-C49 and Y_2Cd-C37, both of which are close to the energy of the two phase region Y↔CdY (figure (21)). We do not find any other stable or metastable phase. *To address the degenerate structures, we further investigate Y_2Cd with PAW-GGA potentials, as described in Section (III). With PAW, C37 is the most stable compound and C49 is higher by 7.7meV/atom.*

Another *ab initio* study, relevant for this system, can be found in reference [188].

Cd-Y system		
Low Temperature Phases comparison chart		
Composition % Cd	Experimental (Massalski [9])	*Ab initio* result
33.3	not studied/ two-phase region	CdY_2 C37/C49 (us-lda) *C37 stable (paw-gga)* *C49 ∼ 7.7meV/at. above C37 (paw-gga)*
50	B2	CdY-B2
66.6	C6	Cd_2Y-C6
75	Cd_3Er	Cd_3Y-Cd_3Er
80.4	$Cd_{45}Y_{11}$-$Cd_{45}Sm_{11}$	unavailable
81.7	$Cd_{58}Y_{13}$-$Pu_{13}Zn_{58}$	unavailable
85.7	Cd_6Y	unavailable

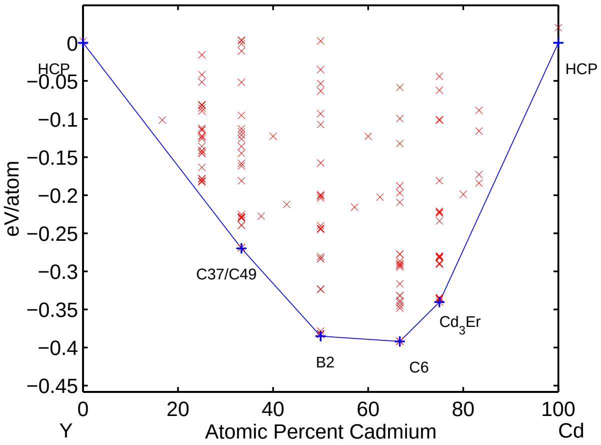

FIG. 21. CdY (Cadmium - Yttrium) ground state convex hull.

Cd-Zr (Cadmium - Zirconium). The Cd-Zr system is poorly characterized [49,9,189], and compounds have been identified at four compositions Cd_3Zr, Cd_2Zr, CdZr, and $CdZr_2$. Massalski [9] reports Cd_3Zr-$L1_0$-AuCu, which we consider a misprint for Cd_3Zr-$L1_2$-$AuCu_3$, while CRYSTMET and Pauling File databases [10,11] report Cd_3Zr-$D0_a$-βCu_3Ti from reference [190]. We confirm the stability of Cd_3Zr-$L1_2$ and $CdZr_2$-$C11_b$. At composition CdZr, Massalski and the Pauling file, report B11 and CdTi compounds, respectively [9,10]. B11 (γCuTi prototype) and CdTi are very similar structures, both tetragonal (tP4) and with the same space group #129. B11 belongs to the bcc superstructure family while CdTi, a slightly distorted version of B11, is a closed packed structure [10]. Therefore, within the formalism of the atomic environments, they represents two different prototypes [10]. The *ab initio* calculation is able to relax one structure into the other, easily. For CdZz, we find CdZr-$L1_0$ instead of CdZr-B11, which has an energy ∼18meV/atom higher than $L1_0$. The prototype of Cd_2Zr is not known: our best guess is Cd_2Zr-$C11_b$. In addition, we find a stable compound $CdZr_3$-A15 not present in Massalski [9], and a metastable $L1_2$ which is 8.5meV/atom higher than A15. *To address the disagreement with the experimental results for compound CdZr, we further investigate $L1_0$ and B11 with PAW-GGA potentials, as described in Section (III). With PAW, CdZr-B11 is the most stable compound and CdZr-$L1_0$ is higher by 13meV/atom.*

Cd-Zr system		
Low Temperature Phases comparison chart		
Composition % Cd	Experimental (Massalski [9])	*Ab initio* result
25	two-phase region not studied	$CdZr_3$-A15 $L1_2$ ∼ 8.5meV/at. above A15
33.3	$C11_b$	$CdZr_2$-$C11_b$
50	B11	CdZr-$L1_0$ (us-lda) B11 ∼ 18meV/at. above $L1_0$ (us-lda). *B11 stable (paw-gga)* *$L1_0$ ∼13meV/at. above $L1_0$ (paw-gga).*
66.6	cubic (unknown)	Cd_2Zr-$C11_b$
75	$L1_2$ [9] $D0_a$ [190,10,11]	Cd_3Zr-$L1_2$

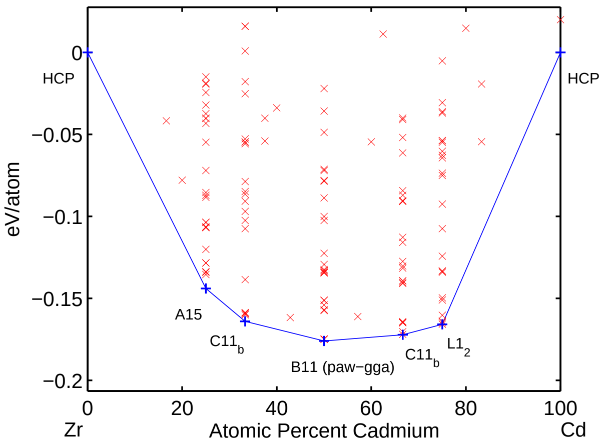

FIG. 22. CdZr (Cadmium - Zirconium) ground state convex hull.

Mo-Nb (Molybdenum - Niobium). The system MoNb has not been studied in great detail and no experimental intermetallic compounds have been found [9,10,47,197]. A bcc solid solution is reported from 2400°C up to the melt. We predict four stable compounds at low temperature: $MoNb_2$-$C11_b$, MoNb-B2, Mo_2Nb-$C11_b$, and Mo_3Nb-$D0_3$, as shown in figure (23).

Other *ab initio* studies, relevant for this system, can be found in references [90,198–200].

Mo-Nb system		
Low Temperature Phases comparison chart		
Composition % Mo	Experimental (Massalski [9])	*Ab initio* result
33.3	not studied	$MoNb_2$-$C11_b$
50	not studied	MoNb-B2
66.6	not studied	Mo_2Nb-$C11_b$
75	not studied	Mo_3Nb -$D0_3$

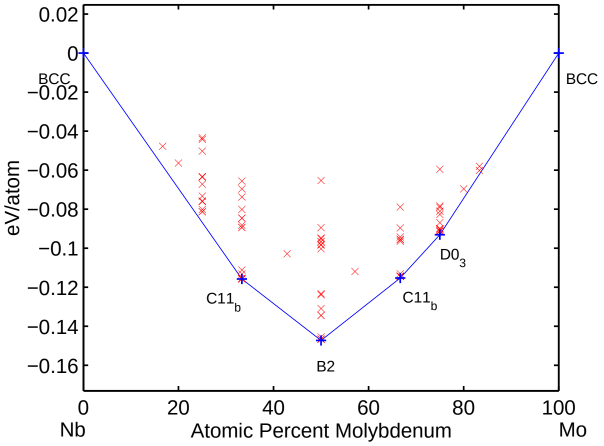

FIG. 23. MoNb (Molybdenum - Niobium) ground state convex hull.

Mo-Pd (Molybdenum - Palladium). The phase diagram of this alloy is known from experimental investigations and thermodynamic calculations [9,10,46,51,201]. The only compound is at composition MoPd$_2$ and is listed in Massalski as having approximatively the MoPt$_2$ structure [9,10,201]. Our *ab initio* method finds that the MoPt$_2$ structure is 8meV/atom higher than MoPd$_2$-ZrSi$_2$. In addition, we find a stable phase MoPd$_4$-D1$_a$ (MoNi$_4$ prototype), previously unknown.

Mo-Pd system		
Low Temperature Phases comparison chart		
Composition % Pd	Experimental (Massalski [9])	*Ab initio* result
66 to 67	~ MoPt$_2$	MoPd$_2$-ZrSi$_2$ MoPt$_2$ ~ 8meV/at. ZrSi$_2$
80	disorder fcc Pd-A1	MoPd$_4$-D1$_a$

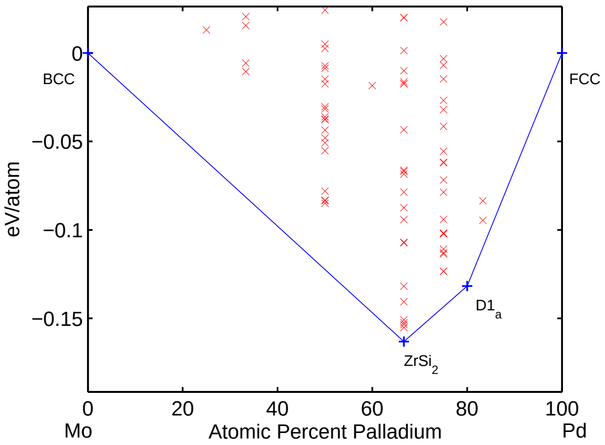

FIG. 24. MoPd (Molybdenum - Palladium) ground state convex hull.

Mo-Pt (Molybdenum - Platinum). The phase diagram of this alloy is known from experimental investigations and thermodynamic modeling [9,10,201–210,277]. We confirm the stability of MoPt-B19 and MoPt$_2$ (with MoPt$_2$ prototype). In the Pt-rich part of the phase diagram, we find a compound MoPt$_4$-D1$_a$ (MoNi$_a$ prototype), previously unknown. The observed high-temperature phase A15, reported as Mo$_6$Pt in Massalski [9] and as Mo$_{3.2}$Pt$_{0.8}$ in the Pauling File [10], is off-stoichiometry. Our *ab initio* method finds a stoichiometric Mo$_3$Pt-A15 to be ~45meV/atom above the two-phase region Mo↔MoPt-B19. For a detailed experimental study of such A15 phase, see reference [210].

Mo-Pt system		
Low Temperature Phases comparison chart		
Composition % Pt	Experimental (Massalski [9])	*Ab initio* result
18.5 20	Mo$_6$Pt-A15 [9] Mo$_{3.2}$Pt$_{0.8}$-A15 [10] above ~1200°C	Mo$_3$Pt-A15 ~45meV/at. above Mo↔MoPt-B19
31.5 to 45	ϵ'-D0$_{19}$ above 1000°C	unavailable at such composition
50	B19	MoPt-B19
66.6	MoPt$_2$	MoPt$_2$
80	two-phase region MoPt$_2$↔Pt	MoPt$_4$-D1$_a$

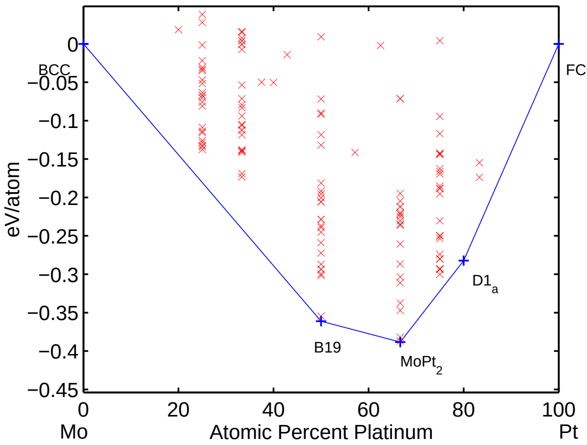

FIG. 25. MoPt (Molybdenum - Platinum) ground state convex hull.

Mo-Rh (Molybdenum - Rhodium). The phase diagram of the system Mo-Rh is known above ∼900°Cand it is based on thermodynamic calculations and experimental results [9,10,51,211–214]. We confirm the stability of the two known compounds MoRh-B19 [9] and $MoRh_3$-$CdMg_3$ [10,213]. At concentration 66.6% Rh, we find the stable phase $MoRh_2$-C37 (prototype Co_2Si), previously not identified [9].

Mo-Rh system		
Low Temperature Phases comparison chart		
Composition % Rh	Experimental (Massalski [9])	*Ab initio* result
∼50	B19	MoRh-B19
66.6	two-phase region above 900°C	Mo_2Rh-C37
∼75	$CdMg_3$ [10,213]	$MoRh_3$-$CdMg_3$

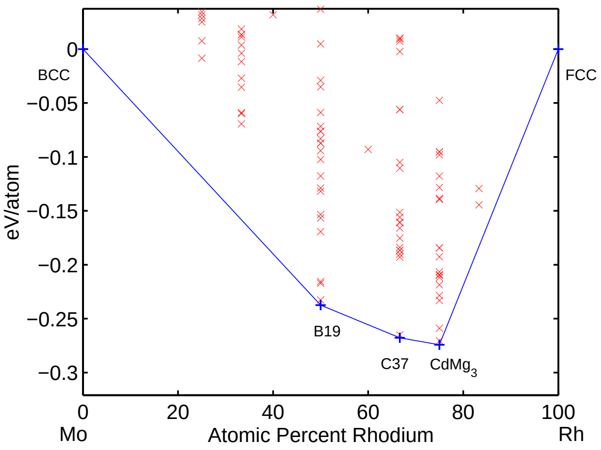

FIG. 26. MoRh (Molybdenum - Rhodium) ground state convex hull.

Mo-Ru (Molybdenum - Ruthenium). The phase diagram of this system is known at medium and high-temperature [9,10,215]. There is a σ phase around 38% Ru, which is quite common when bcc (Mo) and hcp (Ru) elements are mixed. We are not able to confirm the σ phase since we do not have the proper prototype in our library. At concentration 75% Ru, we find the stable phase $MoRu_3$-$D0_{19}$ (formation energy ∼ 60meV/atom), not present in Massalski [9], indicating that it might be a low-temperature ordered structure.

Another *ab initio* study, relevant for this system, can be found in reference [216].

Mo-Ru system		
Low Temperature Phases comparison chart		
Composition % Ru	Experimental (Massalski [9])	*Ab initio* result
75	disorder hcp Ru-A3 above 800°C	$MoRu_3$-$D0_{19}$

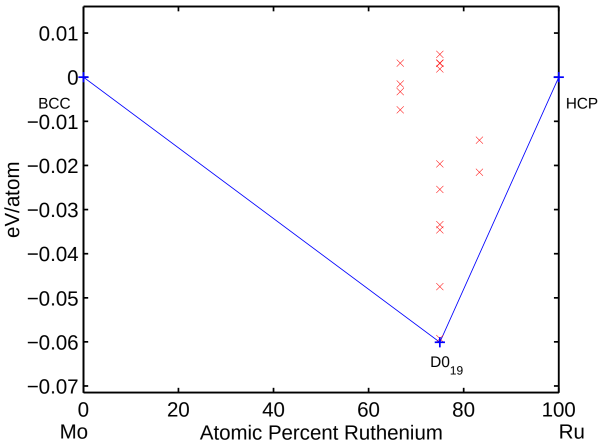

FIG. 27. MoRu (Molybdenum - Ruthenium) ground state convex hull.

Mo-Ti (Molybdenum - Titanium). To our knowledge, no intermetallic compounds have been reported for the system Mo-Ti [9,10,48,218–220], and it is considered a non-compound forming system [10,11]. In contrast to the experimental assessment, we find seven stable compounds. Four of these have bcc superstructures: orthorhombic $MoTi_3$, degenerate with the two-phase region Ti↔$MoTi_2$, with space group Immm #71 and prototype $MoTi_3^{proto}$ (Appendix (XI)); orthorhombic Mo_3Ti with space group Immm #71 and prototype Mo_3Ti^{proto} (Appendix (XI)); trigonal $MoTi_2$-$BCC_{AB2}^{[211]}$, and orthorhombic MoTi with space group Imma #74 and prototype $MoTi^{proto}$ (Appendix (XI)). In addition, we find a stable compound Mo_2Ti-$C11_b$, a compound Mo_4Ti-$D1_a$ degenerate with the tie-line, and finally a monoclinic Mo_5Ti which has space group C2/m #12 and prototype Mo_5Ti^{proto} (Appendix (XII)). Given the relatively large value of the formation energy, the experimental miscibility gap is surprising. This system warrants further study to sort out the apparent discrepancy between experiments and *ab initio* computation.

Another *ab initio* study, relevant for this system, can be found in reference [221].

Mo-Ti system		
Low Temperature Phases comparison chart		
Composition % Mo	Experimental (Massalski [9])	*Ab initio* result
25	two-phase region, (βTi,Mo)-A2↔ (αTi)-A3, above 400°C	$MoTi_3^{proto}$/tie-line Appendix (XI)
33.3	same as above	$MoTi_2$-$BCC_{AB2}^{[211]}$
50	same as above	$MoTi^{proto}$ Appendix (XI)
66.6	same as above	Mo_2Ti-$C11_b$
75	same as above	Mo_3Ti^{proto} Appendix (XI)
80	same as above	Mo_4Ti-$D1_a$/tie-line
83.3	same as above	Mo_5Ti^{proto} Appendix (XII)

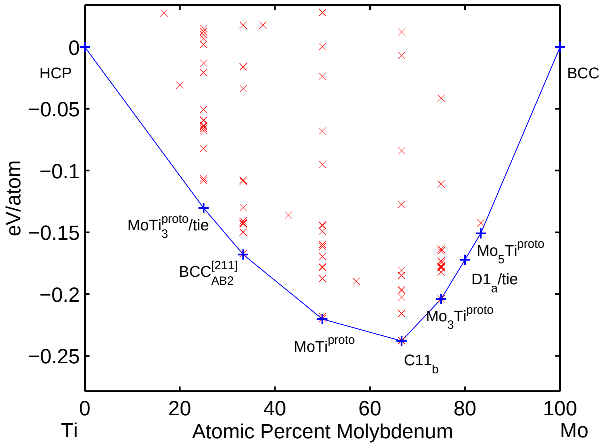

FIG. 28. MoTi (Molybdenum - Titanium) ground state convex hull.

Mo-Zr (Molybdenum - Zirconium). Not much is known of the system Mo-Zr to produce a reliable phase diagram [9,10,49]. We confirm the stability of the only known compound Mo_2Zr-C15. Experimentally, the Zr-rich side of the phase diagram has not been explored in detail at low temperature, and it is reported to have a two-phase region Mo_2Zr-C15↔(αZr)-A3 above 400°C. However, we find two possible new compounds: the orthorhombic phase $MoZr_3$ with space group Imma #74, prototype $MoZr_3^{proto}$ (Appendix (XII)), and the monoclinic compound $MoZr_5$-Mo_5Ti^{proto} with space group C2/m #12, and prototype Mo_5Ti^{proto} (Appendix (XII)). Both compounds $MoZr_3^{proto}$ and $MoZr_5$-Mo_5Ti^{proto} are quasi-degenerate with respect to the two-phase region Mo_2Zr↔(αZr). Hence, the existence of $MoZr_3^{proto}$ and $MoZr_5$-Mo_5Ti^{proto} is uncertain. It is useful mentioning that we find a metastable orthorhombic phase MoZr with space group Imma #74 and prototype similar to $MoTi^{proto}$ (Appendix (XI)) only ∼2meV/atom above the tie-line Mo_2Zr↔(αZr).

Another *ab initio* study, relevant for this system, can be found in reference [110].

Mo-Zr system		
Low Temperature Phases comparison chart		
Composition % Mo	Experimental (Massalski [9])	*Ab initio* result
16.6	two-phase region above 400°C	$MoZr_5$-Mo_5Ti^{proto}/tie-line Appendix (XII)
25	same as above	$MoZr_3^{proto}$/tie-line Appendix (XII)
50	same as above	∼$MoTi^{proto}$ ∼2meV/at. above Mo_2Zr↔(αZr)
60-67	C15	Mo_2Zr-C15

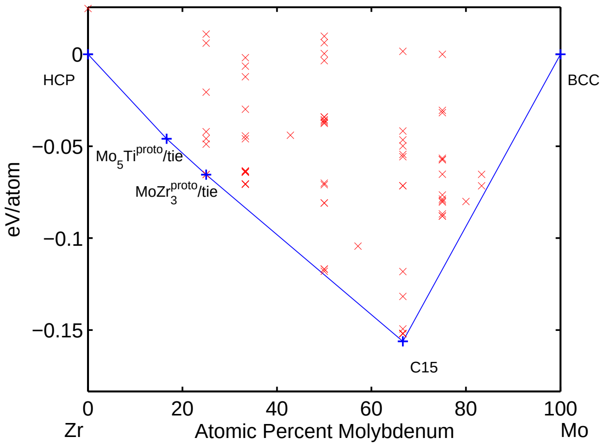

FIG. 29. MoZr (Molybdenum - Zirconium) ground state convex hull.

Nb-Pd (Niobium - Palladium). The Pd-Nb phase diagram is known with reasonable accuracy in the Pd-rich region [9,10,47,259]. The stability of the experimental phase $NbPd_2$-$MoPt_2$ and $\alpha NbPd_3$-$D0_{22}$ is confirmed. In the Nb-rich region, at concentration 33% Nb, we find an orthorhombic compound Nb_2Pd-$BCC^{[011]}_{AB2}$, not present in Massalski [9]. The energy of this phase is ∼11meV/atom below the tie-line of the two-phase region Nb↔$NbPd_2$.

Another *ab initio* study, relevant for this system, can be found in reference [224].

Nb-Pd system		
Low Temperature Phases comparison chart		
Composition % Pd	Experimental (Massalski [9])	*Ab initio* result
33.3	two-phase region above 700°C	Nb_2Pd-$BCC^{[011]}_{AB2}$ ∼11meV/at. below Nb↔$NbPd_2$
66.6	$MoPt_2$	$NbPd_2$-$MoPt_2$
75	α-$D0_{22}$	$NbPd_3$-$D0_{22}$

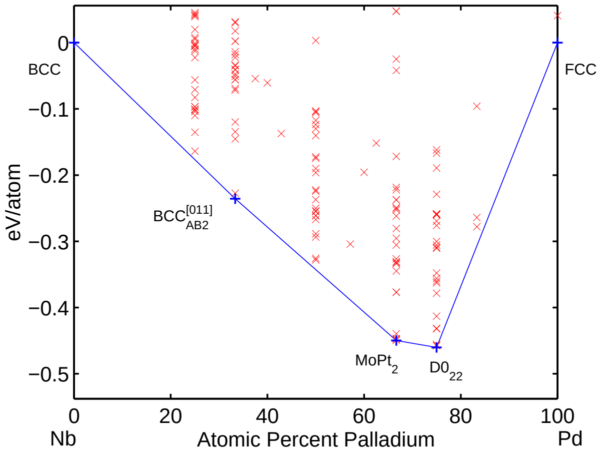

FIG. 30. NbPd (Niobium - Palladium) ground state convex hull.

Nb-Pt (Niobium - Platinum). Several intermetallic compounds have been reported for the system Nb-Pt [9,10,47,225–229]. We confirm the experimental phases Nb_3Pt-A15 and $\alpha NbPt_3$-$D0_a$ (βCu_3Ti prototype). The prototype of $NbPt_2$ is not reported in Massalski [9] (orthorhombic oI6, with space group Immm). We find $NbPt_2$-$MoPt_2$, in agreement with references [10,227,228]. At 50% concentration we do not confirm the stability of NbPt-B19. Instead of B19 we find NbPt-$L1_0$, and B19 to be higher by ∼11meV/atom above $L1_0$. It is possible that $L1_0$ is a ground state and B19 a high-temperature state. We can not say anything about the σ-phase $D8_b$ since we do not have such prototype in our library. *We further investigated NbPt-$L1_0$ and NbPt-B19 with PAW-GGA potentials, as described in Section (III). With PAW, $L1_0$ is the most stable compound and B19 is ∼18.5meV/atom higher than $L1_0$.*

Nb-Pt system		
Low Temperature Phases comparison chart		
Composition % Pt	Experimental (Massalski [9])	*Ab initio* result
19 to 28	A15	Nb_3Pt-A15
31 to 38	$D8_b$	unavailable σ-phase
∼50	$Nb_{1-x}Pt_{1+x}$-B19	NbPt-$L1_0$ B19 ∼ 11meV/at. above $L1_0$ (us-lda) *$L1_0$ stable (paw-gga)* *B19 ∼ 18.5meV/at.* *above $L1_0$ (paw-gga)*
∼67	$MoPt_2$ [10,227,228]	$NbPt_2$-$MoPt_2$
∼76	$D0_a$	$NbPt_3$-$D0_a$

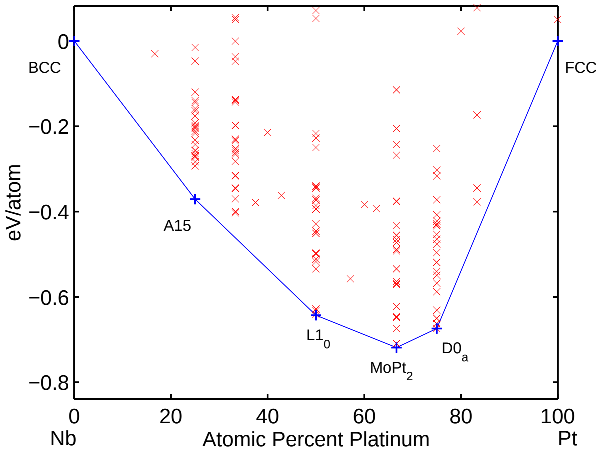

FIG. 31. NbPt (Niobium - Platinum) ground state convex hull.

Nb-Rh (Niobium - Rhodium). The system Nb-Rh is poorly characterized in the range of concentration 50∼80% Rh [9,10,47,226,230,231,51]. We confirm the stability of Nb_3Rh-A15, NbRh-$L1_0$. NbRh-B19, which is observed as a high-temperature state, is ∼27meV/atom above $L1_0$, and it is possibly stabilized by entropic effects. Note: in Massalski and in the Pauling File [9,10] there is no phase at 50% composition, and $Nb_{0.96}Rh_{1.04}$-$L1_0$ appears off-stoichiometry. At concentration 75% Rh, we find the stable phase η-Al_3Pu (Co_3V) and $\kappa NbRh_3$-$L1_2$ to be higher by 8meV/atom. Hence, we think that η prevails at low-temperature over κ, in contrast with the sketched phase diagram of reference [9]. We can not say anything about $D8_b$ and $\xi(Nb_2Rh_3)$ since we do not have the σ-phase $D8_b$ and any A_2B_3 prototypes in our library. *To address the structures with similar energy, we further investigate* $NbRh_3$ *with PAW-GGA potentials, as described in Section (III). With PAW,* $NbRh_3$-Al_3Pu *is the most stable compound and* $NbRh_3$-$L1_2$ *is higher by 5.3meV/atom.* The disagreement at composition $NbRh_3$ is further discussed in Section (IV).

Another *ab initio* study, relevant for this system, can be found in reference [232].

Nb-Rh system		
Low Temperature Phases comparison chart		
Composition % Rh	Experimental (Massalski [9])	*Ab initio* result
25	$\alpha'(Nb_3Rh)$-A15	Nb_3Rh-A15
28.5 to 39.5	$\sigma(Nb_{13}Rh_7)$-$D8_b$	unavailable
∼51.5 to 52	$Nb_{0.96}Rh_{1.04}$-$L1_0$ ($\lesssim 1337°C$)	NbRh-$L1_0$
∼56 to 62	$\epsilon(Nb_2Rh_3)$-B19 (high-temperature $\gtrsim 1330°C$)	NbRh-B19 ∼27meV/at. above $L1_0$ (us-lda)
59 to ∼64	$\xi(Nb_2Rh_3)$-Nb_2Rh_3	unavailable
∼67 to 70	$\eta(Nb_{13}Rh_{27})$-Al_3Pu ($\equiv Co_3V$ in [9])	see below for Al_3Pu
∼71 to 79	$\kappa(NbRh_3)$-$L1_2$	$NbRh_3$-Al_3Pu (us-lda) $L1_2$∼8meV/at. above Al_3Pu (us-lda) *Al_3Pu stable (paw-gga)* *$L1_2$∼5.3meV/at.* *above Al_3Pu (paw-gga)* See Section (IV).

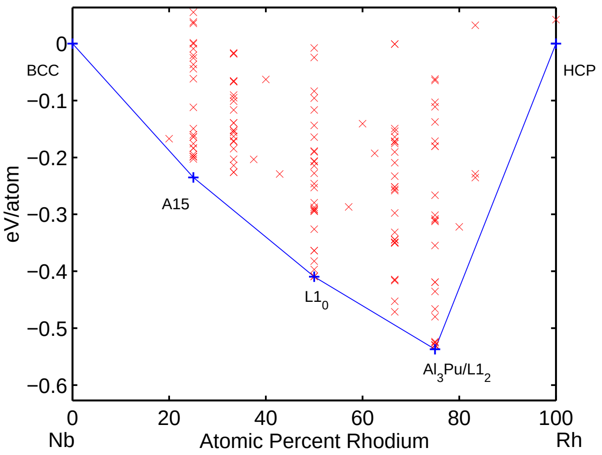

FIG. 32. NbRh (Niobium - Rhodium) ground state convex hull.

Nb-Ru (Niobium - Ruthenium). Very little is known for the alloy Nb-Ru, especially at low-temperature [9,10,47,233–237]. We do not confirm the stability of any low-temperature compound at composition NbRu, but instead find a two-phase field between Nb_3Ru and $NbRu_2$, even though a high and low-temperature phase of NbRu has been observed [233,237]. In the Ru-rich side of the phase diagram, we find $NbRu_3$-$D0_{24}$ to be 8meV/atom lower than $L1_2$ which is suggested experimentally. At 66% Ru we find $NbRu_2$-C37 (with oP12-Co_2Si prototype). With respect to the two-phase field Nb_3Ru↔$NbRu_2$, the structures closest to the tie-line at NbRu composition are B19 (∼13meV/atom), $L1_0$ (∼20meV/atom), B27 (∼23meV/atom), B33 (∼39meV/atom), and B2 (∼45meV/atom). Experiments have not found any other stable compound. However, in the Nb-rich side of the phase diagram, we find Nb_3Ru-$D0_3$ and a monoclinic Nb_5Ru with C2/m #12 space group and prototype Mo_5Ti^{proto}. The structure Nb_5Ru-Mo_5Ti^{proto} is described in Appendix (XII). *To address the disagreements at compositions NbRu and* $NbRu_3$ *we further investigate the relevant compounds with PAW-GGA potentials, as described in Section (III). For composition NbRu, the PAW-GGA result is substantially different from the US-LDA result. GGA gives* $L1_0$ *only 4meV/atom above the tie-line (versus 20meV/atom in LDA), whereas B19 was difficult to converge numerically, and seems to be >100meV/atom above the tie-line. For composition* $NbRu_3$*, also with PAW,* $D0_{24}$ *is the most stable compound and* $L1_2$ *is higher by 2.5meV/atom. Because this number is so small, extremely large* **k***-points sets and high energy cutoff were used to converge it.* The disagreements at compositions NbRu and $NbRu_3$ are further discussed in Section (IV).

Other *ab initio* studies, relevant for this system, can be found in references [238–240].

Nb-Ru system

Low Temperature Phases comparison chart

Composition % Ru	Experimental (Massalski [9])	*Ab initio* result
16.6	disorder Nb-A2	Nb_5Ru-Mo_5Ti^{proto} Appendix (XII)
25	disorder Nb-A2	Nb_3Ru-$D0_3$
∼50	NbRu′-$L1_0$ (room-temperature)	two-phase region Nb_3Ru↔$NbRu_2$. *$L1_0$ ∼4meV/at. (paw-gga)* *B19 >100meV/at.* *above tie-line (paw-gga).*
∼50	NbRu-B2 (high-temperature)	B19∼13meV/at. (us-lda) $L1_0$∼20meV/at. B2 ∼45meV/at. above the tie-line See Section (IV).
66.6	two-phase region above ∼700°C	$NbRu_2$-C37
75	$L1_2$	$NbRu_3$-$D0_{24}$ (us-lda) $L1_2$∼8meV/at. above $D0_{24}$ (us-lda) *$D0_{24}$ stable (paw-gga)* *$L1_2$∼2.5meV/at.* *above $D0_{24}$ (paw-gga)* See Section (IV).

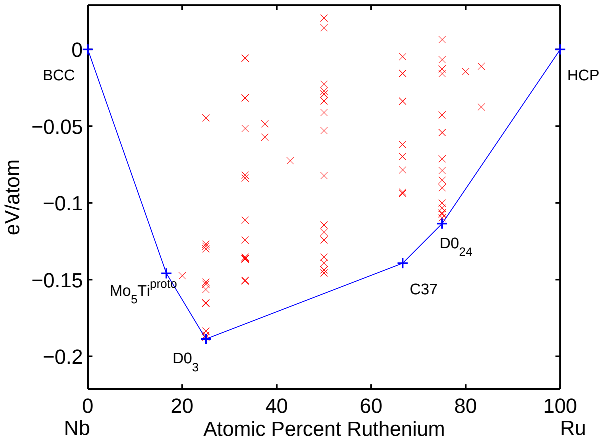

FIG. 33. NbRu (Niobium - Ruthenium) ground state convex hull.

Nb-Tc (Niobium - Technetium). The phase diagram of the system Nb-Tc is not known and only one intermetallic compound, $NbTc_3$ (metallic and superconductor) has been reported with αMn structure [9,10,47,241–243,365]. The compound $NbTc_3$ is classified as phase $Nb_{0.15}Tc_{0.85}$ in the Pauling File [10]. We do not have αMn in our library of prototypes, and, at such stoichiometry, we do not find any stable compound. In the Tc-rich side of the phase diagram, we find a two-phase field NbTc↔Tc, as shown in figure (34). At 50% concentration, we obtain NbTc-B2, and in the Nb-rich side of the diagram, we find Nb_2Tc-$C11_b$ and an orthorhombic phase Nb_3Tc with space group Immm #71, bcc superstructure, and prototype Nb_3Tc^{proto} described in Appendix (XI). Trends of Tc alloys are further discussed in Section (VIII).

Nb-Tc system

Low Temperature Phases comparison chart

Composition % Tc	Experimental (Massalski [9])	*Ab initio* result
25	not studied, unknown	Nb_3Tc^{proto} Appendix (XI)
33.3	same as above	Nb_2Tc-$C11_b$
50	same as above	NbTc-B2
75	$NbTc_3$-αMn [9]	nothing stable
85	$Nb_{0.15}Tc_{0.85}$-αMn [10]	

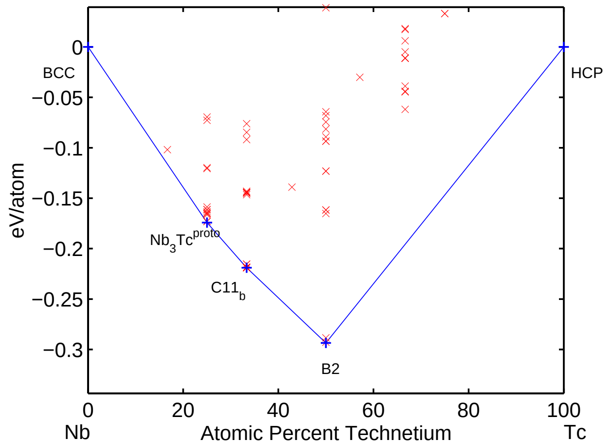

FIG. 34. NbTc (Niobium - Technetium) ground state convex hull.

Pd-Pt (Palladium - Platinum). The low temperature part of the phase diagram is believed to have a miscibility gap at a temperature of about 770°C. This miscibility gap is predicted on the basis of the difference of melting points between Pd an Pt [9,10,43,260,261]. Instead of such gap, we find three unknown stable compounds with fcc superstructures (Pd and Pt are both fcc). We find PdPt-$L1_1$, and two orthorhombic phases, Pd_3Pt and $PdPt_3$, with space group Cmmm #65 and prototypes described in Appendix (XI). The prototypes are labeled as Pd_3Pt^{proto} and $PdPt_3^{proto}$. The compound Pd_3Pt is degenerate with respect the two-phase fields Pd-A1↔PdPt-$L1_1$, therefore its existence is uncertain. As shown in figure (35), all the stable phases have small formation energy (< 50meV/atom) making them difficult to determine experimentally. However, we believe the experimental phase diagram to be in error. *We further investigate PdPt with PAW-GGA potentials, as described in Section (III). With PAW, PdPt-$L1_1$ is the most stable compound and PdPt-$L1_0$ is higher by 5.5meV/atom.* Our results are in disagreement with previous FLAPW-LDA calculations, where $L1_0$ is found to be the most stable compound [262].

Other *ab initio* studies, relevant for this system, can be found in references [13,62].

Pd-Pt system

Low Temperature Phases comparison chart

Composition % Pt	Experimental (Massalski [9])	*Ab initio* result
25	predicted two-phase region Pd-A1↔Pt-A1	Pd_3Pt^{proto}/tie-line (uncertain) Appendix (XI)
50	same as above	PdPt-$L1_1$ $L1_0$~11meV/at. higher than $L1_1$ (us-lda) *$L1_1$ stable* *$L1_0$~5.5meV/at. higher than $L1_1$ (paw-gga)*
75	same as above	$PdPt_3^{proto}$ Appendix (XI)

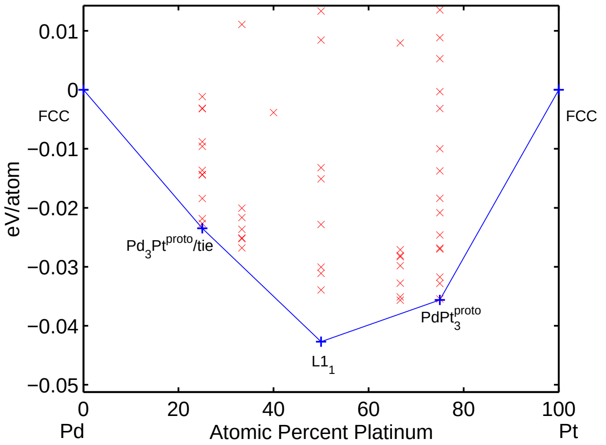

FIG. 35. PdPt (Palladium - Platinum) ground state convex hull.

Pd-Tc (Palladium - Technetium). The phase diagram for the system Pd-Tc is sketched based on the solid solubility data [9,10,43,365,368,275,346]. Experimental results report two solid solutions (fcc Pd-rich) and (hcp Tc-rich) with a two-phase region in between. No intermetallic compounds have been reported [9,10]. However, we find one stable phases $PdTc_3$-$D0_{19}$. In addition, at 50% concentration, we find a hcp superstructure (trigonal lattice, hP4, space group $P\bar{3}m1$) which has an energy ~3meV/atom higher than the tie-line of the two-phase region $PdTc_3$↔Pd. Trends of Tc alloys are further discussed in Section (VIII).

Pd-Tc system		
Low Temperature Phases comparison chart		
Composition % Pd	Experimental (Massalski [9])	*Ab initio* result
25	two-phase region above ~1000°C Pd-A1↔Tc-A3	$PdTc_3$-$D0_{19}$
50	two-phase region above ~1000°C Pd-A1↔Tc-A3	two-phase region $PdTc_3$↔Pd hcp superstr. ~3meV/at. above tie-line

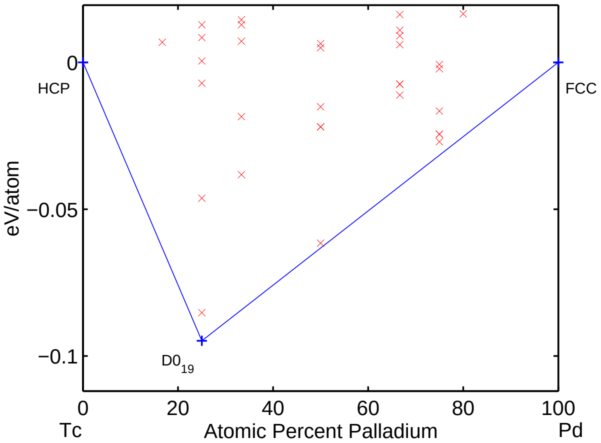

FIG. 36. PdTc (Palladium - Technetium) ground state convex hull.

Pd-Ti (Palladium - Titanium). This system has been subject of conflicting results for several years [9,10,169,276–291]. Our *ab initio* method confirms the stability of the compounds $PdTi_2$-$C11_b$, $PdTi_3$-A15, and Pd_3Ti-$D0_{24}$. Near 80% Pd, Long Period Superstructures (LPS) modulations of $L1_2$ are observed [279]. While we do not have such off-stoichiometric LPS, we find $L1_2$ to be only 6meV/atom above $D0_{24}$ at Pd_3Ti composition. The low energy difference between $L1_2$ and $D0_{24}$ indicates that it may be easy to form antiphase boundaries and LPS near this composition. We find Pd_2Ti-$MoPt_2$ which is an orthorhombic distortion of $C11_b$ ($MoPt_2$ is orthorhombic, while $C11_b$ is tetragonal). We find Pd_2Ti-C49 and Pd_2Ti-$C11_b$ to be higher by 3meV/atom and 14meV/atom above $MoPt_2$, respectively. At low temperature, at concentration 50%, we find a stable compound αTiPd, but two prototypes are degenerate: $L1_0$ and B19 (which is reported experimentally). We can not find the reported phase $PdTi_4$-A15 (off-stoichiometry) [9], which we think should appear inside the two-phase region of Ti ~ $PdTi_3$, or at composition $PdTi_3$. While off-stoichiometric compounds are obviously possible, this usually goes together with significant width of the single-phase field. Hence, we concluded (maybe erroneously) that the placement of A15 at composition $PdTi_4$ in reference [9] is likely a typographical error. *To address the degenerate structures, we further investigate αTiPd with PAW-GGA potentials, as described in Section (III). With PAW, PdTi-B19 is the most stable compound and PdTi-$L1_0$ is higher by 10meV/atom.*

Another *ab initio* study, relevant for this system, can be found in reference [292].

Pd-Ti system		
Low Temperature Phases comparison chart		
Composition % Pd	Experimental (Massalski [9])	*Ab initio* result
20 and 25	A15 at 20%	$PdTi_3$-A15 at 25%
33.3	$C11_b$	$PdTi_2$-$C11_b$
47 to 53	α(TiPd)-B19	PdTi-B19/$L1_0$ (us-lda) *B19 stable (paw-gga)* *$L1_0$~10meV/at. above B19 (paw-gga)*
60	Pd_3Ti_2 ~ Au_2V	unavailable
62.5	Pd_5Ti_3 ~ $C11_b$	unavailable
66.6	orthorhombic distortion of $C11_b$	Pd_2Ti-$MoPt_2$ (distortion of $C11_b$) C49~3meV/at. $C11_b$~14meV/at. above $MoPt_2$
75	$D0_{24}$	Pd_3Ti-$D0_{24}$ $L1_2$~6meV/at. above $D0_{24}$
80	$L1_2$	$L1_2$ metastable at 75% (see text)

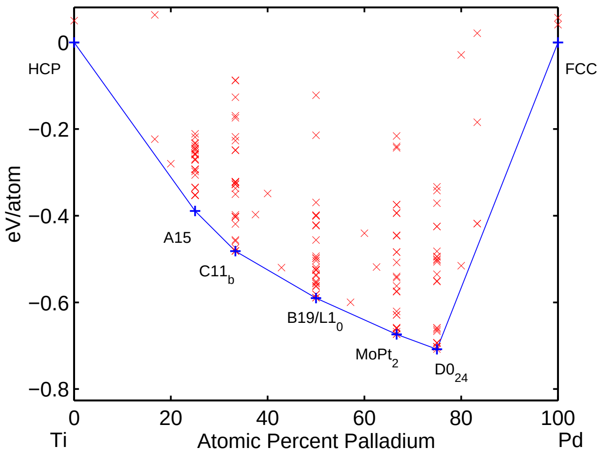

FIG. 37. PdTi (Palladium - Titanium) ground state convex hull.

Pd-Y (Palladium - Yttrium). The phase diagram for the system Pd-Y is known with reasonable accuracy. Several intermetallic compounds have been reported, but not all the structures have been determined experimentally [9,10,293–296]. We confirm the stability of the compounds Pd_3Y-L1$_2$ and PdY_3-D0$_{11}$. The prototype of αPdY is not known [293]. Our best guesses are PdY-B27 and PdY-B33 (CrB), which are degenerate in the calculation. We also find PdY_2-C37, which occurs in a concentration between two known compounds Pd_2Y_3 and Pd_2Y_5 and is very close to the tie-line of the two-phase field $PdY_3 \leftrightarrow PdY$ (5meV/atom) Hence, if Pd_2Y_3 and Pd_2Y_5 were to be included, C37 would likely not be stable. We cannot check this prediction since we do not have Pd_2Y_3 and Pd_2Y_5 prototypes in the set of calculations. *To address the degenerate structures, we further investigate PdY with PAW-GGA potentials, as described in Section (III). With PAW, PdY-B27 is the most stable compound and PdY-B33 is higher by 3.1meV/atom.*

Pd-Y system		
Low Temperature Phases comparison chart		
Composition % Pd	Experimental (Massalski [9])	*Ab initio* result
25	D0$_{11}$	PdY_3-D0$_{11}$
28.6	Pd_2Y_5 unknown	unavailable
33.3	two-phase region	PdY_2-C37 (uncertain)
40	Pd_2Y_3-hR15 unknown	unavailable
50	αPdY unknown	PdY-B27/B33 (us-lda) *B27 stable (paw-gga)* *B33∼3.1meV/at. above B27 (paw-gga)*
57.1	Pd_4Y_3-hR14 unknown	unavailable
60	αPd_3Y_2 unknown	unavailable
66.6	unknown	two phase region
79.5 to 75	L1$_2$	Pd_3Y-L1$_2$
87.5	unknown	unavailable

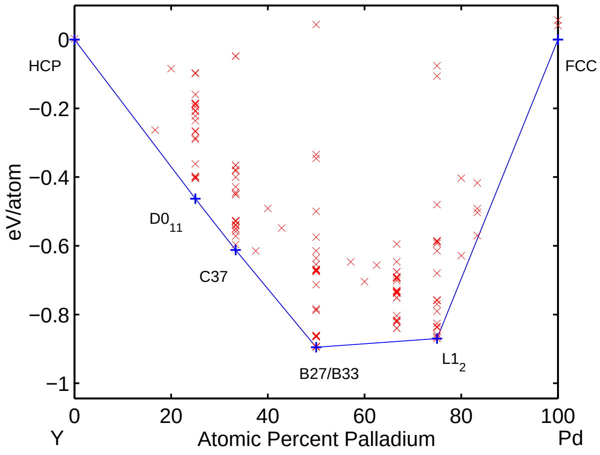

FIG. 38. PdY (Palladium - Yttrium) ground state convex hull.

Pd-Zr (Palladium - Zirconium). The experimental phase diagram for the system Pd-Zr is based on limited information [9,10,297–299,282,300–304]. We are able to confirm stability of Pd_3Zr-D0$_{24}$ and $PdZr_2$-C11$_b$. The stable phase of PdZr is reported to be CrB (B33) [10,304]. At that composition, we find two degenerate structures: PdZr-B27 or PdZr-B33 (CrB). In the Zr-rich side of the phase diagram, we find $PdZr_3$-FCC$^{[001]}_{AB3}$. However, the energy difference between $PdZr_3$-FCC$^{[001]}_{AB3}$ and the two-phase region Zr↔$PdZr_2$-C11$_b$, is very small (∼6meV/atom). Hence, the existence of compound $PdZr_3$-FCC$^{[001]}_{AB3}$ remains uncertain. At low-temperature, instead of a stable phase with stoichiometry Pd_2Zr, we find the two-phase field PdZr↔Pd_3Zr-D0$_{24}$. The least unstable phases are Pd_2Zr-C49, Pd_2Zr-$MoPt_2$, Pd_2Zr-C11$_b$, with energies ∼18meV/atom, ∼24meV/atom, ∼26meV/atom above the tie-line of the two-phase region, respectively. *To address the degenerate structures and the erroneous two phase region PdZr↔Pd_3Zr, we further investigate PdZr and Pd_2Zr with PAW-GGA potentials, as described in Section (III). With PAW, PdZr-B33 is the most stable compound and PdZr-B27 is higher by 3.2meV/atom. In addition, Pd_2Zr-C11$_b$ is degenerate with the tie line PdZr↔Pd_3Zr, and $MoPt_2$ and C49 are higher by ∼1.3meV/atom and ∼7.1meV/atom with respect to C11$_b$ (also the tie-line PdZr↔Pd_3Zr has been recalculated with PAW-GGA potentials).*

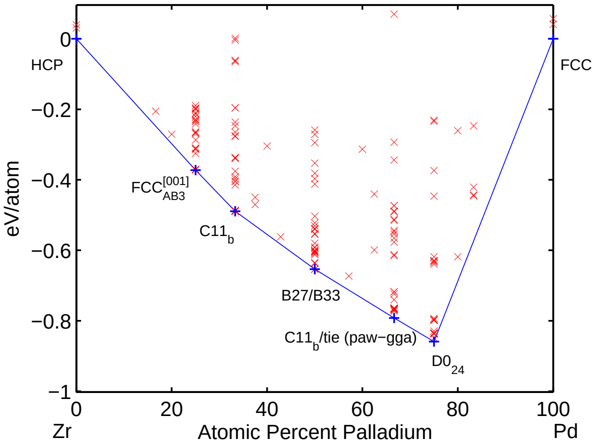

FIG. 39. PdZr (Palladium - Zirconium) ground state convex hull.

Pd-Zr system

Low Temperature Phases comparison chart

Composition % Pd	Experimental (Massalski [9])	*Ab initio* result
25	two-phase region	$PdZr_3$-FCC$^{[001]}_{AB3}$ (uncertain)
33.3	C11$_b$	$PdZr_2$-C11$_b$
50	disorder fcc [9] CrB(B33-TlI) [10,304]	PdZr- B27/B33 (us-lda) *B33 stable (paw-gga)* *B27∼3.2meV/at.* *above B33 (paw-gga)*
66.6	C11$_b$	two-phase region (us-lda). C49∼18meV/at. $MoPt_2$∼24meV/at. C11$_b$∼26meV/at. above the tie-line (us-lda). *C11$_b$/tie-line (paw-gga).* *$MoPt_2$∼1.3meV/at.,* *C49∼7.1meV/at.* *above tie-line (paw-gga).*
75	D0$_{24}$	Pd_3Zr-D0$_{24}$

Pt-Rh (Platinum - Rhodium). The experimental phase diagram of the system Pt-Rh is similar the system Pd-Pt. The low-temperature part of the phase diagram is believed to have a miscibility gap at a temperature of about 760°C [9,10,43,263,305]. Instead of the gap, we find several stable phases, all with fcc superstructure (Pt and Rh are both fcc), similar to previous FLAPW-LDA calculations [262]. We find $\mathrm{Pt_4Rh\text{-}D1}_a$, $\mathrm{Pt_3Rh\text{-}D0_{22}}$, $\mathrm{PtRh_2\text{-}C49}$, $\mathrm{PtRh_3\text{-}D0_{22}}$, $\mathrm{PtRh_4\text{-}D1}_a$, and, at 50% concentration, $\mathrm{PtRh\text{-}FCC}^{[201]}_{A2B2}$ (CH "40" in reference [262]). As shown in figure (40), all the stable phases have very small formation energy (< 30meV/atom) indicating that they may disorder at relatively low temperature.

Another *ab initio* study, relevant for this system, can be found in reference [62].

Pt-Rh system		
Low Temperature Phases comparison chart		
Composition % Rh	Experimental (Massalski [9]) Theoretical ([262])	*Ab initio* result
20	two-phase region [9] $\mathrm{D1}_a$ [262]	$\mathrm{Pt_4Rh\text{-}D1}_a$
25	two-phase region [9] two-phase region [262]	$\mathrm{Pt_3Rh\text{-}D0_{22}}$
50	two-phase region [9] $\mathrm{FCC}^{[201]}_{A2B2}$ [262]	$\mathrm{PtRh\text{-}FCC}^{[201]}_{A2B2}$
66.6	two-phase region [9]	$\mathrm{PtRh_2\text{-}C49}$
71.4	two-phase region [9] X2 [262]	unavailable
75	two-phase region [9] $\mathrm{D0_{22}}$ [262]	$\mathrm{PtRh_3\text{-}D0_{22}}$
80	two-phase region [9] $\mathrm{D1}_a$ [262]	$\mathrm{PtRh_4\text{-}D1}_a$

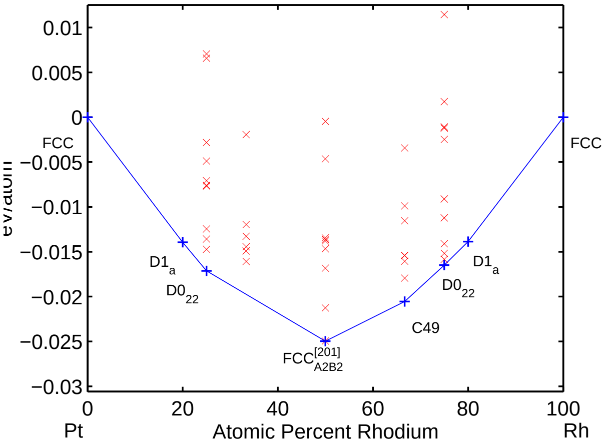

FIG. 40. PtRh (Platinum - Rhodium) ground state convex hull.

Pt-Ru (Platinum - Ruthenium). Only one compound has been found for the system Pt-Ru [9,10,306,307]. At low-temperature, the phase diagram reported in Massalski [9] has Platinum-rich and Ruthenium-rich solid solution with large solubilities of the other element, and a two-phase region for concentration between ∼70% to ∼80% of Ruthenium. However, recent X-ray diffraction experimental work reported the existence of a fcc phase at 50% composition, with unknown prototype [307]. For PtRu, our prediction is $\mathrm{PtRu\text{-}FCC}^{[001]}_{A2B2}$. At 25% Ru composition, we find a stable phase $\mathrm{Pt_3Ru\text{-}FCC}^{[001]}_{AB3}$, degenerate with the two-phase field Pt↔PtRu. Hence, the existence of compound $\mathrm{Pt_3Ru\text{-}FCC}^{[001]}_{AB3}$ remains uncertain. To our knowledge, PtRu is the first known system where the prototype structure $\mathrm{FCC}^{[001]}_{A2B2}$ would be stable.

Pt-Ru system		
Low Temperature Phases comparison chart		
Composition % Ru	Experimental (Massalski [9])	*Ab initio* result
25	disorder Pt-A1 [9]	$\mathrm{Pt_3Ru}$ $\mathrm{FCC}^{[001]}_{AB3}$/tie-line (uncertain)
50	disorder Pt-A1 [9] PtRu-fcc [307]	$\mathrm{PtRu\text{-}FCC}^{[001]}_{A2B2}$

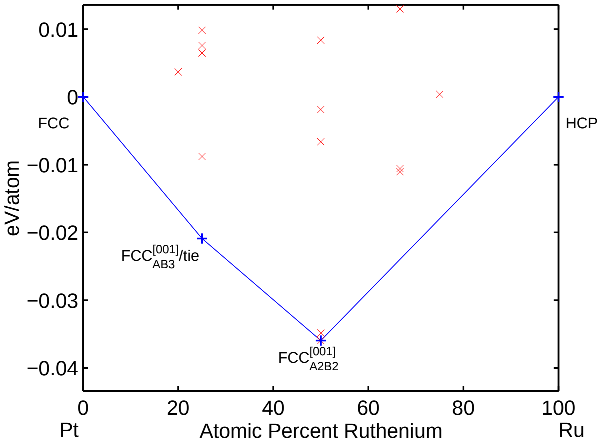

FIG. 41. PtRu (Platinum - Ruthenium) ground state convex hull.

Pt-Tc (Platinum - Technetium). The phase diagram for the system Pt-Tc has been determined from experimental solid solubility data [9,10,43,365,368]. No intermetallic compounds have been reported [9]. However, we find two stable phases: Pt$_3$Tc-FCC$_{AB3}^{[001]}$ and PtTc$_3$-D0$_{19}$. PtTc$_3$-D0$_{19}$ appears in the composition range of a two-phase region Pt-A1 and Tc-A3, that is present at temperatures higher than ∼ 1000°C. Trends of Tc alloys are further discussed in Section (VIII).

Pt-Tc system

Low Temperature Phases comparison chart

Composition % Tc	Experimental (Massalski [9])	*Ab initio* result
25	disorder Pt-A1	Pt$_3$Tc-FCC$_{AB3}^{[001]}$
75	two-phase region above ∼1000°C Pt-A1↔Tc-A3	PtTc$_3$-D0$_{19}$

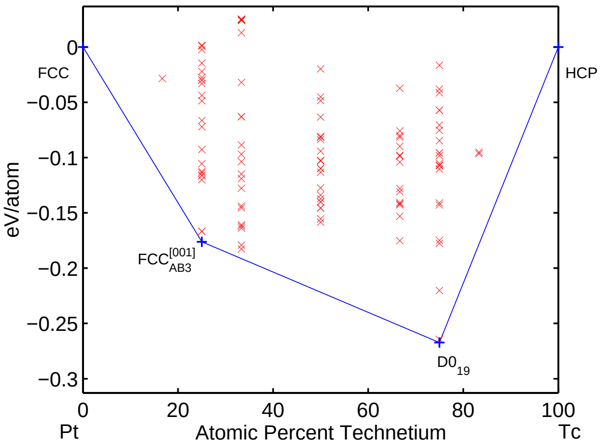

FIG. 42. PtTc (Platinum - Technetium) ground state convex hull.

Pt-Ti (Platinum - Titanium). Not much is known of Pt-Ti system to produce a precise phase diagram [9,10,48,285,290,308–311,283,312]. Some intermetallic compounds are reported [308–311,283,312,288]. We confirm the stability of phases PtTi$_3$-A15, αPtTi-B19, Pt$_3$Ti-D0$_{24}$. B19 is stable at 50% composition, and L1$_0$ and B33 are higher by ∼20meV/atom and ∼30meV/atom, respectively. At concentration 25%Ti, we confirm the existence of γ-L1$_2$, which has an energy that is ∼5meV/atom higher than Pt$_3$Ti-D0$_{24}$. However, L1$_2$ has been reported to be stable away from stoichiometry < 25% Ti [9]. At composition 33% Ti, Pt$_2$Ti, Massalski reports a two-phase region above 600°C [9,10]. Instead of the two-phase field, we find a stable compound Pt$_2$Ti: two structures, C49 and C37, are degenerate. We cannot say anything about Pt$_8$Ti-D1$_a$, because our library does not contain off-stoichiometry D1$_a$. *To address the degenerate structures, we further investigate Pt$_2$Ti with PAW-GGA potentials, as described in Section (III). With PAW, Pt$_2$Ti-C49 is the most stable compound and Pt$_2$Ti-C37 is higher by 1.9meV/atom.*

Another *ab initio* study, relevant for this system, can be found in reference [292].

Pt-Ti system

Low Temperature Phases comparison chart

Composition % Ti	Experimental (Massalski [9])	*Ab initio* result
1 to 12	Pt$_8$Ti-D1$_a$	unavailable
20 to 27	D0$_{24}$ (>25%Ti) γ-L1$_2$ (<25%Ti)	Pt$_3$Ti-D0$_{24}$ L1$_2$∼5meV/at. above D0$_{24}$
33.3	two-phase region above 600°C [9]	Pt$_2$Ti-C49/C37 (us-lda) *C49 stable* *C37∼1.9meV/at.* *above C49 (paw-gga)*
46 to 54	αPtTi-B19	PtTi-B19 L1$_0$∼20meV/at. above B19
71 to 78	A15	PtTi$_3$-A15

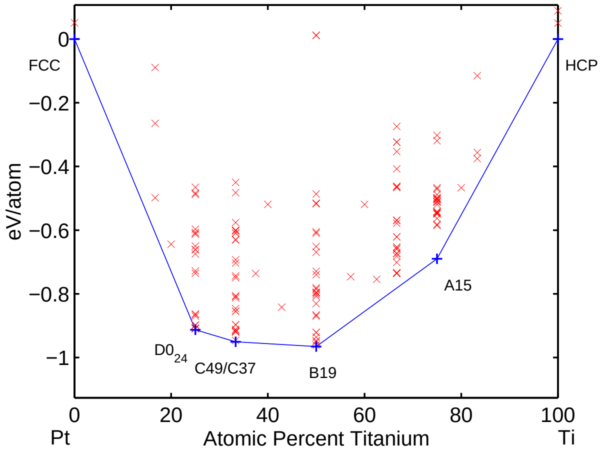

FIG. 43. PtTi (Platinum - Titanium) ground state convex hull.

Pt-Y (Platinum - Yttrium). The experimental phase diagram of the system Pt-Y has been sketched by analogy with other Rare Earth-Platinum diagrams [9]. Several intermetallic compounds have been reported [9,10,43,156,277,285,313–320,324]. The stability of the compounds Pt_3Y-$L1_2$, Pt_2Y-C15, and PtY_3-$D0_{11}$ is confirmed. At 50% concentration, we do not find any stable PtY-B27. Instead of B27, we find PtY-B33 (CrB prototype) to have lowest energy with B2 and B27 having energies ∼50meV/atom above B33. At 66.6% Y concentration, we find PtY_2-C37 which is the prototype of Co_2Si and Ni_2Si. Hence our calculations confirm the correct experimental structure. At concentration 62.5% Y, we do not find Pt_3Y_5-$D8_8$, but the two-phase field PtY↔PtY_2. $D8_8$ and W_5Si_3 are higher by ∼24meV/atom and ∼80meV/atom with respect to the tie-line PtY↔PtY_2 (this problem is solved with PAW-GGA potentials). As shown in figure (44), at concentration 16.6% Y, we find a two-phase region instead of the reported stable compound Pt_5Y with unknown structure [9]. Our best guess is Pt_5Y-$D2_d$ which is the least-metastable structure we have at such composition (∼18meV/atom above the tie-line Pt↔Pt_3Y). We conclude that further experimental and theoretical investigations are necessary to determine the behavior of PtY. *To address the disagreement with the experimental results for compounds PtY and* Pt_3Y_5*, we further investigate the relevant structures with PAW-GGA potentials, as described in Section (III). With PAW, PtY-B33 is stable and PtY-B27 is higher by 60meV/atom. For compound* Pt_3Y_5*,* $D8_8$ *is stable with an energy 6.9meV/atom lower than the tie-line PtY↔*PtY_2*, which has also been recalculated with PAW-GGA potentials.* The disagreement at composition PtY is further discussed in Section (IV).

Pt-Y system		
Low Temperature Phases comparison chart		
Composition % Y	Experimental (Massalski [9])	*Ab initio* result
16.6	unknown	Pt_5Y-$D2_d$ metastable. $D2_d$ ∼18meV/at. above the tie-line
25	$L1_2$	Pt_3Y-$L1_2$
33.3	C15	Pt_2Y-C15
42.9	Pt_4Y_3-Pd_4Pu_3	unavailable
50	B27	PtY-B33 B2/B27 ∼50meV/at. above B33 *B33 stable (paw-gga)* *B27 ∼60meV/at.* *above B33. (paw-gga)* See Section (IV).
55.6	Pt_4Y_5-Pu_5Rh_4	unavailable
62.5	Pt_3Y_5-$D8_8$	two-phase region PtY↔PtY_2. (us-lda) $D8_8$ ∼24meV/at. above the tie-line (us-lda) *$D8_8$ stable (paw-gga).* *∼6.9meV/at. below* *PtY↔PtY_2 (paw-gga).*
66.6	PtY_2-Ni_2Si [9] (Co_2Si)	PtY_2-C37 (Co_2Si)
70	Pt_3Y_7-$D10_2$	unavailable
75	$D0_{11}$	PtY_3-$D0_{11}$

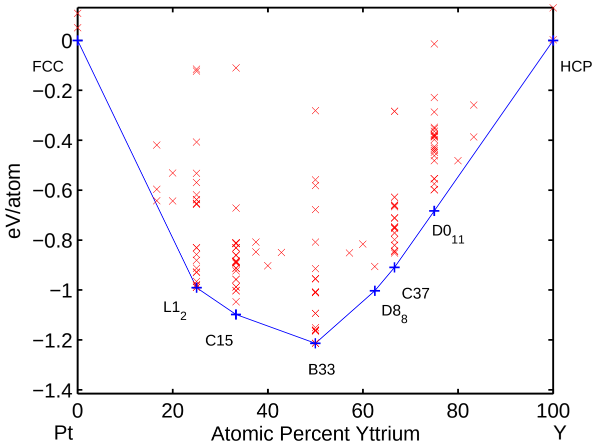

FIG. 44. PtY (Platinum - Yttrium) ground state convex hull.

Pt-Zr (Platinum - Zirconium). The system Pt-Zr is quite interesting. Our *ab initio* method confirms the stability of αPtZr-B33 (CrB prototype). Two crystal structures have been reported for Pt_3Zr: $D0_{24}$ and $L1_2$ [9,10,321,323,322,324,285,302]. We confirm the stability of Pt_3Zr-$D0_{24}$ and we find $L1_2$ to be higher by 10meV/atom with respect to $D0_{24}$. In the Zr-rich part of the phase diagram, we find two stable phases $PtZr_2$-C16 and $PtZr_3$-A15. At concentration 62.5% Zr, we do not find Pt_3Zr_5-$D8_8$, but the two-phase field PtZr↔$PtZr_2$. W_5Si_3 and $D8_8$ are higher by ∼26meV/atom and ∼36meV/atom with respect to the tie-line PtZr↔$PtZr_2$. *To address the phase instability at composition* Pt_3Zr_5*, we further investigate the relevant compounds with PAW-GGA potentials, as described in Section (III). With PAW, at concentration* Pt_3Zr_5*, there is a two-phase region PtZr↔*$PtZr_2$*. In addition,* Pt_3Zr_5*-*W_5Si_3 *and* Pt_3Zr_5*-*$D8_8$ *have energies higher by 23meV/atom and 26meV/atoms with respect to the tie-line PtZr↔*$PtZr_2$*, respectively.* The disagreement at composition Pt_3Zr_5 is further discussed in Section (IV).

Pt-Zr system

Low Temperature Phases comparison chart

Composition % Zr	Experimental (Massalski [9])	*Ab initio* result
25	$D0_{24}$ in [322,302,324,285] $L1_2$ in [323]	Pt_3Zr-$D0_{24}$ $L1_2$∼10meV/at. above $D0_{24}$
50	αPtZr-B33 (CrB)	PtZr-B33
62.5	Pt_3Zr_5-$D8_8$	two-phase region (us-lda) W_5Si_3∼26meV/at. $D8_8$∼36meV/at. above tie-line (us-lda). *two-phase region (paw-gga)* *W_5Si_3∼23meV/at.* *$D8_8$∼26meV/at.* *above tie-line (paw-gga).* See Section (IV).
66.6	two-phase region above 600°C	$PtZr_2$-C16 (uncertain)
75	two-phase region above 600°C	$PtZr_3$-A15 (uncertain)

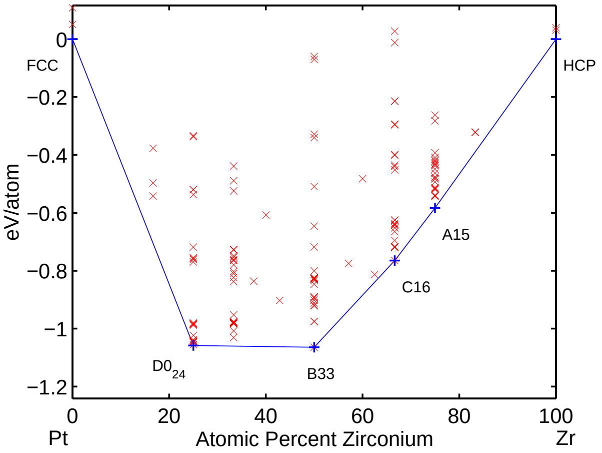

FIG. 45. PtZr (Platinum - Zirconium) ground state convex hull.

Rh-Ru (Rhodium - Ruthenium). The phase diagram for the system Rh-Ru is based on the solid solubility data [9,10,43,326]. Experimental results report two solid solutions (fcc Rh-rich) and (hcp Ru-rich) with a two-phase region in between (from 34.5% to 40% atomic percent Ruthenium). No intermetallic compounds have been reported [325–327] and the system is considered to be no compound forming [10]. However, we find two stable phases: an orthorhombic oC12 RhRu_2^{proto}, with hcp superstructure and Cmcm #63 space group, and a trigonal hP4 RhRu^{proto}, with hcp superstructure and $\mathrm{P\bar{3}m1}$ #164 space group. Both prototypes are described in Appendix (XI). As shown in figure (46), all the stable phases have small formation energy (< 10meV/atom) making them difficult to determine experimentally. *To better describe the stability of this system, we further investigate all the structures with negative formation energies with PAW-GGA potentials, as described in Section (III). Also with PAW,* RhRu_2^{proto} *and* RhRu^{proto} *are the most stable structures, with formation energies of -8.3meV/atom and -8.8meV/atom, respectively.*

Rh-Ru system		
Low Temperature Phases comparison chart		
Composition % Rh	Experimental (Massalski [9])	*Ab initio* result
33	solid solution Ru-A3	RhRu_2^{proto} stable both us-lda and *paw-gga*, $E_f \sim -8.3meV/atom$ *(paw-gga).*
50	solid solution Ru-A3	RhRu^{proto} stable both us-lda and *paw-gga*, $E_f \sim -8.8meV/atom$ *(paw-gga).*

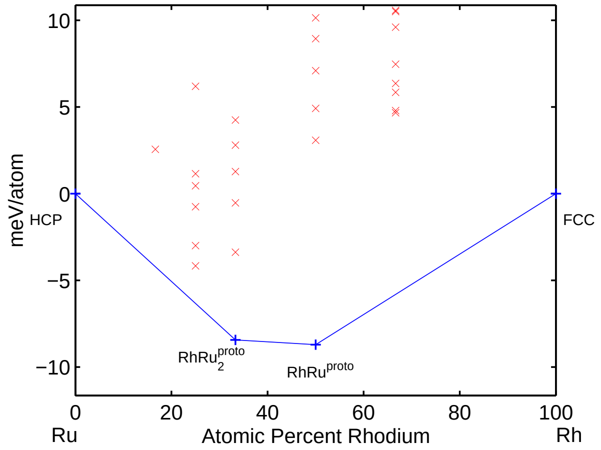

FIG. 46. RhRu (Rhodium - Ruthenium) ground state convex hull.

Rh-Tc (Rhodium - Technetium). The phase diagram for the system Rh-Tc is based on the solid solubility data [9,10,43,366,368]. Experimental results report two solid solutions (fcc Rh-rich) and (hcp Tc-rich) with a two-phase region in between. No intermetallic compounds have been reported [366,368]. However, we find three stable phases: $\mathrm{RhTc_3}$-$\mathrm{D0_{19}}$, RhTc-B19, and $\mathrm{Ru_2Tc}$-$\mathrm{ZrSi_2}$. Trends of Tc alloys are further discussed in Section (VIII).

Rh-Tc system		
Low Temperature Phases comparison chart		
Composition % Rh	Experimental (Massalski [9])	*Ab initio* result
25	solid solution Tc-A3	$\mathrm{RhTc_3}$-$\mathrm{D0_{19}}$
50	solid solution Tc-A3	RhTc-B19 B27∼29meV/at. above B19 (us-lda).
66.6	two-phase region above ∼1000°C Pt-A1↔Tc-A3	$\mathrm{Rh_2Tc}$-$\mathrm{ZrSi_2}$

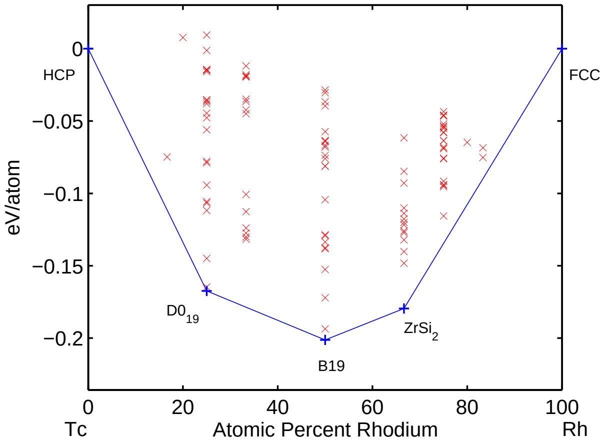

FIG. 47. RhTc (Rhodium - Technetium) ground state convex hull.

Rh-Ti (Rhodium - Titanium). There are qualitative disagreements about the phase diagram of the Rh-Ti system [9,10,48,322,328–332]. We confirm the stable phases that where found by all investigators [328–331]: $RhTi_2$, $\alpha RhTi$-$L1_0$, and Rh_3Ti-$L1_2$. References [10,322,332] report $RhTi_2$-$CuZr_2$ instead of $RhTi_2$-$C11_b$. The prototype $CuZr_2$ is a distortion of $C11_b$ and has the same lattice type (tetragonal, tI6) and space group (I4/mmm #139) [10]. We find $RhTi_2$-$C11_b$ and $RhTi_2$-$CuZr_2$ to have degenerate energy. In the Rh-rich part of the phase diagram we find a stable phase Rh_2Ti-C37. However, we do not have Rh_5Ti_3 in our library, so C37 might likely be unstable with respect to the two-phase field $Rh_5Ti_3 \leftrightarrow L1_2$. At concentration ≈ 84% Rh, we do not find any stable compound, in agreement with [330] and in contrast with [328]. *To address the degenerate structures* $RhTi_2$-$C11_b/CuZr_2$*, we further investigate* $RhTi_2$ *with PAW-GGA potentials, as described in Section (III). Also with PAW,* $C11_b$ *and* $CuZr_2$ *remain degenerate.*

Other *ab initio* studies, relevant for this system, can be found in references [232,292].

Rh-Ti system		
Low Temperature Phases comparison chart		
Composition % Rh	Experimental (Massalski [9])	*Ab initio* result
33.3	$C11_b$ [9]/$CuZr_2$ [10]	$RhTi_2$ $C11_b/CuZr_2$ (us-lda,) $C11_b/CuZr_2$ (*paw-gga*)
∼38 to 58	$\alpha RhTi$-$L1_0$	$RhTi$-$L1_0$
62.5	Rh_5Ti_3-Ge_3Rh_5	unavailable
66.6	two-phase region above 600°C	Rh_2Ti-C37
73 to 78	$L1_2$	Rh_3Ti-$L1_2$
∼83.8	Rh_5Ti (unknown)	nothing stable

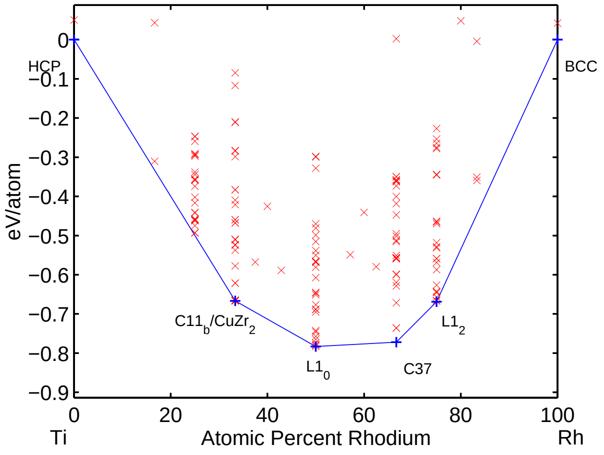

FIG. 48. RhTi (Rhodium - Titanium) ground state convex hull.

Rh-Y (Rhodium - Yttrium). Several compounds have been reported for the system Rh-Y at low-temperature [9,10,43,333,277,334,335,337]. The stability of Rh_2Y-C15, RhY-B2, RhY_3-$D0_{11}$ is confirmed. At composition Rh_5Y, where a $D2_d$ structure has been seen at high-temperature (but not stable at low-temperature), we find the $D2_d$ to be the lowest energy structure (of all the structures at that composition), even though it is metastable with respect to the phase separation into Rh_2Y-C15↔Rh. At composition Rh_3Y one compound has been reported to be stable with prototype $CeNi_3$ and space group $P6_3/mmc$ #194 [10,336,338]. We do not have such prototype in our library and we do not find any stable phase: Rh_3Y-$D0_{19}$ is the least metastable prototype we obtain. Rh_3Y-$D0_{19}$ is higher by 130 meV/atom with respect the tie-line, which is at least one order of magnitude bigger than the accuracy of the calculations. We also find RhY_2-C37, which appears in a concentration between two known compounds, Rh_3Y_5 and Rh_3Y_7, that are not present in our set of calculations. Therefore C37 might be unstable with respect to the two-phase region $Rh_3Y_5 \leftrightarrow Rh_3Y_7$.

Rh-Y system		
Low Temperature Phases comparison chart		
Composition % Rh	Experimental (Massalski [9])	*Ab initio* result
25	$D0_{11}$	RhY_3-$D0_{11}$
30	Rh_3Y_7-$D10_2$	unavailable
33.3	two-phase region above 0°C	RhY_2-C37 (uncertain)
37.5	Rh_3Y_5 (unknown)	unavailable
40	Rh_2Y_3 (unknown) tI140-I4/mcm	unavailable
50	B2	RhY-B2
66.6	C15	Rh_2Y-C15
75	Rh_3Y (unknown) hP24-$P6_3/mmc$	$D0_{19}$∼130meV/at. above tie-line
83.5	Rh_5Y-$D2_d$ (high-temperature)	$D2_d$∼110meV/at. above tie-line

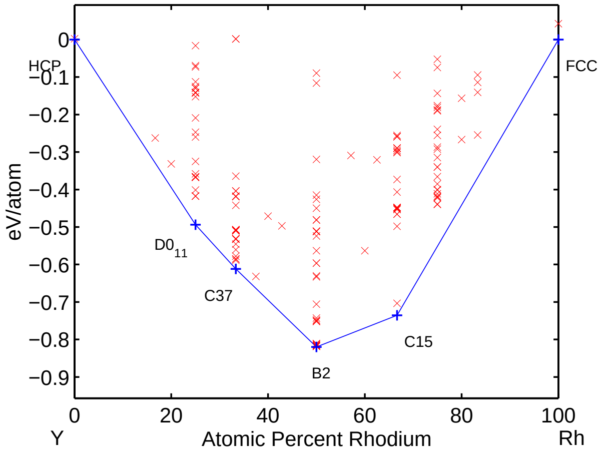

FIG. 49. RhY (Rhodium - Yttrium) ground state convex hull.

Rh-Zr (Rhodium - Zirconium). Although the system Zr-Rh is well known for its superconducting phases [9,10,339,342], further investigations are needed to clarify the stability and presence of intermediate phases [340,341]. Our *ab initio* method confirms the stability of $RhZr_2$-C16 and Rh_3Zr-$L1_2$. Massalski does not report the prototype of the low-temperature phase αRhZr [9]. References [342–344] report αRhZr-B27. We confirm the stability of αRhZr-B27 (BFe prototype) with no other metastable compounds with similar energy. In addition, we find three new phases Rh_2Zr-C37, $RhZr_4$-$D1_a$ and $RhZr_3$-$FCC^{[001]}_{AB3}$, which are degenerate with the two-phase fields RhZr↔Rh_3Zr, Zr ↔RhZr, and Zr ↔RhZr, respectively.

Other *ab initio* studies, relevant for this system, can be found in references [232,345].

Rh-Zr system		
Low Temperature Phases comparison chart		
Composition % Rh	Experimental (Massalski [9])	*Ab initio* result
20	two-phase region above 0°C	$RhZr_4$-$D1_a$/tie-line
25	two-phase region above 0°C	$RhZr_3$-$FCC^{[001]}_{AB3}$/tie-line
33.3	C16	$RhZr_2$-C16
50 to ?	αRhZr unknown [9] B27 [342–344]	RhZr-B27
57.1	Rh_4Zr_3 (unknown)	unavailable
62.5	Rh_5Zr_3-Pd_3Pu_3	unavailable
66.6	two-phase region above 0°C	Rh_2Zr-C37/tie-line
72 to 82	$L1_2$	Rh_3Zr-$L1_2$

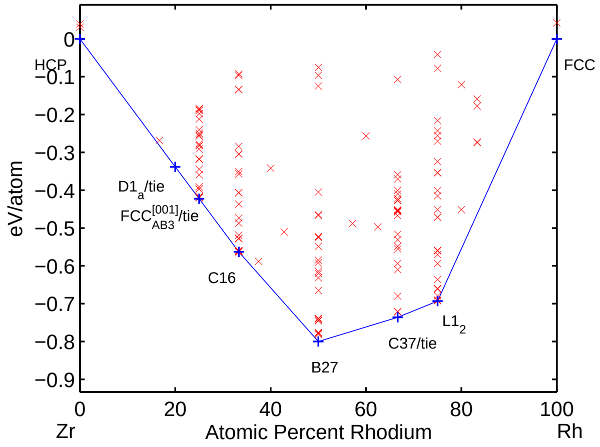

FIG. 50. RhZr (Rhodium - Zirconium) ground state convex hull.

Ru-Tc (Ruthenium - Technetium). The phase diagram for the system Ru-Tc is considered to have a continuous disordered hcp solid solution at low-temperature [9,10,365,368,346]. We find three stable ordered phases Ru_3Tc-$D0_{19}$, RuTc-B19, and $RuTc_3$-$D0_{19}$, all of which are hcp superstructures. Hence, it is possible that they are low-temperature phases of the system Ru-Tc. Trends of Tc alloys are further discussed in Section (VIII).

Ru-Tc system		
Low Temperature Phases comparison chart		
Composition % Ru	Experimental (Massalski [9])	*Ab initio* result
25	disorder solution (Ru,Tc)-A3	$RuTc_3$-$D0_{19}$
50	same as above	RuTc-B19
75	same as above	Ru_3Tc-$D0_{19}$

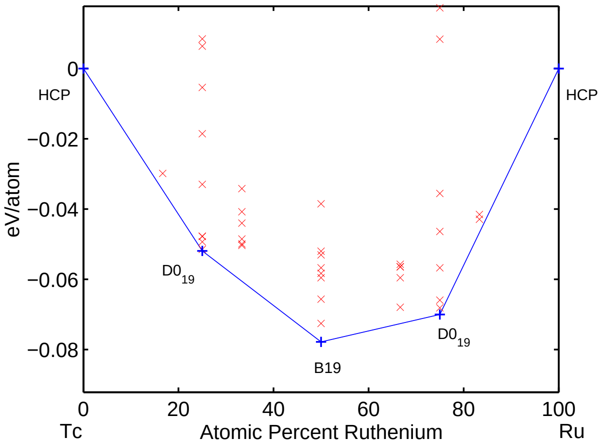

FIG. 51. RuTc (Ruthenium - Technetium) ground state convex hull.

Ru-Ti (Ruthenium - Titanium). The phase diagram of Ru-Ti is well determinated by several investigators. A single low-temperature compound RuTi-B2 has been reported [9,10,48,285,347,348,350,349,351–354], and our *ab initio* method confirms its stability. In addition, we find two stable phases: $RuTi_2$-C49, and orthorhombic $RuTi_3$ with space group Immm #71, bcc superstructure, and prototype $RuTi_3^{proto}$ described in Appendix (XI). Such compounds are close to the tie-line Ti↔RuTi. In fact, for C49 and $RuTi_3^{proto}$, the formation energies are lower by ∼34meV/atom and ∼37meV/atom with respect to the two-phase field Ti↔RuTi.

Ru-Ti system		
Low Temperature Phases comparison chart		
Composition % Ru	Experimental (Massalski [9])	*Ab initio* result
25	two-phase region above 600°C	$RuTi_3^{proto}$ Appendix (XI) ∼37meV/at. below Ti↔RuTi
33.3	same as above	$RuTi_2$-C49 ∼34meV/at. below Ti↔RuTi
45 to 52 ±1	B2	RuTi-B2

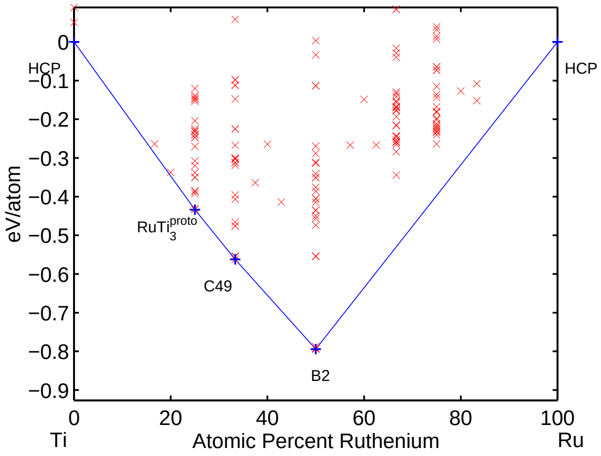

FIG. 52. RuTi (Ruthenium - Titanium) ground state convex hull.

Ru-Y (Ruthenium - Yttrium). Several compounds have been reported for the system Ru-Y [9,10,43,333,355–359]. We confirm the stability of RuY_3-$D0_{11}$ and Ru_2Y-C14. Also, we find RuY_2-C16, which appears in a concentration between two known compounds $Ru_{25}Y_{44}$ and Ru_2Y_5 that are not in our library of calculations. Hence, the existence of RuY_2-C16 is uncertain. At concentration 50%, we do not find any stable RuY compound, in agreement with [358].

Ru-Y system		
Low Temperature Phases comparison chart		
Composition % Ru	Experimental (Massalski [9])	*Ab initio* result
25	$D0_{11}$	RuY_3-$D0_{11}$
28.6	Ru_2Y_5-C_2Mn_5 mS28 C12/c1 [10,355,356,358]	unavailable
33.3	two-phase region above 0°C	RuY_2-C16 (uncertain)
36.2	$Ru_{25}Y_{44}$ (unknown) oP276 Pnna [10,355,359]	unavailable
40	Ru_2Y_3-Er_3Ru_2 hP10 $P6_3/m$ [360]	unavailable
66.6	Ru_2Y-C14	Ru_2Y-C14

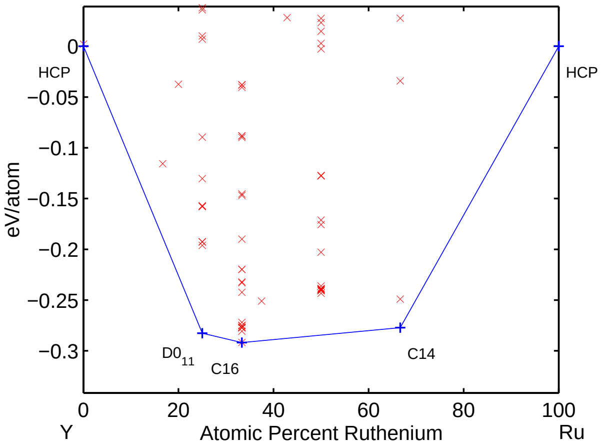

FIG. 53. RuY (Ruthenium - Yttrium) ground state convex hull.

Ru-Zr (Ruthenium - Zirconium). The phase diagram of RuZr is known accurately [9,10,362,361]. Our *ab initio* method confirms the stability of the low-temperature phase RuZr-B2. In agreement with experiments, we find no ground state at composition Ru$_2$Zr, though the lowest energy structure at that composition in our calculations is C14 which appears in the phase diagram at high-temperature. Ru$_2$Zr-C14 is higher by ∼60meV/atom with respect to the two-phase field Ru↔RuZr. In the Zr-rich region we find one stable compound, RuZr$_4$-D1$_a$, previously unknown. In addition, we find three metastable phases: RuZr$_5$, RuZr$_3$, and RuZr$_2$-C49, with energies higher by 21meV/atom, 16.6meV/atom, and 14meV/atom, with respect to the two-phase fields RuZr$_4$↔Zr, RuZr↔RuZr$_4$, and RuZr↔RuZr$_4$, respectively. The structure of RuZr$_5$ is similar to MoZr$_5^{proto}$ (Appendix (XII)), while the structure of RuZr$_3$ is similar to RuTi$_3^{proto}$ (Appendix (XI)).

Other *ab initio* studies, relevant for this system, can be found in references [238–240,363].

Ru-Zr system		
Low Temperature Phases comparison chart		
Composition % Ru	Experimental (Massalski [9])	*Ab initio* result
16.6	two-phase region RuZr↔Zr above 400°C	RuZr$_5$≈MoZr$_5^{proto}$ ∼21meV/at. above RuZr$_4$↔Zr
20	same as above	RuZr$_4$-D1$_a$
25	same as above	RuZr$_3$≈RuTi$_3^{proto}$ ∼16.6meV/at. above RuZr↔RuZr$_4$
33.3	same as above	RuZr$_2$-C49 ∼14meV/at. above RuZr↔RuZr$_4$
48 to 52	B2	RuZr-B2
66 to 68	C14 (high T)	Ru$_2$Zr-C14 ∼60meV/at. above Ru↔RuZr

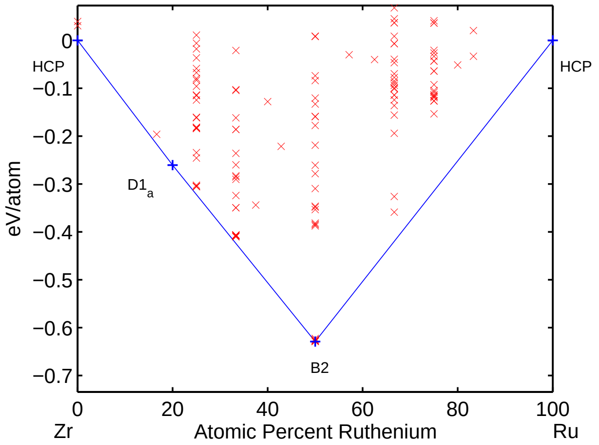

FIG. 54. RuZr (Ruthenium - Zirconium) ground state convex hull.

Tc-Ti (Technetium - Titanium). The phase diagram of the system TcTi has been constructed by analogy with chemically related systems [9,10,48,364,365]. Two intermetallic compound, TcTi-B2 and χ are reported [364,365]. We confirm the stability of TcTi-B2, but we can not say anything about χ since we do not have prototypes at composition 85% Ru. In addition, we find Tc$_2$Ti-C11$_b$, TcTi$_2$-C49, and an orthorhombic phase TcTi$_3$ with space group Immm #71 and prototype TcTi$_3^{proto}$ described in Appendix (XI). These intermetallics have large negative formation energy, therefore they are expected to be very stable. Trends of Tc alloys are further discussed in Section (VIII).

Tc-Ti system		
Low Temperature Phases comparison chart		
Composition % Tc	Experimental (Massalski [9])	*Ab initio* result
25	disorder βTi-A2	TcTi$_3^{proto}$ Appendix (XI)
33.3	disorder βTi-A2	TcTi$_2$-C49
∼50	B2	TcTi-B2
66.6	two-phase region TcTi↔χ	Tc$_2$Ti-C11$_b$
∼85	χ-A12	unavailable

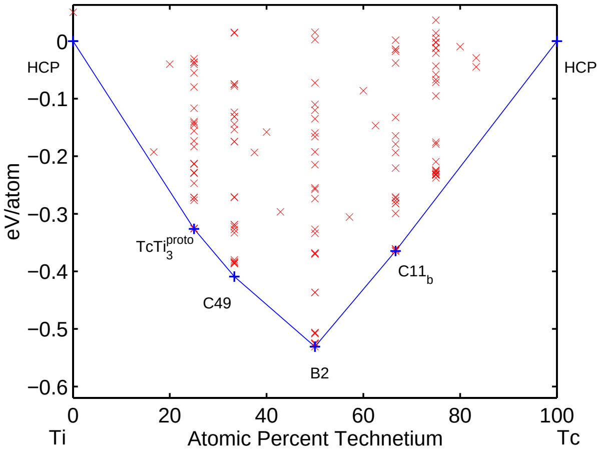

FIG. 55. TcTi (Technetium - Titanium) ground state convex hull.

Tc-Y (Technetium - Yttrium). Not enough information exists in order to construct a phase diagram for the system Tc-Y [9,10]. Only one intermetallic compound has been reported: Tc_2Y-C14 (Friauf-Laves/Frank-Kasper phase) [367,369]. We confirm the stability of Tc_2Y-C14. In addition, we find another stable phase TcY_3-$D0_{11}$. Trends of Tc alloys are further discussed in Section (VIII).

Tc-Y system

Low Temperature Phases comparison chart

Composition % Tc	Experimental (Massalski [9])	*Ab initio* result
25	no information	TcY_3-$D0_{11}$
66.6	C14 [367,369]	Tc_2Y-C14 (Laves phase)

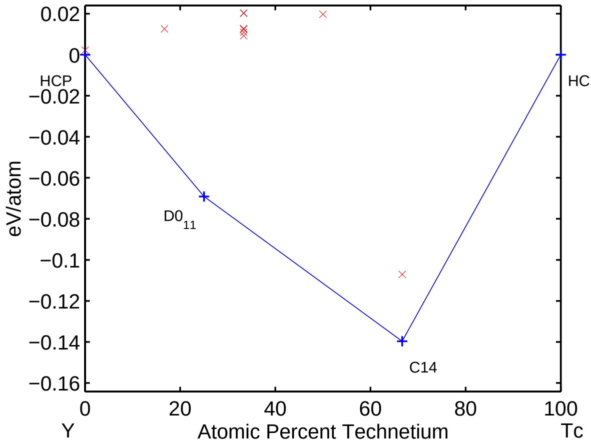

FIG. 56. TcY (Technetium - Yttrium) ground state convex hull.

Tc-Zr (Technetium - Zirconium). Not enough information exists in order to construct a phase diagram for the system Tc-Zr [9,10]. Only two intermetallic compounds have been reported: Tc_2Zr-C14 (Friauf-Laves/Frank-Kasper phase) and Tc_6Zr-A12 [9,10,365,370]. We confirm the stability of Tc_2Zr-C14, but we cannot determine A12 since we do not have the proper prototype in our library. At 50% composition, Miedema *et-al.* reported the existence of a TcZr compound with unknown structure [10,285]. At such composition we find TcZr-B2. In addition, we find other stable phases: $TcZr_4$-$D1_a$ and $TcZr_2$-C49. These intermetallics have large negative formation energy, therefore they are expected to be very stable. Trends of Tc alloys are further discussed in Section (VIII).

Tc-Zr system

Low Temperature Phases comparison chart

Composition % Tc	Experimental (Massalski [9])	*Ab initio* result
20	no information	$TcZr_4$-$D1_a$
33.3	no information	$TcZr_2$-C49
50	TcZr (unknown) [285]	TcZr-B2
66.6	C14 [365,370]	Tc_2Zr-C14 (Laves phase)
85.7	Tc_6Zr-A12	unavailable

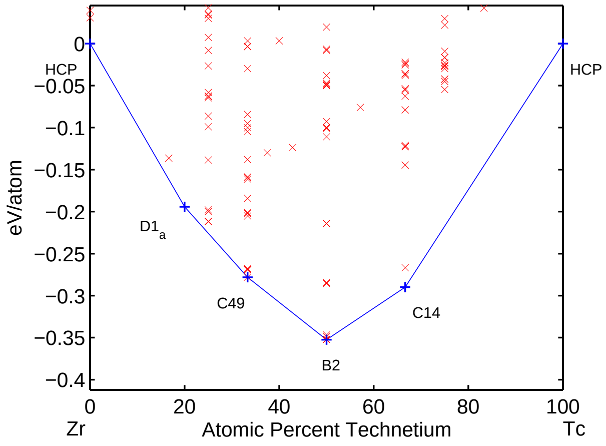

FIG. 57. TcZr (Technetium - Zirconium) ground state convex hull.

VIII. TREND FOR TECHNETIUM ALLOYS

In our set of calculations, we have noticed that the phase $D0_{19}$ appears in systems MTc_3 where M is a transition metal in the columns on the right of Tc (Tc is in column 7B) while $D0_{19}$ is not present if M is in the columns on the left of Tc: $D0_{19}$ is stable in $PdTc_3$, $PtTc_3$, $RhTc_3$, $RuTc_3$, and unstable in NbTc, TcTi, TcY, and TcZr.

IX. ACKNOWLEDGMENTS

The research was supported by the Department of Energy, Office of Basic Energy Science under Contract No. DE-FG02-96ER45571 and National Science Foundation Information Technology Research (NSF-ITR) Grant No. DMR-0312537.

It has benefited from discussion with John Rodgers, Kristin Persson, Frank Hadley Cocks, Chris Fischer, Aleksey Kolmogorov, Vincent Crespi and Zi-Kui Liu.

X. TABLES OF RESULTS

A. Experimental compounds in agreement with ab initio solutions

Experimental compound ⇔ *ab initio* compound					
System	Experimental result	*Ab initio* result	System	Experimental result	*Ab initio* result
Ag-Cd	AgCd-B2 [10,67–70]	AgCd-B2/B19/B27	Nb-Pd	NbPd$_3$-D0$_{22}$	NbPd$_3$-D0$_{22}$
Ag-Mg	Ag$_3$Mg-D0$_{23}$ [76]	AgMg-D0$_{23}$/D0$_{24}$	Nb-Pt	Nb$_3$Pt-A15	Nb$_3$Pt-A15
Ag-Mg	AgMg-B2	AgMg-B2	Nb-Pt	NbPt$_2$-MoPt$_2$	NbPt$_2$-MoPt$_2$
Ag-Na	Ag$_2$Na-C15	Ag$_2$Na-C15	Nb-Pt	NbPt$_3$-D0$_\alpha$	NbPt$_3$-D0$_\alpha$
Ag-Ti	AgTi$_2$-C11$_b$	AgTi$_2$-C11$_b$	Nb-Rh	Nb$_3$Rh-α'-A15	Nb$_3$Rh-A15
Ag-Ti	AgTi-B11	AgTi-B11 (γCuTi)	Nb-Rh	NbRh-L1$_0$	NbRh-L1$_0$
Ag-Y	AgY-B2	AgY-B2	Nb-Rh	ϵ(Nb$_2$Rh$_3$)-B19 (high T)	NbRh-B19
Ag-Y	Ag$_2$Y-C11$_b$	Ag$_2$Y-C11$_b$	Nb-Rh	η(Nb$_{13}$Rh$_{27}$)-Al$_3$Pu	NbRh$_3$-Al$_3$Pu
Ag-Zr	AgZr$_2$-C11$_b$	AgZr$_2$-C11$_b$	Pd-Ti	PdTi$_3$-A15 at 20%	PdTi$_3$-A15 at 25%
Ag-Zr	AgZr-B11	AgZr-B11 (γCuTi)	Pd-Ti	PdTi$_2$-C11$_b$	PdTi$_2$-C11$_b$
Al-Sc	AlSc$_2$-B8$_2$	AlSc$_2$-B8$_2$	Pd-Ti	α(TiPd)-B19	PdTi-B19
Al-Sc	AlSc-B2	AlSc-B2	Pd-Ti	Pd$_3$Ti-D0$_{24}$	Pd$_3$Ti-D0$_{24}$
Al-Sc	Al$_2$Sc-C15	Al$_2$Sc-C15	Pd-Y	PdY$_3$-D0$_{11}$	PdY$_3$-D0$_{11}$
Al-Sc	Al$_3$Sc-L1$_2$	Al$_3$Sc-L1$_2$	Pd-Y	Pd$_3$Y-L1$_2$	Pd$_3$Y-L1$_2$
Au-Cd	β'AuCd-B19	AuCd-B19	Pd-Zr	PdZr$_2$-C11$_b$	PdZr$_2$-C11$_b$
Au-Cd	βAuCd-B2 (high T)	AuCd-B2	Pd-Zr	PdZr-B33	PdZr-B33
Au-Nb	Au$_2$Nb-C32	Au$_2$Nb-C32 (paw-gga)	Pd-Zr	Pd$_2$Zr-C11$_b$	Pd$_2$Zr-C11$_b$/tie-line (paw-gga)
Au-Sc	Au$_4$Sc-D1$_a$	Au$_4$Sc-D1$_a$	Pd-Zr	Pd$_3$Zr-D0$_{24}$	Pd$_3$Zr-D0$_{24}$
Au-Sc	Au$_2$Sc-C11$_b$	Au$_2$Sc-C11$_b$/MoPt$_2$	Pt-Ti	Pt$_3$Ti-D0$_{24}$	Pt$_3$Ti-D0$_{24}$
Au-Sc	AuSc-B2	AuSc-B2/B19	Pt-Ti	αPtTi-B19	PtTi-B19
Au-Ti	Au$_4$Ti-D1$_a$	Au$_4$Ti-D1$_a$	Pt-Ti	PtTi$_3$-A15	PtTi$_3$-A15
Au-Ti	Au$_2$Ti-C11$_b$	Au$_2$Ti-C11$_b$/MoPt$_2$	Pt-Y	Pt$_3$Y$_5$-D8$_8$	Pt$_3$Y$_5$-D8$_8$ (paw-gga)
Au-Ti	αAuTi-B11	AuTi-B11	Pt-Y	Pt$_3$Y-L1$_2$	Pt$_3$Y-L1$_2$
Au-Ti	AuTi$_3$-A15	AuTi$_3$-A15	Pt-Y	Pt$_2$Y-C15	Pt$_2$Y-C15
Au-Y	Au$_3$Y-D0$_a$	Au$_3$Y-D0$_a$	Pt-Y	PtY$_2$-C37	PtY$_2$-C37
Au-Y	Au$_2$Y-C11$_b$	Au$_2$Y-C11$_b$	Pt-Y	PtY$_3$-D0$_{11}$	PtY$_3$-D0$_{11}$
Au-Zr	Au$_3$Zr-D0$_a$	Au$_3$Zr-D0$_a$	Pt-Zr	Pt$_3$Zr-D0$_{24}$	Pt$_3$Zr-D0$_{24}$
Au-Zr	Au$_2$Zr-C11$_b$	Au$_2$Zr-C11$_b$	Pt-Zr	PtZr-B33	PtZr-B33
Au-Zr	AuZr$_2$-CuZr$_2$/C11$_b$	AuZr$_2$-CuZr$_2$ (paw-gga)	Rh-Ti	RhTi$_2$-C11$_b$ [9]/CuZr$_2$ [10]	RhTi$_2$-C11$_b$/CuZr$_2$
Au-Zr	AuZr$_3$-A15	AuZr$_3$-A15	Rh-Ti	αRhTi-L1$_0$	RhTi-L1$_0$
Cd-Pd	CdPd-β_1-L1$_0$	CdPd-L1$_0$	Rh-Ti	Rh$_3$Ti-L1$_2$	Rh$_3$Ti-L1$_2$
Cd-Pt	CdPt-α'_1-L1$_0$	CdPt-L1$_0$	Rh-Y	RhY$_3$-D0$_{11}$	RhY$_3$-D0$_{11}$
Cd-Ti	CdTi$_2$-C11$_b$	CdTi$_2$-C11$_b$	Rh-Y	RhY-B2	RhY-B2
Cd-Ti	CdTi-B11	CdTi-B11 (γCuTi)	Rh-Y	Rh$_2$Y-C15	Rh$_2$Y-C15
Cd-Y	CdY-B2	CdY-B2	Rh-Zr	RhZr$_2$-C16	RhZr$_2$-C16
Cd-Y	Cd$_2$Y-C6	Cd$_2$Y-C6	Rh-Zr	αRhZr-B27	RhZr-B27
Cd-Y	Cd$_3$Y-Cd$_3$Er	Cd$_3$Y-Cd$_3$Er	Rh-Zr	Rh$_3$Zr-L1$_2$	Rh$_3$Zr-L1$_2$
Cd-Zr	CdZr$_2$-C11$_b$	CdZr$_2$-C11$_b$	Ru-Ti	RuTi-B2	RuTi-B2
Cd-Zr	CdZr-B11	CdZr-B11 (paw-gga)	Ru-Y	RuY$_3$-D0$_{11}$	RuY$_3$-D0$_{11}$
Cd-Zr	Cd$_3$Zr-L1$_2$	Cd$_3$Zr-L1$_2$	Ru-Y	Ru$_2$Y-C14	Ru$_2$Y-C14
Mo-Pt	MoPt-B19	MoPt-B19	Ru-Zr	RuZr-B2	RuZr-B2
Mo-Pt	MoPt$_2$	MoPt$_2$	Tc-Ti	TcTi-B2	TcTi-B2
Mo-Rh	MoRh-B19	MoRh-B19	Tc-Y	Tc$_2$Y-C14	Tc$_2$Y-C14
Mo-Zr	Mo$_2$Zr-C15	Mo$_2$Zr-C15	Tc-Zr	Tc$_2$Zr-C14	Tc$_2$Zr-C14
Nb-Pd	NbPd$_2$-MoPt$_2$	NbPd$_2$-MoPt$_2$			

TABLE 5: Experimental compounds in agreement with *ab initio* solutions (89 entries).

B. Experimentally unknown, non-identified or speculated compounds and ab initio predictions

Experimental unknown/speculated compound ⇔ *ab initio* compound		
System	Experimental result	*Ab initio* result
Ag-Cd	β'-bcc ordered	AgCd-B2/B19/B27
Ag-Mg	cF* (unknown)	$AgMg_3$-$D0_{19}$ (hP8) / $D0_a$ (oP8)
Au-Cd	Au_3Cd-α_2-hP? (unknown)	Au_3Cd-$D0_{24}$/$D0_{19}$/Al_3Pu
Au-Cd	$\alpha'' \sim$ AuCd (unknown)	AuCd-$L1_0$/$FCC^{[201]}_{A2B2}$
Au-Cd	$\epsilon' \sim AuCd_3$ (unknown)	$AuCd_3$-$L6_0$
Au-Pd	Au_3Pd-$L1_2$ (speculated) (wide concentration range)	Au_3Pd-$D0_{23}$/$D0_{22}$/$L1_2$ Au_4Pd-$D1_a$/tie-line
Au-Pd	AuPd (speculated and unknown)	AuPd-$FCC^{[201]}_{A2B2}$
Au-Pd	$AuPd_3$-$L1_2$ (speculated)	$AuPd_3$-$D0_{23}$/$D0_{22}$/$L1_2$/tie-line
Au-Sc	$AuSc_2$-C37 (speculated)	$AuSc_2$-C37
Cd-Pd	γ'-(unknown)	Cd_3Pd-$D0_{19}$/$D0_{24}$/$NbPd_3$/Al_3Pu
Cd-Pt	γ_1-(unknown)	Cd_3Pt-$D0_{11}$/$D0_a$/$D0_{22}$
Cd-Pt	Cd_2Pt-(unknown)	Cd_2Pt-C37/C16/tie-line
Cd-Zr	cubic (unknown)	Cd_2Zr-$C11_b$
Mo-Pd	$MoPd_2$ $\sim MoPt_2$	$MoPd_2$-$ZrSi_2$
Mo-Rh	$MoRh_3$ (unknown)	$MoRh_3$-$CdMg_3$
Nb-Pt	Nb two-phase region$_{1-x}$Pt$_{1+x}$-B19	NbPt-$L1_0$
Pd-Ti	orthorhombic distortion of Pd_2Ti-$C11_b$	Pd_2Ti-$MoPt_2$ (distortion of $C11_b$)
Pd-Y	αPdY (unknown)	PdY-B27
Pt-Ru	PtRu-FCC (unknown)	PtRu-$FCC^{[001]}_{A2B2}$
Pt-Y	Pt_5Y (unknown)	Pt_5Y-$D2_d$ metastable
Tc-Zr	TcZr (unknown)	TcZr-B2

TABLE 6: Experimentally unknown, non-identified or speculated compounds and *ab initio* predictions (21 entries).

C. Experimental solid solutions, two-phases and “not studied” regions and possible ab initio predictions

Experimental non-compound ⇔ *ab initio* compound		
System	Experimental result	*Ab initio* result
Ag-Au	short-range order $\gtrsim$950°C	Ag_4Au-$D1_a$/tie-line
Ag-Au	short-range order $\gtrsim$950°C	Ag_3Au-$L1_2$/$D0_{23}$/Al_3Pu/$NbPd_3$/$D0_{22}$/$D0_{24}$
Ag-Au	short-range order $\gtrsim$950°C	Ag_2Au-C37/$MoPt_2$
Ag-Au	short-range order $\gtrsim$950°C	AgAu-$L1_0$
Ag-Au	short-range order $\gtrsim$950°C	$AgAu_2$-C37/$MoPt_2$
Ag-Au	short-range order $\gtrsim$950°C	$AgAu_3$-$L1_2$/$D0_{22}$/$D0_{23}$
Ag-Cd	fcc solid solution	Ag_3Cd-$D0_{22}$/$D0_{24}$
Ag-Cd	fcc solid solution	Ag_2Cd-C37
Ag-Cd	none	$AgCd_2$-$ZrSi_2$
Ag-Cd	hcp solid solution	$AgCd_3$-$D0_{19}$
Ag-Pd	solid solution $\gtrsim$900°C	AgPd-$L1_1$
Ag-Pd	solid solution $\gtrsim$900°C	Ag_2Pd-C37
Ag-Pd	solid solution $\gtrsim$900°C	Ag_3Pd- $L1_2$/$D0_{22}$
Ag-Y	two-phase region above 200°C	AgY_2-C37/tie-line (uncertain)
Ag-Y	two-phase region above 200°C	Ag_3Y-$D0_a$ (uncertain)
Ag-Zr	two-phase region above 700°C	$AgZr_3$-$FCC^{[001]}_{AB3}$/tie-line (uncertain)
Ag-Zr	two-phase region above 700°C	Ag_2Zr-C32
Al-Sc	two-phase region above 0°C	$AlSc_3$-$D0_{19}$
Au-Nb	two-phase region (calculated)	$AuNb_2$-$BCC^{[011]}_{AB2}$
Au-Pd	solid solution	Au_2Pd-C49/C37
Au-Ti	two-phase region above 500°C	Au_4Ti_3-Cu_4Ti_3/tie
Au-Y	not studied	AuY_2-C37
Au-Zr	two-phase region	Au_4Zr_3-Cu_4Ti_3 (unreliable)
Au-Zr	two-phase region	AuZr-B11/$FCC^{[001]}_{A2B2}$ (unreliable)
Cd-Pd	Pd phase above 100°C	$CdPd_3$-$D0_{22}$/$NbPd_3$
Cd-Pd	two-phase region above 100°C	$CdPd_2$-C37
Cd-Rh	not studied	Cd_2Rh-C37
Cd-Rh	not studied	Cd_3Rh-Al_3Pu
Cd-Ti	two-phase region above 200°C	Cu_4Ti_3/tie-line
Cd-Y	not studied/two-phase region	CdY_2-C37
Cd-Zr	not studied/two-phase region	$CdZr_3$-A15
Mo-Nb	not studied	$MoNb_2$-$C11_b$
Mo-Nb	not studied	MoNb-B2
Mo-Nb	not studied	Mo_2Nb-$C11_b$
Mo-Nb	not studied	Mo_3Nb -$D0_3$
Mo-Pd	disorder fcc Pd-A1	$MoPd_4$-$D1_a$
Mo-Pt	two-phase region $MoPt_2$↔Pt	$MoPt_4$-$D1_a$
Mo-Rh	two-phase region above 900°C	Mo_2Rh-C37
Mo-Ru	disorder hcp Ru-A3 above 800°C	$MoRu_3$-$D0_{19}$
Mo-Ti	not studied/two-phase region above 400°C	$MoTi_3^{proto}$/tie-line (uncertain), Appendix (XI)
Mo-Ti	not studied/two-phase region above 400°C	$MoTi_2$-$BCC^{[211]}_{AB2}$
Mo-Ti	not studied/two-phase region above 400°C	$MoTi^{proto}$, Appendix (XI)
Mo-Ti	not studied/two-phase region above 400°C	Mo_2Ti-$C11_b$
Mo-Ti	not studied/two-phase region above 400°C	Mo_3Ti^{proto}, Appendix (XI)
Mo-Ti	not studied/two-phase region above 400°C	Mo_4Ti-$D1_a$/tie-line
Mo-Ti	not studied/two-phase region above 400°C	Mo_5Ti^{proto}, Appendix (XII)
Mo-Zr	two-phase region above 400°C	$MoZr_5^{proto}$/tie-line, Appendix (XII) (uncertain)
Mo-Zr	two-phase region above 400°C	$MoZr_3^{proto}$/tie-line, Appendix (XII) (uncertain)
Mo-Zr	two-phase region above 400°C	∼ $MoTi^{proto}$ (uncertain) (∼2meV above two-phase reg.)

TABLE 7a: Experimental solid solutions, two-phases and “not studied” regions and possible *ab initio* predictions. The table continues in the next page.

Experimental non-compound ⇔ *ab initio* compound		
System	Experimental result	*Ab initio* result
Nb-Pd	two-phase region above 700°C	Nb$_2$Pd-BCC$^{[011]}_{AB2}$
Nb-Ru	disorder Nb-A2	Nb$_5$Ru ^{proto}, Appendix (XII)
Nb-Ru	disorder Nb-A2	Nb$_3$Ru-D0$_3$
Nb-Ru	two-phase region above 700°C	NbRu$_2$-C37
Nb-Tc	not studied/unknown	Nb$_3$Tc^{proto}, Appendix (XI)
Nb-Tc	not studied/unknown	Nb$_2$Tc-C11$_b$
Nb-Tc	not studied/unknown	NbTc-B2
Pd-Pt	two-phase region Pd↔Pt	Pd$_3$Pt^{proto}/tie-line (uncertain), Appendix (XI)
Pd-Pt	two-phase region Pd↔Pt	PdPt-L1$_1$
Pd-Pt	two-phase region Pd↔Pt	PdPt$_3^{proto}$, Appendix (XI)
Pd-Tc	two-phase region above ∼1000°C	PdTc$_3$-D0$_{19}$
Pd-Y	two-phase region	PdY$_2$-C37 (uncertain)
Pd-Zr	two-phase region	PdZr$_3$-FCC$^{[001]}_{AB3}$ (uncertain)
Pt-Rh	two-phase region Pt↔Rh [9], D1$_a$ [262]	Pt$_4$Rh-D1$_a$
Pt-Rh	two-phase region Pt↔Rh	Pt$_3$Rh-D0$_{22}$
Pt-Rh	two-phase region Pt↔Rh	PtRh-NbP
Pt-Rh	two-phase region Pt↔Rh	PtRh$_2$-C49
Pt-Rh	two-phase region Pt↔Rh	PtRh$_3$-D0$_{22}$
Pt-Rh	two-phase region Pt↔Rh [9], D1$_a$ [262]	PtRh$_4$-D1$_a$
Pt-Ru	disorder Pt-A1	Pt$_3$Ru-FCC$^{[001]}_{AB3}$/tie-line (uncertain)
Pt-Tc	disorder Pt-A1	Pt$_3$Tc-FCC$^{[001]}_{AB3}$
Pt-Tc	two-phase region above ∼1000°C	PtTc$_3$-D0$_{19}$
Pt-Zr	two-phase region above 600°C	PtZr$_2$-C16 (uncertain)
Pt-Zr	two-phase region above 600°C	PtZr$_3$-A15 (uncertain)
Rh-Ru	solid solution Ru-A3	RhRu$_2$^{proto}
Rh-Ru	solid solution Ru-A3	RhRu^{proto}
Rh-Tc	solid solution Tc-A3	RhTc$_3$-D0$_{19}$
Rh-Tc	solid solution Tc-A3	RhTc-B19
Rh-Tc	two-phase region above 1000°C	Rh$_2$Tc$_2$-ZrSi$_2$
Rh-Ti	two-phase region above 600°C	Rh$_2$Ti-C37
Rh-Y	two-phase region above 0°C	RhY$_2$-C37 (uncertain)
Rh-Zr	two-phase region above 0°C	RhZr$_4$-D1$_a$/tie-line
Rh-Zr	two-phase region above 0°C	RhZr$_3$-FCC$^{[001]}_{AB3}$/tie-line
Rh-Zr	two-phase region above 0°C	Rh$_2$Zr-C37/tie-line
Ru-Tc	disorder solution (Ru,Tc)-A3	RuTc$_3$-D0$_{19}$
Ru-Tc	disorder solution (Ru,Tc)-A3	RuTc-B19
Ru-Tc	disorder solution (Ru,Tc)-A3	Ru$_3$Tc-D0$_{19}$
Ru-Ti	two-phase region above 600°C	RuTi$_3^{proto}$, Appendix (XI)
Ru-Ti	two-phase region above 600°C	RuTi$_2$-C49
Ru-Y	two-phase region above 0°C	RuY$_2$-C16 (uncertain)
Ru-Zr	two-phase region above 400°C	RuZr$_4$-D1$_a$
Tc-Ti	disorder βTi-A2	TcTi$_3^{proto}$, Appendix (XI)
Tc-Ti	disorder βTi-A2	TcTi$_2$-C49
Tc-Ti	two-phase region TcTi↔χ	Tc$_2$Ti-C11$_b$
Tc-Y	no information	TcY$_3$-D0$_{11}$
Tc-Zr	no information	TcZr$_4$-D1$_a$
Tc-Zr	no information	TcZr$_2$-C49

TABLE 7b: Experimental solid solutions, two-phases and “not studied” regions and possible *ab initio* predictions (Table 7a + Table 7b = 96 entries). The table starts in the previous page.

D. Experimental compounds that could not be checked by our calculations

Experimental compound ⇔ unavailable compound		
System	Experimental result	*Ab initio* result
Ag-Mg	$AgMg_4$-hP* (unknown)	unknown experimental compound
Ag-Y	$Ag_{51}Y_{14}$-$Ag_{51}Gd_{14}$	unavailable prototype
Au-Cd	η' (unknown)	unknown experimental compound
Au-Cd	$\alpha_1 Au_3Cd$-Ag_3Mg	unavailable prototype
Au-Cd	Au_3Cd_5-$D8_m$	unknown experimental compound
Au-Nb	Au_2Nb_3 (unknown)	unknown experimental compound
Au-Ti	βAuTi-B19	unavailable prototype off-stoichiometry B19
Au-Y	AuY_3 (unknown)	unknown experimental compound
Au-Zr	Au_4Zr (oP20 - Pnma)	unavailable prototype
Au-Zr	$Au_{10}Zr_7$ (tI34)	unavailable prototype
Au-Zr	Au_4Zr_5 (unknown prototype)	unknown experimental compound
Cd-Pd	γ_1-(unknown)	unknown experimental compound
Cd-Pd	γ-$D8_3$	unavailable prototype
Cd-Pt	γ-(unknown)	unknown experimental compound
Cd-Pt	γ_2-(unknown)	unknown experimental compound
Cd-Y	$Cd_{45}Y_{11}$-$Cd_{45}Sm_{11}$	unavailable prototype
Cd-Y	$Cd_{58}Y_{13}$-$Pu_{13}Zn_{58}$	unavailable prototype
Cd-Y	Cd_6Y	unavailable prototype
Mo-Pt	ϵ'-$D0_{19}$ above 1000°C	unavailable prototype off-stoichiometry $D0_{19}$
Nb-Pt	$D8_b$	unavailable prototype σ phase
Nb-Rh	$\sigma(Nb_{13}Rh_7)$-$D8_b$	unavailable prototype
Nb-Rh	$\xi(Nb_2Rh_3)$-Nb_2Rh_3	unavailable prototype
Nb-Tc	$NbTc_3$,$Nb_{0.15}Tc_{0.85}$-αMn	unavailable prototype
Pd-Ti	$Pd_3Ti_2 \sim Au_2V$	unavailable prototype
Pd-Ti	$Pd_5Ti_3 \sim C11_b$	unavailable prototype
Pd-Y	unknown at 66.6% Pd	unknown experimental compound
Pd-Y	unknown at 87.5% Pd	unknown experimental compound
Pd-Y	Pd_2Y_5 (unknown)	unknown experimental compound
Pd-Y	Pd_2Y_3-hR15 (unknown)	unknown experimental compound
Pd-Y	Pd_4Y_3-hR14 (unknown)	unknown experimental compound
Pd-Y	αPd_3Y_2 (unknown)	unknown experimental compound
Pt-Ti	Pt_8Ti-$D1_\alpha$	unavailable prototype off-stoichiometry $D1_\alpha$
Pt-Ti	Pt_2Ti-$ReSi_2$	unavailable prototype
Pt-Y	Pt_4Y_3-Pd_4Pu_3	unavailable prototype
Pt-Y	Pt_4Y_5-Pu_5Rh_4	unavailable prototype
Pt-Y	Pt_3Y_7-$D10_2$	unavailable prototype
Rh-Ti	Rh_5Ti (unknown)	unknown experimental compound
Rh-Ti	Rh_5Ti_3-Ge_3Rh_5	unavailable prototype
Rh-Y	Rh_3Y (unknown), hP24-$P6_3$/mmc	unknown experimental compound
Rh-Y	Rh_3Y_7-$D10_2$	unavailable prototype
Rh-Y	Rh_3Y_5 (unknown)	unknown experimental compound
Rh-Y	Rh_2Y_3 (unknown), tI140-I4/mcm	unknown experimental compound
Rh-Zr	Rh_4Zr_3 (unknown)	unknown experimental compound
Rh-Zr	Rh_5Zr_3-Pd_3Pu_3	unavailable prototype
Ru-Y	Ru_2Y_5-C_2Mn_5	unavailable prototype
Ru-Y	$Ru_{25}Y_{44}$ (unknown)	unknown experimental compound
Tc-Ti	χ-A12	unavailable prototype
Tc-Zr	Tc_6Zr-A12	unavailable prototype

TABLE 8: Experimental compounds that could not be checked by our calculations, because the proper structure prototype or concentration is not known or not in our library. The table contains 21 *"unknown experimental compounds"* and 27 *"unavailable prototypes"* (48 entries total).

E. Experimental compounds in disagreement with other ab initio compounds or two-phase regions

Experimental compound ⇔ *ab initio* wrong compound or two-phases					
System	Experimental result	*Ab initio* result	ΔE_f (us-lda) (meV/atom)	ΔE_f *(paw-gga) (meV/atom)*	Note
Au-Nb	$AuNb_3$-A15	two-phase region	7	6.5	(a)
Au-Y	AuY-B2 [170]	AuY-B33	26	25	(b)
Cd-Nb	Cd_3Nb-$L1_2$	immiscible system	70	>100	(c)
Cd-Pt	$CdPt_3 - \alpha'$-$L1_2$ [181]	$CdPt_3^{proto}$, Appendix (XI)	25	10.4	(b)
Nb-Rh	$\kappa(NbRh_3)$-$L1_2$	$NbRh_3$-Al_3Pu	8	5.3	(a)
Nb-Ru	$NbRu_3$-$L1_2$	$NbRu_3$-$D0_{24}$	8	2.5	(a)
Nb-Ru	$NbRu'$-$L1_0$	two-phase region	20	4	(a)
Pt-Y	PtY-B27	PtY-B33	50	60	(c)
Pt-Zr	Pt_3Zr_5-$D8_8$	two-phase region	36	23	(c)

TABLE 9: Experimental compounds (which we have in the library as prototypes) in disagreement with other *ab initio* compounds or two-phase regions. We include the differences between the formation energies of the phases in disagreement, both for US-LDA and PAW-GGA potentials. (9 entries). Note **(a)**: the *ab initio* ground state is within less than 10meV/atom of the experimental ground state (4). Note **(b)**: the assigned experimental structures are poorly justified (2) [170,181]. Note **(c)**: unambiguous significant disagreement (3).

XI. APPENDIX: NEW STRUCTURE PROTOTYPES WHICH ARE SUPERSTRUCTURES OF FCC, BCC, HCP

System	$CdPt_3$, $PdPt_3$, Pd_3Pt	MoTi,	$MoTi_3$, Mo_3Ti, Nb_3Tc, $RuTi_3$, $TcTi_3$	RhRu	$RhRu_2$
Superlattice	FCC AB_3	BCC A_2B_2	BCC AB_3	HCP A_2B_2	HCP A_2B_4
Lattice	Orthorhombic	Orthorhombic	Orthorhombic	Trigonal	Orthorhombic
Space Group	Cmmm #65	Imma #74	Immm #71	$P\bar{3}m1$ #164	Cmcm #63
Pearson symbol	oC8	oI8	oI8	hP4	oC12
Primitive vectors (cart.)					
$\mathbf{a}_1$/a	$(1, -1/2, 1/2)$	$(3/2, 1/2, -1/2)$	$(3/2, 1/2, -1/2)$	$(1/2, -\sqrt{3}/2, 0)$	$(-1/2, 3\sqrt{3}/2, 0)$
$\mathbf{a}_2$/a	$(-1, -1/2, 1/2)$	$(1/2, 3/2, 1/2)$	$(1/2, 3/2, 1/2)$	$(1/2, \sqrt{3}/2, 0)$	$(-1/2, -3\sqrt{3}/2, 0)$
$\mathbf{a}_3$/a	$(0 - 1/2, -1/2)$	$(-1/2, -3/2, 1/2)$	$(-1/2, -3/2, 1/2)$	$(0, 0, 2\sqrt{8/3})$	$(0, 0, \sqrt{8/3})$
Atomic positions (fract.)					
A1	$(0, 0, 0)$	$(0, 0, 0)$	$(0, 0, 0)$	$(0, 0, 0)$	$(0, 0, 0)$
A2	–	$(1/4, 3/4, 1/2)$	–	$(1/3, 2/3, 1/4)$	$(5/9, 4/9, 1/2)$
B1	$(0, 1/2, 1/2)$	$(1/2, 1/2, 0)$	$(1/4, 3/4, 1/2)$	$(0, 0, 1/2)$	$(2/9, 7/9, 1/2)$
B2	$(1/2, 0, 1/2)$	$(3/4, 1/4, 1/2)$	$(1/2, 1/2, 0)$	$(1/3, 2/3, 3/4)$	$(1/3, 2/3, 0)$
B3	$(1/2, 1/2, 0)$	–	$(3/4, 1/4, 1/2)$	–	$(2/3, 1/3, 0)$
B4	–	–	–	–	$(8/9, 1/9, 1/2)$

TABLE 10. Geometry of FCC, BCC, HCP superstructures which appear as new prototypes in our study. Positions are given as unrelaxed positions in the parent lattice.

XII. APPENDIX: RELAXED STRUCTURE PROTOTYPES

System	$MoZr_3$ (AB_3)	Mo_5Ti^* (AB_5)	$MoZr_5^*$ (AB_5)	Nb_5Ru^* (AB_5)
Lattice	Orthorhombic	Monoclinic	Monoclinic	Monoclinic
Space Group	Imma #74	C2/m #12	C2/m #12	C2/m #12
Prototype	$MoZr_3$	Mo_5Ti see note*	Mo_5Ti see note*	Mo_5Ti see note*
Primitive vectors				
(a, b, c) (Å)	$(5.678, 5.678, 5.678)$	$(5.192, 5.192, 9.879)$	$(5.695, 5.695, 10.881)$	$(5.339, 5.339, 10.178)$
(α, β, γ) degrees	$(145.5, 128.9, 63.1)$	$(139.8, 139.8, 35.0)$	$(138.5, 138.5, 34.1)$	$(139.8, 139.8, 35.1)$
Atomic positions (fract.)				
A1	$(0, 0, 0)$	$(0, 0, 0)$	$(0, 0, 0)$	$(0, 0, 0)$
B1	$(0.259, 0.722, 0.537)$	$(0.166, 0.166, 0.833)$	$(0.205, 0.205, 0.864)$	$(0.170, 0.170, 0.836)$
B2	$(0.524, 0.500, 0.024)$	$(0.334, 0.334, 0.665)$	$(0.349, 0.349, 0.692)$	$(0.335, 0.335, 0.672)$
B3	$(0.815, 0.278, 0.537)$	$(0.500, 0.500, 0.499)$	$(0.495, 0.495, 0.513)$	$(0.501, 0.501, 0.500)$
B4	–	$(0.667, 0.667, 0.334)$	$(0.642, 0.642, 0.313)$	$(0.666, 0.666, 0.328)$
B5	–	$(0.834, 0.834, 0.166)$	$(0.800, 0.800, 0.160)$	$(0.831, 0.831, 0.164)$

TABLE 11. Geometry of relaxed structures which appear as new prototypes in our study. Positions are given as fractional positions of the primitive vectors. Note *: Mo_5Ti, $MoZr_5$, and Nb_5Ru are slight distorsion of the prototype Mo_5Ti^{proto}, monoclinic lattice, space group C2/m #12, with atoms in the following Wyckoff positions: Ti in 2a, Mo(1) in 2c, Mo(2) in 4i ($x = 1/3, z = 1/6$), Mo(3) in 4i ($x = 2/3, z = 1/3$), and primitive vectors $\mathbf{a}_1$/a=$(3.171, 1, 0)$, $\mathbf{a}_2$/a=$(-0.315, 1, 0)$, $\mathbf{a}_3$/a=$(-0.638, -0.201, 1.987)$ [17].

REFERENCES

[1] D. de Fontaine, in *Solid State Physics*, edited by H. Ehrenreich and D. Turnbull (Academic Press 1994), Vol. 47, pp. 33-176.

[2] M. Sluiter, P. Turchi, F. Zezhong, and D. de Fontaine, *Tight Binding Calculation of Ti-Rh-Type Phase Diagram*, Phys. Rev. Lett. **60**, 716 (1988).

[3] S. Curtarolo, D. Morgan, K. Persson, J. Rodgers, and G. Ceder, Phys. Rev. Lett. **91**, 135503 (2003).

[4] S. Curtarolo, H. Cocks, and A. N. Kolmogorov, *High-Throughput ab initio analysis of the Bi-Mg, Bi-In, In-Mg, Mg-Sb, In-Sb, and Bi-Sb systems*, submitted (2005).

[5] S. Curtarolo and A. N. Kolmogorov, *Prediction of possible metastable alloy phases in the Mg-B system*, internal report (2004).

[6] D. Morgan, G. Ceder, and S. Curtarolo, Mat. Res. Soc. Symp. Proc. **804**, JJ9.25 (2004).

[7] D. Morgan, G. Ceder, and S. Curtarolo, J. Measurement Science & Technology, Special Feature Combinatorial and High-Throughput Materials Research, Meas. Sci. Technol. **16**, 296-301 (2005).

[8] Y. Wang, S. Curtarolo, C. Jiang, R. Arroyave, T. Wang, G. Ceder, L.-Q. Chen, and Z.-K. Liu, Calphad **28**, 79 (2004).

[9] *Binary Alloy Phase Diagrams*, edited by T. B. Massalski (ASM International, Metals Park, OH, 1992)

[10] P. Villars, K. Cenzual, J. L. C. Daams, F. Hulliger, T. B. Massalski, H. Okamoto, K. Osaki, A. Prince, and S. Iwata, Crystal Impact, *Pauling File. Inorganic Materials Database and Design System*, Binaries Edition, ASM International, Metal Park, OH (2003)

[11] P. S. White, J. R. Rodgers, and Y. Le Page, CRYSTMET*: a database of the structures and powder patterns of metals and intermetallics*, Acta Cryst. B **58**, 343 (2002).

[12] J. M. Sanchez and D. de Fontaine, *Theoretical Prediction of Ordered Superstructures in Metallic Alloys*, in "Structure and Bonding in Crystals", Vol. II, Academic Press (1981).

[13] Z. W. Lu, S.-H. Wei, A. Zunger, S. Frota-Pessoa, and L. G. Ferreira, Phys. Rev. B **44**, 512 (1991).

[14] C. Wolverton and A. Zunger, Phys. Rev. B **50**, 10548 (1994).

[15] S. Curtarolo, *Coarse-Graining and Data Mining Approaches to the Prediction of Structures and their Dynamics*, Ph.D. Thesis, MIT (2003).
Download: burgaz.mit.edu and alpha.mems.duke.edu

[16] Appendix B, pp. 196-210 of reference [15].

[17] *International Table of Crystallography*, edited by T. Hahn, (Kluwer Academic Publishers, 2002)

[18] J. P. Perdew and A. Zunger, Phys. Rev. B **23**, 5048 (1981).

[19] D. Vanderbilt, Phys. Rev. B **41**, 7892 (1990).

[20] G. Kresse and J. Furthmuller, Comput. Mater. Sci. **6**, 15 (1996).

[21] H. J. Monkhorst and J. D. Pack, Phys. Rev. B **13**, 5188 (1976).

[22] H. J. Monkhorst and J. D. Pack, Phys. Rev. B **16**, 1748 (1977).

[23] P. E. Blöchl, Phys. Rev. B **50**, 17953 (1994).

[24] G. Kresse and D. Joubert, Phys. Rev. B **59**, 1758 (1999).

[25] J. P. Perdew and Y. Wang, Phys. Rev. B **45**, 13244 (1992).

[26] J. B. Neaton and N. W. Ashcroft, Phys. Rev. Lett. **86**, 2830 (2001).

[27] A. K. McMahan and J. A. Moriarty, Phys. Rev. B **27**, 3235 (1983).

[28] J. E. Jaffe, Z. Lin, and A. C. Hess, Phys. Rev. B **57**, 11834 (1998).

[29] M. M. Dacorogna and M. L. Cohen, Phys. Rev. B **34**, 4996 (1986).

[30] M. I. Katsnelson, G. V. Sinko, N. A. Smirnov, A. V. Trefilov, and K. Yu. Khromov, Phys. Rev. B **61**, 14420 (2000).

[31] C. S. Barrett and O. R. Trautz, Trans. Am. Inst. Min. Metall. Pet. Eng. **175**, 579 (1948).

[32] S. Barrett, Acta Crystallogr. **9**, 671 (1956).

[33] A. W. Overhauser, Phys. Rev. Lett. **53**, 64 (1984).

[34] G. Ernst, C. Artner, O. Blaschko, and G. Krexner, Phys. Rev. B **33**, 6465 (1986).

[35] H. G. Smith, R. Berliner, J. D. Jorgensen, M. Nielsen, and J. Trivisonno, Phys. Rev. B **41**, 1231 (1990).

[36] W. Schwarz and O. Blaschko, Phys. Rev. Lett. **65**, 3144 (1990).

[37] W. Schwarz, O. Blaschko, and I. Gorgas, Phys. Rev. B **44**, 6785 (1991).

[38] O. Blaschko, V. Dmitriev, G. Krexner, P. Tolèdano, Phys. Rev. B **59**, 9095 (1999).

[39] L. Vegard, Z. Phys. **5**, 17 (1921).

[40] The reference CPU is Compaq/HP - Alpha 21264 EV67 667MHz.

[41] M. Hansen and K. Anderko, *Constitution of Binary Alloys*, McGraw-Hill, New-York (1958).

[42] W. B. Pearson, *Handbook of Lattice Spacings and Structures of Metals and Alloys*, Metals Park, Oh: American Society for Metals (1985).

[43] W. G. Moffatt, Ed., *Handbook of Binary Phase Diagrams*, Business Growth Services, General Electric Co., Schenectady, NY (1976).

[44] F. A. Shunk, *Constitution of Binary Alloys, Second Supplement*, McGraw-Hill, New-York; General Electric Co., Business Growth Services, Schenectady, New York (1969).

[45] M. Venkatraman, J. P. Neumann, *Phase Diagrams of Binary Titanium Magnesium*, ASM International (1988).

[46] L. Brewer, *Molybdenum: Physico-Chemical Properties of its Compounds and Alloys*, edited by O. Kubaschewski, Atomic Energy Review Special Issue No. 7, International Atomic Energy Agency, Vienna (1980).

[47] V. I. Lavrentev, Ya. I. Gerassimov, P. Feschotte, D.

T. Livey, O. von Goldbeck, H. Nowotny, K. Seifert, R. Ferro, A. L. Dragoo, *Niobium: Physico-Chemical Properties of its Compounds and Alloys*, edited by O. Kubaschewski, Atomic Energy Review Special Issue No. 2, International Atomic Energy Agency, Vienna (1968).

[48] J. L. Murray, *Phase Diagrams of Binary Titanium Alloys*, ASM International (1987).

[49] C. B. Alcock, K. T. Jacob, S. Zador, O. von Goldbeck, H. Nowotny, K. Seifert, O. Kubaschewski, *Zirconium: Physico-Chemical Properties of its Compounds and Alloys*, edited by O. Kubaschewski, Atomic Energy Review Special Issue No. 6, International Atomic Energy Agency, Vienna (1976).

[50] D. R. Lide (editor), *CRC Handbook of Chemistry and Physics*, CRC Press Inc., Cleveland, OH (2003).

[51] L. Kaufman, Calphad **14**, 163 (1990).

[52] C. Wagner, Acta Metall. **2**(2), 242 (1954).

[53] J. L. White, R. L. Orr, and R. Hultgren, Acta Metall. **5**(12), 747 (1957).

[54] J. L. White, Trans. AIME **215**(1), 178 (1959).

[55] C. J. Cooke and W. Hume-Rothery, Acta Metall. **9**(10), 982 (1961).

[56] S.-H. Wei, A. A. Mbaye, L. G. Ferreira, and A. Zunger, Phys. Rev. B **36**, 4163 (1987).

[57] T. Mohri, K. Terakura, T. Oguchi, and K. Watanabe, Acta Metall. **36**, 547 (1988).

[58] R. A. Johnson, Phys. Rev. B **41**, 9717 (1990).

[59] T. Mohri, K. Terakura, S. Takizawa, and J. M. Sanchez, Acta. Metall. Mater. **39**, 493 (1991).

[60] T. Mohri, S. Takizawa, and K. Terakura, J. Physics: Cond. Matt. **5**, 1473 (1993).

[61] Z. W. Lu, B. M. Klein, and A. Zunger, Superlattice Microst. **18**, 161 (1995).

[62] Z. W. Lu, B. M. Klein, and A. Zunger, J. Phase Equilib. **16**, 36 (1995).

[63] Z. W. Lu, B. M. Klein, and A. Zunger, Model. Simul. Mater Sc. **3**, 753 (1995).

[64] V. Ozolins, C. Wolverton, and A. Zunger, Phys. Rev. B **57**, 4816 (1998).

[65] V. Ozolins, C. Wolverton, and A. Zunger, Phys. Rev. B **57**, 6427 (1998).

[66] A. Zunger, L. G. Wang, G. L. W. Hart, and M. Sanati, Model. Simul. Mater Sc. **10**, 685 (2002).

[67] A. Tonejc, A. M. Tonejc, and A. Bonefacic, Phys. Lett. A **49**, 145 (1974).

[68] O. S. Zarechnyuk and V. V. Kinzhibalo, Russ. Metall. **6**, 153 (1978).

[69] Y. Matsuo, S. Minamigawa, and K. Katada, Script. Metall. **12**, 821 (1978).

[70] Y. Matsuo, T. Makita, T. Suzuki, and A. Nagasawa, J. Phys. Soc. Japan **50**, 1209 (1981).

[71] W. Hume-Rothery and E. Butchers, J. Inst. Met. **60**, 345 (1937).

[72] R. J. M. Payne and J. L. Haughton, J. Inst. Met. **60**, 351 (1937).

[73] K. Schubert, B. Kiefer, M. Wilkens, and R. Haufler, Z. Metallkd. **46**, 1692 (1955).

[74] K. Fujiwara, M. Hirabayashi, D. Watanabe, and S. Ogawa, J. Phys. Soc. Japan **13**, 167 (1958).

[75] M. V. Prokof'ev and V. E. Kolesnichenko, Inorg. Mater. **21**(8), 1168 (1985).

[76] J. Kulik, S. Takeda, and D. de Fontaine, Acta Metall. **35**(5), 1137 (1987).

[77] V. E. Kolesnichenko, V. V. Karonik, S. N. Tsyganova, T. A. Kupriyanova, and L. N. Sysoeva, Russ. Metall. (5) 199 (1988).

[78] Y. Liu, R. G. Jordan, and S. L. Qiu, Phys. Rev. B **49**, 4478 (1994).

[79] O. I. Velikokhatnyi, S. V. Eremeev, I. I. Naumov, and A. I. Potekaev J. Physics: Cond. Matt. **12**, 8825 (2000).

[80] N. M. Rosengaard and H. L. Skriver, Phys. Rev. B **49**, 14666 (1994).

[81] F. V. Linen, Trans. Metall, Soc. AIME **175**, 878 (1948).

[82] X. D. Dai, H. R. Gong, and B. X. Liu, J. Phys. Soc. Jpn. **73**, 1222 (2004).

[83] G. J. Lamprecht and P. Crowther, Trans. AIME **242**, 2169 (1968).

[84] J. R. Weeks, Trans. ASM **62**, 304 (1969).

[85] M. W. Chase, Bull. Alloy Phase Diagrams **4**, 124 (1983).

[86] R. Kieffer, H. Nowotny, Metallwissenschaft Technick **17**, 669 (1963).

[87] M. R. Baren, Bull. Alloy Phase Diagrams **10**(6) (1989).

[88] I. Karakaya, and W. T. Thompson, Bull. Alloy Phase Diagrams **9** (3) (1988).

[89] N. V. Skorodumova, S. I. Simak, E. A. Smirnova, and Yu. Kh. Vekilov, Phys. Lett. A **208**, 157-60 (1995).

[90] E. Bruno, B. Ginatempo, E. S. Guiliano, A. V. Ruban, and Yu. Kh. Vekilov, Phys. Rep. **249**, 353 (1994).

[91] E. Bruno, B. Ginatempo, and E. S. Giuliano, Phys. Rev. B **52**, 14544 (1995).

[92] E. Bruno, B. Ginatempo, and E. S. Giuliano, Nuovo Cimento D **20**D, 1367-76 (1998).

[93] W. Olovsson, I. A. Abrikosova, and B. Johansson, J. Electron Spectrosc. Relat. Phenom. **127**, 65-9 (2002).

[94] A. A. Rudnitskii and A. N. Khotinskaya, Russ. J. Inorg. Chem. **4**, 1053 (1959).

[95] I. Barin, O. Knacke, and O. Kubaschewski, *Thermodynamical Properties of Inorganic Substances (Supplement)*, 590, Springer-Verlag, Berlin (1977).

[96] I. Karakaya and W. T. Thompson, Bull. Alloy Phase Diagrams **7**(4), 259 (1986).

[97] A. A. Rudnitskii and O. A. Novikova, Russ. J. Inorg. Chem. **4**, 719 (1959).

[98] J. H. Li, L. T. Kong, and B. X. Liu, J. Phys. Chem. B **108**, 16071-16076 (2004).

[99] B. B. Gulyaev and G. F. Dvorshkaya, in *Phase Diagrams of Metallic Systems*, E. M. Savitskii, Ed., Nauka Pub., Moscow, 267 (1968).

[100] V. N. Emerenko, Y. I. Buyanov, and N. M. Panchenko, Sov. Powder Metall. Met. Cer. **8**(7), 562 (1969).

[101] M. R. Plichta and H. I. Aaronson, Acta Metall. **26**, 1293 (1978).

[102] E. Gebhardt, M. von Erdberg, and U. Lüty, Nucl. Met. **10**, 303 (1964).

[103] K. A. Gschneidner, O. D. McMasters, D. G.Alexander, and R. F. Venteicher, Metall. Trans. **1**, 1961 (1970).

[104] O. D. McMasters, K. A. Gschneidner, and R. F. Venteicher, Acta Crystallogr. B**26** 1224 (1970).

[105] I. Barin, O. Knacke, and O. Kubaschewski, *Thermochemical Properties of Inorganic Substances*, Springer-Verlag, Berlin (1977).

[106] I. Karakaya and W. T. Thompson, Bull. Alloy Phase Diagrams **8**(4), 326 (1987).

[107] O. P. Naumkin, V. F. Terekhova, and E. M. Savitskii, Russ. Metall. (4) 176 (1965).

[108] M. E. Drits, E. S. Kadaner, T. V. Dobatkina, and N. I. Turkina, Russ. Metall. (4) 152 (1973).

[109] S. Fujikawa, M. Sugaya, H. Takei, and K. Hirano, J. Less-Common Met. **63**, 87 (1979).

[110] H. Anton and P. C. Schmidt, Intermetallics **5**, 449-65 (1997).

[111] M. Asta, S. M. Foiles, and A. A. Quong, Phys. Rev. B **57**, 11265 (1998)

[112] M. Asta and V. Ozolins, Phys. Rev. B **64**, 094104 (2001).

[113] V. Ozolins and M. Asta, Phys. Rev. Lett. **86**, 448 (2001).

[114] B. Mayer, H. Anton, E. Bott, M. Methfessel, J. Sticht, J. Harris, and P. C. Schmidt, P.C. Intermetallics **11**, 23-32 (2003).

[115] E. Clouet, M. Nastar, and C. Sigli, Phys. Rev. B **69**, 64109 (2004).

[116] H. Okamoto and T. B. Massalski, Bull. Alloy Phase Diagrams **5**(4) (1984).

[117] H. Okamoto and T. B. Massalski, Bull. Alloy Phase Diagrams **6**(1) (1985).

[118] T. B. Massalski, H. Okamoto, and L. Brewer, Bull. Alloy Phase Diagrams **7**(5) (1986).

[119] T. B. Massalski, H. Okamoto, and L. Brewer, in *Phase Diagrams of Binary Gold Alloys*, ASM International (1987).

[120] L. Dreibholz, Z. Phys. Chem. **108**, 1 (1924).

[121] G. A. Geach and E. Summersmith, J. Inst. Met. **82**, 471 (1953).

[122] J. A. Rodriguez and M. Kuhn, Surf. Sci. **330**, L657-64 (1995).

[123] H. Hirabayashi and S. Ogawa, Acta Metall. **9**(4), 264 (1961).

[124] J. D. Filby and J. N. Pratt, Trans. Faraday Soc. **60**, 1934 (1964).

[125] M. Hirabayashi, K. Hiraga, S. Yamaguchi, and N. Ino, J. Phys. Soc. Jpn. **27**(1), 80 (1969).

[126] K. L. Komarek, E. Reiffenstein, and G. Stummerer, Monatsh. Chem. **104**(6), 1570 (1973).

[127] E. A. Wood and B. T. Matthias, Acta Crystallogr. **9**, 534 (1956).

[128] A. E. Dwight, Metall. Soc. Conf. Proc. **10**, 383 (1961).

[129] R. Flükiger, P. Spitzli, F. Helniger, and J. Muller, Phys. Lett. A **29**, 407 (1969).

[130] M. Bernasson, P. Descouts, R. Flükiger, and A. Treyvaud, Solid State Comm. **8**, 837 (1970) .

[131] E. Ehrenfreund, A. C. Gossard, and J. H. Wernick, Solid State Comm. **8**, 1925 (1970).

[132] E. Röschel, C. J. Raub, and O. Loebich, Jr., Z. Metallkd. **64**(5), 359 (1973).

[133] H. R. Khan, E. Röschel, and C. J. Raub, Z. Physik **262**, 279 (1973).

[134] E. Z. Kurmaev, F. Werfel, O. Brümmer, and R. Flükiger, Solid State Comm. **21**, 239 (1977).

[135] R. Flükiger, S. Foner, E. J. McNiff Jr., and O. Fischer, Solid State Comm. **30**, 723 (1979).

[136] M. S. Wire and G. W. Webb, J. Phys. Chem. Solids **42**, 233 (1981).

[137] N. Savvides, C. M. Hurd, and S. P. McAlister, Solid State Comm. **41**, 735 (1982).

[138] M. S. Wire, G. W. Webb, D. E. Cox, C. L. Snead Jr., and A. R. Sweedler, Solid State Comm. **48**, 125 (1983).

[139] S. Ramakrishnan, G. Chandra, and M. C. Saxena, Physica B & C **141**, 185 (1986).

[140] L. M. Di and H. Bakker, J. Phys. Cond. Matt. **3**, 9319 (1991).

[141] M. Baier, R. Wordel, F. E. Wagner, T. E. Antonova, aV. E. Antonov, J. Less-Common Met. **172/174**, 358 (1991).

[142] R. Ruer, Z. Anorg. Chem. **51**, 391 (1906).

[143] A. Nagasawa, Y. Matsuo, and J. Kakinoki, J. Phys. Soc. Jpn. **20**(10), 1881 (1965).

[144] Y. Matsuo, A. Nagasawa, and J. Kakinoki, J. Phys. Soc. Jpn. **21**(12), 2633 (1966).

[145] Y. Kawasaki, S. Ino, and S. Ogawa, J. Phys. Soc. Jpn. **30**(6), 1758 (1971).

[146] F. Doerinckel, Z. Anorg. Allg. Chem. **34**, 333 (1907).

[147] C. H. Johnsson and J. O. Linde, Ann. Phys. **5**(6), 762 (1930).

[148] A. S. Darling, R. A. Mintern, and J. C. Chaston, J. Inst. Met. **81**, 125 (1952-1953).

[149] A. A. Rudnitskii and A. N. Khotinskaya, Zh. Neorg. Khim. **4**, 2518 (1959); TR: Russ. J. Inorg. Chem. **4**, 1160 (1969).

[150] E. Raub and G. Falkenburgh, Z. Metallkd. **55**(7), 392 (1964).

[151] A. A. Rudnitskii and A. N. Khotinskaya, Zh. Neorg. Khim. **4**, 1601 (1959); TR: Russ. J. Inorg. Chem. **4**, 722 (1969).

[152] M. Kuhn, J. A. Rodriguez, J. Hrbek, A. Bzowski, and T. K. Sham, Surf. Sci. **341**, L1011-18 (1995).

[153] A. T. Aldred, Trans. AIME **224**, 1082 (1962).

[154] H. Reule, S. Steeb, and C. Donolato, J. Less-Common Met. **24**, 108 (1971).

[155] P. E. Rider and K. A. Gschneidner, Jr., O. D. McMasters, Trans. AIME **233**, 1488 (1965).

[156] A. R. Miedema, J. Less-Common Met. **46**, 67 (1976).

[157] B. T. Matthias, E. Corenzwit, J. M. Vandenberg, H. Barz, M. B. Maple, and R. N. Shelton, J. Less-Common Met. **46**, 339 (1976).

[158] A. E. Dwight, J. W. Downey, and R. A. Conner, Jr., Acta Crystallogr. **22**, 745 (1967).

[159] H. J. M. van Rongen, B. Knook, and G. G. van den Berg, Low-Temperature Physics LT9, Proc. IXth Int. Conf. on Low-Temperature Physics, Columbus, OH, B1041 (1964).

[160] E. Raub, P. Walter, and M. Engel, Z. Metallkd. **43**, 112 (1952).

[161] M. K. McQuillan, J. Inst. Metals **82**, 511 (1954).

[162] P. Pietrokowsky, E. P. Frink, and P. Duwez, Trans. AIME **206**, 930 (1956).

[163] K. Schubert, H. G. Meissner, M. Pötzschke, W. Rossteutscher, and E. Stolz, Naturwissenschaften **49**, 57 (1962).

[164] P. Pietrokowsky, J. Inst. Metals **90**, 434 (1961/62).

[165] H. Vonphilipsborn and F. Laves, Acta Crystallogr. **17**, 213 (1964).

[166] E. Vielhaber and H. L. Luom, Solid State Comm. **5**, 221 (1967).

[167] J. B. Vetrano, G. L. Guthrie, and H. E. Kissinger, Phys. Lett. A **26** 45 (1967).

[168] P. Pietrokowsky, Scripta Metall. **2**, 379 (1968).

[169] S. A. Shabalovskaya, Solid State Comm. **70**, 23-26 (1989).

[170] C. C. Chao, H. L. Luo, and P. Dumez, J. Appl. Phys. **34**, 1971 (1963).

[171] H. R. Kirchmayr, Z. Metallkd. **56**, 767 (1965).

[172] J. B. Kusma and E. Laube, Monatsh. Chem. **96**, 1496 (1965).

[173] Y. Sadagopan, B. C. Giessen, and N. J. Grant, J. Less-Common Met. **14**, 279 (1968).

[174] E. Raub and M. Engel, Z. Metallkd. **39**, 172 (1948).

[175] K. Schubert, M. Balk, S. Bhan, M. Breimer, P. Esslinger, and E. Stolz, Naturwissenschaften **49**, 647 (1962).

[176] M. V. Nevitt and J. W. Downey, Trans. AIME **224**, 194 (1962).

[177] E. Stolz and K. Schubert, Z. Metallkd. **53**, 433 (1962).

[178] H. Holleck, Acta Crystallogr. **21**(3), 451 (1966).

[179] l. Arnberg, Acta Crystallogr. B **36**, 527 (1980).

[180] J. P. Neumann, A. Mikula, and Y. A. Chang, Metall. Trans. A **13**(7), 1123 (1982).

[181] H. Nowotny, E. Bauer, A. Stampfl, and H. Bittner, Monatsh. Chem. **83**, 221 (1952).

[182] M. G. Chasanov, I. Johnson, and R. V. Schablaske, J. Less-Common Met. **7**, 1127 (1964).

[183] M. G. Chasanov, P. D. Hunt, I. Johnson, and H. M. Feder, Trains AIME **224**, 935 (1962).

[184] W. M. Robertson, Metall. Trans. **3** 1443 (1972).

[185] R. Elmendorf and E. Ryba, Acta Crystallogr. B**24**, 462 (1968).

[186] E. Ryba, P. K. Kejriwal, and R. Elmendorf, J. Less-Common Met. **18**, 419 (1969).

[187] G. Bruzzone, M. L. Fornasini, and F. Merlo, J. Less-Common Met. **30**, 361 (1973).

[188] Y. Ishii, K. Nozawa, and T. Fujiwara, Mat. Res. Soc. Symp. Proc. **805**, 129-134 (2003)

[189] W. Rossteutscher, K. Schubert, Z. Metallkd. **56**, 730 (1965).

[190] Arunsingh and B. Dayal, Acta Crystallogr. B **25**, 1010 (1969).

[191] E. Montignie, Bull. Soc. Chim. Fr. Mem. **5**, 567 (1938).

[192] J. D. Grogan and J. L. Haughton, J. Inst. Met. **69**, 241-248 (1943).

[193] N. Tiner, Trans. Am. Inst. Mining, Metallurgical and Petroleum Eng. **161**, 351-359 (1945).

[194] H. Nowotny, Z. Metallkd. **37**, 130-136 (1946).

[195] N. I. Varich and B. N. Litvin, Phys. Met. Metallogr. **16**(4), 29-32 (1963).

[196] J. J. Hauser, J. V. Waszczak, and B. A. Davidson, Solid State Comm. **62**, 835-836 (1987).

[197] E. Rudy, Compendium of Phase Diagram Data, Air Force Materials Laboratory, Wright-Patterson AFB, OH, Rep. No. AFML-TR-65-2, Part V (1969).

[198] J. Chao, C. Wolverton, J. Sofo, L.-Q. Chen, and Z.-K. Liu, Phys. Rev. B **69**, 214202 (2004).

[199] S. S. Rajput, R. Prasad, R. M. Singru, S. Kaprzyk, and A. Bansil, Mater. Sci. Forum **175-178**, 925 (1995).

[200] C. MoBecker and J. Hafner, J. Physics: Cond. Matt. **7**, 5843-56 (1995).

[201] A. Maldonado and K. Shubert, Z. Metallkd. **55**, 619 (1964).

[202] E. Raub, Z. Metallkd. **45**, 23-30 (1954).

[203] K. Schubert, W. Burkhardt, P. Esslinger, E. Günzel, H. G. Meissner, W. Schütt, J. Wegst, and M. Wilkens, Naturwissenschaften **43**, 248-249 (1956).

[204] A. G. Knapton, Planseeber. Pulvermet. **7**, 2-3 (1959).

[205] K. Schubert, K. Frank, R. Gohle, A. Maldonado, H. G. Meissner, A. Raman, and W. Rossteutscher, Naturwissenschaften **50**, 41 (1963).

[206] H. P. Rooksby and B. Lewis, J. Less-Common Met. **6**, 451-460 (1964).

[207] H. Ocken and J. H. N. Van Vucht, J. Less-Common Met. **15**, 193-199 (1968).

[208] R. Flükiger, A. Paoli, R. Roggen, K. Yvon, and J. Müller, Solid State Comm. **11**, 61-63 (1972).

[209] R. Flükiger, K. Yvon, C. Susz, R. Roggen, A. Paoli, and J. Müller, J. Less-Common Met., **32**, 207 (1973).

[210] R. Flükiger, A. Paoli, and J. Müller, Solid State Comm. **14**, 443-447 (1974).

[211] C. W. Haworth and W. Hume-Rothery, J. Inst. Met. **87**, 265 (1958/1959).

[212] E. Anderson and W. Hume-Rothery, J. Less-Common Met. **2**, 19 (1960).

[213] B. C. Giessen, U. Jaehnigen and N, J, Grant, J. Less-Common Met. **10**, 147 (1966).

[214] R. Gurler and J. N. Pratt, J. Alloys Compd. **177**, 321 (1991).

[215] H. Kleykamp, J. Less-Common Met. **136**, 271 (1988).

[216] S. Ferreira, J. Duarte Jr., and S. Frota-Pessoa, Phys. Rev. B **41**, 5627 (1990).

[217] P. Souvatzis, M. I. Katsnelson, S. Simak, R. Ahuja, O. Eriksson, and P. Mohn, Phys. Rev. B **70**, 12201 (2004).

[218] G. N. Ronami, Krist. Tech. **7**(6), 615 (1972).

[219] R. G. Baggerly, Metallography **8**, 361 (1975).

[220] D. L. Moffatt and U. R. Kattner, Metall. Trans. **19**, 2389 (1988).

[221] G. Rubin and A. Finel, J. Physics: Cond. Matt. **7**, 3139-52 (1995).

[222] K. A. Gschneidner, Jr. *Rare Earth Alloys*, Van Nostrand, Princeton, NJ, 221 (1961).

[223] L. T. Kong, J. B. Liu, and B. X. Liu, J. Mater. Res. **17**, 528-531 (2002).

[224] R. E. Watson, M. Weinert, and M. Alatalo, Phys. Rev. B **65**, 014103 (2002).

[225] B. T. Matthias, V. B. Compton, and E. Corenzwit, Phys. Chem. Solids **19**, 130 (1961).

[226] B. C. Giessen and N. J. Grant, Acta Crystallogr. **17** 615 (1964).

[227] A. Maldonado and K. Shubert, Z. Metallkd. **55**, 619 (1964).
[228] B. C. Giessen and N. J. Grant, J. Less-Common Met. **8**, 114 (1965).
[229] R. M. Waterstrat and B. C. Giessen, Metall. Trans. A **16**(11), 1943 (1985).
[230] D. L. Ritter, B. C. Giessen, and N. J. Grant, Trans. AIME **230**, 1250 (1964).
[231] D. L. Ritter, B. C. Giessen, and N. J. Grant, Trans. AIME **230**, 1259 (1964).
[232] M. Rajagopalan and M. Sundareswari, J. Alloys Compd. **379**, 8-15 (2004).
[233] D. Bender, E. Bucher, and J. Muller, Phys. Kondens. Mater. **1**, 225 (1963).
[234] E. Raub and W. Fritzsche, Z. Metallkd. **54** 317 (1963).
[235] G. F. Hurley and J. H. Brophy, J. Less-Common Met. **7**, 267 (1964).
[236] T. Tsukamoto, K. Koyama, A. Oota, and S. Noguchi, Nippon Kinzoku Gakkai-shi **53**(3), 253 (1989).
[237] B. H. Chen, H. F. Franzen, J. Less-Common Met. **153**, L13 (1989).
[238] J. M. Sanchez and J. D. Becker, Mat. Res. Soc. Symp. Proc. **291**, 115-27 (1993).
[239] J. D. Becker and J. M. Sanchez, J. Mater. Sci. **A170**, 161-167 (1993).
[240] J. D. Becker, J. M. Sanchez, and J. K. Tien, Mat. Res. Soc. Symp. Proc. **213**, 113-18 (1991).
[241] V.B. Compton, E. Corenzwit, J. P. Maita, B. T. Matthias, and F. J. Morin, Phys. Rev. **123**, 1567 (1961).
[242] D. O. Van Ostenburg, D. J. Lam, M. Shimizu, and A. Katsuki, J. Phys. Soc. Japan **18**, 1744-1754 (1963).
[243] A. L. Giorgi and E. G. Szklarz, J. Less-Common Met. **20**(2), 173-175 (1970).
[244] O. N. Carlson, V. C. Marcotte, and D. E. Williams, USAEC Rep. ISC-1050, 53 (1959).
[245] O. N. Carlson, W. L. Larsen, V. C. Marcotte, and D. E. Williams, USAEC Rep. IS-17, 76 (1959).
[246] C. E. Lundin and D. T. Klodt, J. Inst. Met. **90**, 341 (1961).
[247] A. Taylor, W. M. Hickam, and N. J. Doyle, J. Less-Common Met. **9**, 214 (1965).
[248] L. T. Kong, J. B. Liu and B. X. Liu, J. Phys. Soc. Jpn. **71**, 141-3 (2002).
[249] A. G. Rabinkin, L. A. Klishanova, and L. N. Pronina, *Problems of Superconducting Materials* **141** (1970).
[250] P. Van Effenterre, Report CEA0R04330, Atomic Energy Commission, Saclay, France (1972).
[251] P. E. J. Flewitt, J. Appl. Crystallogr. **5**, 423 (1972).
[252] P. E. J. Flewitt, Acta Metall. **22**, 47 (1974).
[253] J. P. Abriata and J. C. Bolcich, Bull. Alloy Phase Diagrams **3**(1) (1982).
[254] H. v. Leuken, A. Lodder, M. T. Czyzyk, F. Springelkamp, and R. A. de Groot, Phys. Rev. B **41**, 5613 (1990).
[255] J. M. Sanchez and J. D. Becker, Prog. Theor. Phys. Sul. **115**, 131-45 (1994).
[256] G. B. Grad, A. F. Guillermet, and J. R. Granada, Z. Metallkd. **87**, 726-731 (1996).
[257] G. B. Grad, G. M. Benites, G. Aurelio, and A. F. Guillermet, Mat. Sci. Eeng. A-Struct. **A273-275**, 175-180 (1999).
[258] J. Kudrnovsky and V. Drchal, Z. Phys. B Cond. Mat. **73**, 489-93 (1989).
[259] B. C. Giessen, N. J. Grant, D. P. Parker, R. C. Manuszewski, and R. M. Waterstrat, Metall. Trans. A **11**, 709 (1980).
[260] E. Raub, J. Less-Common Met. **1**(1), 3 (1959).
[261] D. T. Hawkins, in *Metals Handbook, Metallography, Structures and Phase Diagrams*, Vol. 8, 8th ed., American Society for Metals, Metal Park, Ohio (1973).
[262] Z. W. Lu, S.-H. Wei, and A. Zunger, Phys. Rev. Lett. **66**, 1753 (1991).
[263] E. Raub, J. Less-Common Met. **1**(1), 3 (1959).
[264] E. Raub, H. Beeskow, and D. Menzel, Z. Metallkd. **50**, 428 (1959).
[265] P. E. A. Turchi, G. M. Stocks, W. H. Butler, D. M. Nicholson, and A. Gonis, Phys. Rev. B **37**, 5982 (1988).
[266] J. E. Shield, and R. K. Williams, Scr. Metall. **21**, 1475 (1987).
[267] M. Asato, T. Hoshino, and K. Masuda-Jindo, J. Magn. Magn. Mater. **226-230**, 1051-2 (2001).
[268] M. Asato, T. Mizuno, T. Hoshino, and H. Sawada Mater. Trans. **42**, 2216-2224 (2001).
[269] C. Wolverton and D. de Fontaine, Mat. Res. Soc. Symp. Proc. **291**, 431-6 (1993).
[270] F. M. Marquez, C. Cienfuegos, B. K. Pongsai, M. Yu. Lavrentiev, N. L. Allan, J. A. Purton, and G. D. Barrera, Model. Simul. Mater Sc. **11**, 115-26 (2003).
[271] A. A. Rudnitskii and R. S. Plyakova, Zh. Neorg. Khim. **4**, 1014 (1959); Russ. J. Inorg. Chem. **4**, 631 (1959).
[272] A. S. Darling and J. M. Yorke, Platinum Met. Rev. **4**, 104 (1960).
[273] H. Kleykamp, J. Nucl. Mater. **167**, 49 (1989).
[274] H.B. Guo, X.Y. Li, and B. X. Liu, J. Phys. Soc. Jpn. **71**, 2933-5 (2002).
[275] H. R. Haines, P. E. Potter, and M. H. Rand, Thermodynamics of Nuclear Materials, Proceedings of a Symposium, 4th, Vienna **1**, 471-501 (1980).
[276] A. A. Rudnitskii and N. A. Birun, Russ. J. Inorg. Chem. **5**, 1169-1173 (1960).
[277] A. E. Dwight, R. A. Jr. Conner, and J. W. Downey, Acta Crystallogr. **18**, 835-839 (1965).
[278] H. W. Rosenberg and D. B. Hunter, Trans. AIME **233**, 681-685 (1965).
[279] E. Raub and E. Röschel, Z. Metallkd. **59**, 112-114 (1968).
[280] P. Krautwasser, S. Bhan, and K. Schubert, Z. Metallkd. **59**, 724-729 (1968).
[281] H. Schulz, K. Ritapal, W. Bronger, and W. Klemm, Z. Anorg. und Allg. Chem. **358**, 299-313 (1968).
[282] I. R. Harris and M. Norman, J. Less-Common Met. **22**, 127-130 (1970).
[283] H. C. Donkersloot and J. H. N. Van Vucht, J. Less-Common Met. **20**, 83-91 (1970).
[284] V. N. Eremenko and T. D. Shtepa, Sov. Powder Metall. Metal Cer. **11**, 228-233 (1972).
[285] A. R. Miedema, K. H. J. Buschow, and H. H. Van Mal, J. Less-Common Met. **49**, 463-472 (1976).

[286] V. P. Sivokha, A. S. Savvinov, V. P. Voronin, and V. N. Khachin, Phys. Met. Metallogr., translated from Fizika Metallov, Metallovedenie **56**(3), 112-116 (1983).

[287] S. A. Shabalovskaya, A. I. Lotkov, A. G. Narmonev, and A. I. Zakharov, Solid State Comm. **62**, 93-95 (1987).

[288] N. Selhaoui, J. C. Gachon, and J. Hertz, J. Less-Common Met. **154**, 137-147 (1989).

[289] S. Pick and P. Mikusik, Solid State Comm. **80**, 897-899 (1991).

[290] P. Mikusik and S. Pick, Solid State Comm. **86**, 467-469 (1993).

[291] J. M. Zhang and G. Y. Guo, J. Phys. Cont. Mat. **7**, 6001-60017 (1995).

[292] C. Wolverton, G. Ceder, D. de Fontaine, and H. Dreysse, Phys. Rev. B **48**, 726 (1993).

[293] O. Loebich and E. Raub, J. Less-Common Met. **30**(1), 47 (1973).

[294] J. Le Roy, J. M. Moreau, and D. Paccard, Acta Crystallogr. B **33**(8), 2414 (1977).

[295] R. Sanjines-Zeballos, R. Chabot, and E. Parthé, J. Less-Common Met. **72**(1), P17 (1980).

[296] K. Takao, Y. Sakamoto, and M. Yoshida, J. Less-Common Met. **152**, 115 (1989).

[297] K. Anderko, Z. Metallkd. **50**, 681 (1959).

[298] E. Stolz and K. Schubert, Z. Metallkd. **53**, 433 (1962).

[299] I. R. Harris and M. Norman, J. Less-Common Met. **18**, 333 (1969).

[300] E. M. Savistky, V. P. Polyakova, N. Gorina, and N. Roshan, *Physical Metallurgy of Platinum Metals*, MIR, Moscow (1978).

[301] M. S. Chandrasekharaiah, M. J. Stickney, K. A. Gingerich, and J. A. Speed, J. Alloy Phase Diagrams **6**, 59 (1990).

[302] V. N. Kuznetsov, G. P. Zhmurko, and E. M. Sokolovskaya, J. Less-Common Met. **163**, 1 (1990).

[303] S. Stolen and T. Matsui, J. Nucl. Mater. **186**, 242 (1992).

[304] L. A. Bendersky, J. K. Stalick, R. Portier, and R. M. Waterstrat, J. Alloys Compd. **236**, 19 (1996).

[305] E. Gaganidze, P. Esquinazi, and R. König, Europhys. Lett. **31**, 13 (1995).

[306] J. M. Hutchinson, Platinum Met. Rev. **16**, 88 (1972).

[307] G. A. Camara, M. J. Giz, V. A. Paganin, and E. A. Ticianelli, J. Electronal. Chem. **537**, 21 (2002).

[308] N. Nishimura and T. Hiramatsu, Nippon Kinzoku Gakkaishi **21**, 469 (1957).

[309] T. Sato, S. Hukai, and Y. C. Huang, J. Austr. Inst. Met. **5**(2), 149 (1960).

[310] P. Pietrokowsky, Nature **206**, 291 (1965).

[311] A. K. Sinha, Trans. AIME **245**, 237 (1969).

[312] P. J. Meschter and W. L. Worrell, Metall. Trans. A **7**, 299 (1976).

[313] V.B. Compton and B. T. Matthias, Acta Crystallogr. **12**, 651 (1959).

[314] T. H. Geballe, B. T. Matthias, V.B. Compton, E. Corenzwit, G. W. Hull, and L. D. Longinotti, Phys. Rev. **137**, 119 (1965).

[315] W. Bronger, J. Less-Common Met. **12**, 63 (1967).

[316] N. H. Krikorian, J. Less-Common Met. **23**, 271 (1971).

[317] A. Raman, J. Less-Common Met. **26**, 199 (1972).

[318] B. Erdmann and C. Keller, J. Solid State Chem. **7**, 40 (1973).

[319] J. Le Roy, J. M. Moreau, D. Paccard, and E. Parthé, Acta Crystallogr. B **34**, 3315 (1978).

[320] X. Yifen and O. Loebich, J. Less-Common Met. **144**, 301 (1988).

[321] H. J. Wallbaum, Naturwissenschaften **31**, 91 (1943).

[322] A. Raman and K. Schubert, Z. Metallkd. **55**, 704 (1964).

[323] K. Shubert, S. Bhan, T. K. Biswas, K. Frank, and P. K. Pandy, Naturwissenschaften **55**, 542 (1968).

[324] A. R. Miedema, R. Boom, and F. R. De Boer, J. Less-Common Met. **41**, 283 (1975).

[325] A. Hellawell, and W. Hume Rothery, Phil. Mag. **45**, 797 (1954).

[326] J. O. A. Paschoal, H. Kleykamp, and F. Thmmler, J. Less-Common Met. **98**, 279 (1984).

[327] R. Gurler, J. Alloys Compd. **191**, 31 (1993).

[328] E. Raub and E. Roeschel, Z. Metallkd. **57** 546 (1966).

[329] V. N. Eremenko, T. D. Shtepa, and V. G. Sirotenko, Sov. Powder Metall. Metal Cer. **5**, 487 (1966).

[330] V. N. Eremenko and T. D. Shtepa, Colloq. Int. CNRS **205**, 403 (1972).

[331] T. D. Shetpa, Fiz. Khim. Kondens. Faz. Sverkhtverd. Mater. 175 (1975).

[332] R. Kuentzler and R. M. Waterstrat, Solid State Comm. **68**, 85 (1988).

[333] V. B. Compton and B. T. Matthias, Acta Crystallogr. **12**, 651 (1959).

[334] T. H. Geballe, B. T. Matthias, V. B. Compton, E. Corenzwit, G. W. Hull, and L. D. Longinotti, Phys. Rev. A **137**, 119 (1965).

[335] A. Raman, J. Less-Common Met. **26**(2), 199 (1972).

[336] H. Ghassem and A. Raman, Z. Metallkd. **64**(3), 197 (1973).

[337] J. M. Moreau, D. Paccard, and E. Parthé, Acta Crystallogr. B **32**, 1767 (1976).

[338] O. Loebich and E. Raub, J. Less-Common Met. **46**, 1 (1976).

[339] S. T. Zegler, J. Phys. Chem. Solids **26**, 1347 (1965).

[340] V. N. Eremenko, E. L. Semenova, and T. D. Shtepa, Russ. Metall. (2), 158 (1978).

[341] V. N. Eremenko, E. L. Semenova, and T. D. Shtepa, Diag. Sostoyaniya Tugoplavk Sistem Kiev, 119 (1980).

[342] J. L. Jorda, T. Graf, L. Schellenberg, J. Müller, K. Cenzual, J. C. Gachon, and J. Hertz, J. Less-Common Met. **136**, 313 (1988).

[343] R. Kuentzler and R. M. Waterstrat, Solid State Comm. **68**, 85 (1988).

[344] E. L. Semenova and Y. V. Kudryavtsev, J. Alloys Compd. **203**, 165 (1994).

[345] A. Szajek and A. Jezierski, Solid State Commun. **71**, 917-22 (1989).

[346] N. Y. Alekseyevskiy, O. A. Balakhovskii, and I. V. Kirillov, Phys. Met. Metallogr., translated from Fizika Metallov, Metallovedenie **40**, 38 (1975).

[347] C. B. Jordan, Trans. Am. Inst. Mining, Metallurgical and Petroleum Eng. **203**, 832-833 (1955).

[348] A. E. Dwight, Trans. Am. Inst. Mining, Metallurgical

and Petroleum Eng. **215**, 283-286 (1959).

[349] D. D. Gulamova, M. V. Raevskaya, I. G. Sokolova, F. S. Litvak, and E. M. Sokolovskaya, Moscow Univ. Chem. Bull. **27**(4), 96 (1972).

[350] E. Raub and E. Roeschel, Z. Metallkd. **54**(8) 455 (1963).

[351] Y. Tamminga, B. Barkman, and F. R. De Boer, Solid State Comm. **12**, 731-735 (1973).

[352] V. N. Eremenko, T. D. Shtepa, and V. T. Khoruzhaya, Russ. Metall. (2), 155-156 (1973).

[353] N. G. Boriskina and I. I. Kornilov, Russ. Metall. (2), 162 (1976).

[354] J. M. Zhang and G. Y. Guo, J. Phys. Cond. Matt. **7**, 6001-6017 (1995).

[355] O. Loebich and E. Raub, J. Less-Common Met. **46**, 7 (1976).

[356] K. Cenzual, A. Palenzona, and E. Parthé, Acta Crystallogr. B **36**(7), 1631 (1980).

[357] R. Sanjines-Zaballos, B. Chabot, and E. Parthé, J. Less-Common Met. **72**, P17 (1980).

[358] P. Sharifrazi, R. C. Mohanty, and A. Raman, Z. Metallkd. **75**(10), 801 (1984).

[359] M. L. Fornasini, A. Mugnoli, and A. Palenzona, J. Less-Common Met. **154**, 149 (1989).

[360] A. Palenzona and E. Canepa, J. Less-Common Met. **162**, 267 (1990).

[361] V. N. Eremenko, E. L. Semenova, and T. D. Shtepa, Russ. Metall. (2), 177 (1980).

[362] V. N. Eremenko, V. T. Khoruzhaya, and T. D. Shtepa, Russ. Metall. (1), 194 (1988).

[363] M. J. Mehl, J. E. Osburn, D. A. Papaconstantopoulos, and B. M. Klein, Mat. Res. Soc. Symp. Proc. **186**, 277-82 (1991).

[364] C. C. Koch, J. Less-Common Met. **6**, 177 (1976).

[365] J. B. Darby, Jr., D. J. Lam, L. J. Norton, and J. W. Downey, J. Less-Common Met. **4**, 558 (1962).

[366] J. B. Darby, Jr., L. J. Norton, and J. W. Downey, J. Less-Common Met. **5**, 397 (1963).

[367] J. B. Darby, Jr., L. J. Norton, and J. W. Downey, J. Less-Common Met. **6**, 165 (1964).

[368] J. Niemiec, Bull. Acad. Pol. Sci. Ser. Sci. Chem. **11**. 665 (1963).

[369] E. G. Szklarz and A. L. Giorgi, J. Less-Common Met. **81**, 2349 (1981).

[370] A. L. Giorgi and E. G. Szklarz, J. Less-Common Met. **22**, 246 (1970).

[371] P. A. Farrar and S. Adler, Trans. AIME **236**, 1061 (1966).

[372] D. Chatterji, M. T. Hepworth, and S. J. Hruska, Metall. Trans. **2**, 1271 (1971).

[373] J. Etchessahar and J. Debuigne, Mem. Sci. Rev. Metall. **74**(3), 195 (1977).

[374] J. P. Auffredic, E. Etchessahar, and J. Debuigne, J. Less-Common Met. **84**, 49 (1982).

[375] C. E. Lundin, *Rare Earth Symposium*, Annual Meeting, Am. Soc. Metals, Chicago (1959).

[376] J. C. Uy, D. J. Lam, L. C. Ianiello, R. A. Proebstle, A. P. Lee, B. T. M. Loh, and A. A. Burr, Final Report AT(30-1)-2159, Rensselaer Polytechnic Institute (1961).

[377] C. E. Lundin, D. T. Klodt, Trans. AIME **224**, 367 (1962).

[378] R. Wang, Metall. Trans. **3**, 1213 (1972).

[379] R. Wang and Y. B. Kim, Metall. Trans. **5**, 1973 (1974).

[380] R. Wang, Mater. Sci. Eng. **23**, 135 (1976).

[381] A. van de Walle and G. Ceder, Rev. Mod. Phys. **74**(1), 11 (2002).

[382] C. Wolverton and V. Ozolins, Phys. Rev. Lett. **86**, 5518 (2001).